

UNCLASSIFIED

AD NUMBER
ADC008446
NEW LIMITATION CHANGE
TO Approved for public release, distribution unlimited
FROM Distribution: Further dissemination only as directed by Hq Naval Research Lab., Washington, D.C.
AUTHORITY
NRL ltr 22 Jan 2004

THIS PAGE IS UNCLASSIFIED

UNCLASSIFIED



AD NUMBER

C008 446

CLASSIFICATION CHANGES

TO

UNCLASSIFIED

FROM

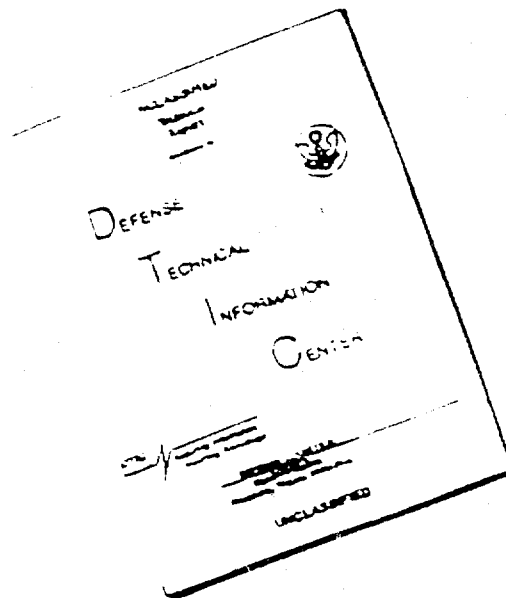
CONFIDENTIAL

AUTHORITY

CMDR NRL

THIS PAGE IS UNCLASSIFIED

DISCLAIMER NOTICE



THIS DOCUMENT IS BEST QUALITY AVAILABLE. THE COPY FURNISHED TO DTIC CONTAINED A SIGNIFICANT NUMBER OF PAGES WHICH DO NOT REPRODUCE LEGIBLY.

~~EX~~ MOST Project -4

NRL Memorandum Report 1273

FG

003630

ADC008446

Good

PROJECT ARTEMIS

High Power Acoustic Source

THIRD INTERIM REPORT ON ACOUSTIC PERFORMANCE

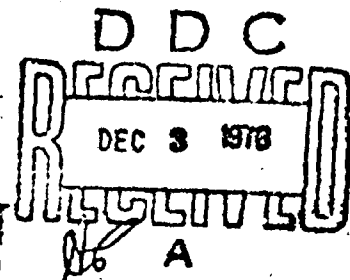
(UNCLASSIFIED TITLE)

A. T. McClinton
R. H. Ferris

SOUND DIVISION

COPY AVAILABLE TO DDC DOES NOT
PERMIT FULLY LEGIBLE PRODUCTION

23 April 1962



NATIONAL SECURITY INFORMATION

*Unauthorized Disclosure Subject to Criminal
Sanctions*



640124-0742

U. S. NAVAL RESEARCH LABORATORY
Washington, D.C.

W 2-7-3
DDC FILE COPY

DO NOT REPRODUCE AT 10-YEAR INTERVALS
BUT AUTOMATICALLY DECLASSIFIED
DDC LST 600 10

Further distribution of this report is to be made only
at the discretion of the Director, Naval Research Laboratory,
Washington 25, D.C., and the activities mentioned
in the research referred therein, as appropriate.

14
NRL MEMORANDUM REPORT 1273

PROJECT ARTEMIS
HIGH POWER ACOUSTIC SOURCE

6 THIRD INTERIM REPORT ON
ACOUSTIC PERFORMANCE (U).
(Unclassified Title)

12 8 p.p.

10 by
A. T./McClinton
R. H./Ferris

1) Intercept. no. 3 Sep-Oct 61,

23 April 1962

Electrical Applications Branch
Sound Division
U. S. NAVAL RESEARCH LABORATORY
Washington 25, D. C.

This document contains information affecting the national defense of the United States within the meaning of the Espionage Laws, Title 18, U.S.C. Section 793 and 794. The transmission or the revelation of its contents in any manner to an unauthorized person is prohibited by law.

CONFIDENTIAL SECURITY INFORMATION

Unauthorized Disclosure Subject to Criminal
Sanctions

251 950

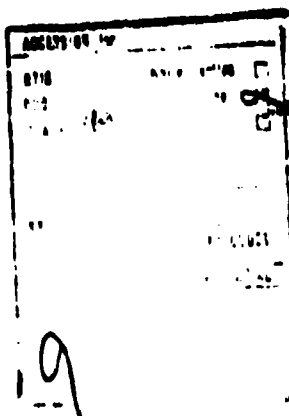
mt

DISTRIBUTION

CNO		
Attn: Op-03EG		1
Op-07		1
Op-31		1
Op-70		1
Op-714D		1
ONR		
Attn: Code 467		11
BUSHIPS		
Attn: Code 370		1
Code 688		1
BUWEPS		
Attn: RUDC		1
NEL		2
NOL		1
NAVUWTRSOUNDREFLAB		1
NAVUWTRSOUNDLAB		2
Hudson Laboratories, Columbia University 145 Palisade Street, Dobbs Ferry, New York		
Attn: D. R. A. Froesch		10
Admiralty Research Laboratory Teddington, Middlesex, England		1

CONTENTS

Distribution	ii
Abstract	iv
Problem Authorisation	iv
Problem Status	iv
Introduction	1
Purpose	2
Experimental Procedure	3
Results	5
Impedance Measurements	5
Acoustic Measurements	6
Displacement Amplitude	7
Displacement Phase	9
Equivalent Loading	9
Especially Instrumented Element	10
Alternating Current Measurements	11
Waveforms	12
Constant Voltage Drive	12
Conclusions	13
List of Illustrations	15



ABSTRACT

U. S. Naval Research Laboratory Reports 1205 and 1214 presented the results of initial tests with an interim ARTEMIS source consisting of a one wave length square array. This report describes additional tests with an enlarged array in which fifteen of the twenty transducer modules of the full array were installed. While the enlarged array results in improved operating characteristics with respect to acoustic loading and velocity distribution, it was found that the permissible operating power level is still severely restricted by abnormally high transducer displacements which can cause mechanical destruction of the transducer elements.

Evidence is presented which supports the theory that anomalous behavior is caused by acoustic interaction effects.

PROBLEM AUTHORIZATION

ONR NR 287 002 (Special)
NRL Problem Number 55S02-11

PROBLEM STATUS

This is an interim report on one phase of the project. Work is continuing.

INTRODUCTION

The high power acoustic source for Project ARTEMIS is planned to consist of 1440 variable reluctance transducer elements close-packed in a rectangular plane array having the approximate dimensions of four wave lengths vertically by two and one-half wave lengths horizontally at the resonant frequency. Each element is 11-1/8 inches square on the radiating face and 11-3/4 inches deep. They are assembled in modules six elements wide by twelve elements high. The final array configuration will consist of four rows of five modules each.

Initial tests were conducted on a one wave length square array composed of two modules mounted side by side on the array structure which was installed on the USNS MISSION CAPISTRANO (T-AG 162). U. S. Naval Research Laboratory Memorandum Reports 1205 and 1214 present the results of these tests indicating that displacement amplitude and phase of individual elements varied widely with element position and operating frequency. The principal deleterious effect of the nonuniform displacement amplitude is that for a given power level some of the elements have larger displacement amplitudes than would be required if the displacement distribution were constant. This requires that the power input to the array be limited to a level consistent with safe operation for those elements having the highest amplitudes.

This report describes the results of tests conducted during September and October 1961 with a larger array configuration. When they became available, fifteen modules were installed on the array structure in three rows of five modules each, forming an array approximately three wave lengths high by two and one-half wave lengths wide. Four oil-filled component tanks and a junction box were installed in the base of the array structure. The double armored cables which provide power and instrumentation connections from the ship to the transducer were terminated in the junction box. Connections are made within the junction box to distribute the power and instrumentation conductors to the four component tanks. The junction box also houses remotely operated contactors which can connect or disconnect power to each tank. Each component tank serves one row of transducer modules and houses the necessary electrical components to appropriately transform and distribute the signal driving current and the polarizing current to each module in the row which it serves. It also contains sensors which measure these currents and transmit the information for remote indication. Polarizing power is transmitted from the ship to the component tanks as three phase, sixty

[REDACTED]

cycle alternating current. A twelve phase silicon diode rectifier with appropriate transformer rectifies the alternating current to provide ten amperes polarizing current to each of the transducer elements. Each component tank contains a transformer having five secondary windings. These transformers distribute the signal driving current through appropriate tuning and blocking capacitors to each of the five modules in the row served by that tank. The transformer primaries are connected in parallel in the junction box. Since three rows of modules were installed for this test, only three of the four component tanks were used.

Acoustic radiation from the rear of the transducer is suppressed by a system of compliant resonant reflectors installed on the back face of each transducer module. Each reflector is a flattened stainless steel tube six feet long and approximately six inches wide. The tubes are filled with nitrogen and pressure compensated by a pressure regulating system. There are twelve tubes on each module, one behind each row of elements. The tubes are separated from the elements by a distance of approximately one-half inch.

Thirty-five accelerometers were available for measuring displacement amplitude and phase of both the transducer elements and the resonant reflectors. These accelerometers were tested and their calibration shown to be independent of the ambient static pressure and the acoustic field. Twelve current sensors were used to sample the signal driving current in rows of elements. The signal current connections to each module were such that the six elements in each row were connected in series and the twelve rows connected in parallel. Thus, the twelve current sensors were adequate to monitor the currents in each row of any one module. The accelerometer and current sensor outputs were transmitted to the ship through a watertight junction box containing a remotely controlled, fifty position stepping switch and a preamplifier. Thus, the sensor outputs were sampled sequentially. One channel was used to transmit a calibration voltage through the preamplifier. The remaining two channels transmitted the outputs of two accelerometers which were installed internally in a special transducer element. A view of the fifteen module installation on the USNS MISSION CAPISTRANO is shown in figure 1.

PURPOSE

The purposes of this test were to obtain information concerning the acoustic and motional characteristics of the enlarged transducer array.

CONFIDENTIAL

to investigate the nature and causes of the anomalous displacement behavior observed in previous tests with a 144 element array, and to determine if the enlarged array exhibited improved acoustic loading characteristics. Instrumentation was provided specifically to:

1. Obtain impedance characteristics of the enlarged array,
2. Measure the free field current response of the enlarged array and obtain an approximate representation of the directivity characteristics in the vicinity of the acoustic axis,
3. Obtain a reasonable statistical sample of the displacement amplitude and phase of the radiating faces of the transducer elements,
4. By means of a specially instrumented transducer element, determine the motional characteristics of the element reaction mass as a function of frequency and element position, and
5. Determine the relative impedance of rows of elements within a module for one or more module positions, and to examine the relative impedance of each module with respect to the other modules in the array.

EXPERIMENTAL PROCEDURE

Experiments were conducted in the Cape Charles area of the Chesapeake Bay in a water depth of eighty feet, at 27° 29' north latitude and 75° 19' west longitude in a water depth of 2540 fathoms, and at various areas within Exuma Sound. The purpose of the shallow water tests in the Chesapeake Bay was to check the operation of the acoustic source and instrumentation. All data presented in this report, with the exception of the air impedance data, were obtained in deep water operations. Figure 1 illustrates the dead reckoning tracks for operations in Exuma Sound. All operations were conducted while lying-to. Drifting towards the western limit of the Sound required repositioning on two occasions.

The transducer elements used in the ARTEMIS array consist of two unequal masses coupled by a spring with a magnetic driving force acting between the masses. The larger mass is in the form of a rigid box which completely encloses the smaller reaction mass. The reaction mass is supported inside the box by a system of springs. Acoustic projection is accomplished at both the front and back outside surfaces

CONFIDENTIAL

of the outer mass. However, the resonant reflectors previously described suppress radiation to the rear of the elements. To measure displacement amplitude and phase of an element, an accelerometer having a threaded stud was screwed into a tapped hole in the center of the front radiating face. Thus, the displacements measured were those of the outer or radiating mass. One special element was constructed with internal accelerometers such that the acceleration of both the inner and outer masses could be measured. Displacement of the rear surface of the resonant reflector tubes was measured at a number of locations by attaching accelerometers to special bosses which had been cemented to the tubes. The close spacing of the tubes to the elements prevented measurements on the front side of the tubes. The results of the measurements on the reflector tubes therefore represent the total motion of the rear face and does not necessarily provide a measure of the compression of the tube. In a similar manner, displacements were measured at a few locations on the component tanks and junction box. All accelerometers were calibrated in terms of displacement for sinusoidal motion over the frequency range of interest.

The operating procedure consisted of attaching the accelerometers in one set of positions, installing branch current sensors in one selected module, replacing one pre-selected element with the especially instrumented element and then lowering the array to operating depth. The sensor outputs were then measured as the array was driven for a number of frequencies over the range from 350 to 450 cycles per second. In one experiment the frequency range was extended to 250 and 600 cycles per second. The accelerometer and current sensor amplitude data were automatically recorded in digital form. All other data including displacement phase and current phase; input power, current, and voltage; hydrophone outputs; and frequency were manually recorded. At the completion of an experiment, the array was raised and the sensors repositioned.

Acoustic intensity was measured by a hydrophone suspended 34 feet in front of the array on a collapsible boom. As this range is too short to represent a far field measurement, these data were used only to indicate consistent performance from run to run and were not accepted as a quantitative measure of acoustic performance. In one experiment, a weighted hydrophone was suspended from a small boat at a range of approximately sixty yards. The range was measured acoustically for each intensity measurement. The hydrophone was moved in azimuth and

CONFIDENTIAL

depth until a maximum response indicated a position on the acoustic axis. At this position acoustic intensity and range were measured and the bearing of the small boat was noted by means of a transit on the deck of the source ship. The small boat was then repositioned to a new bearing and measurements repeated. In this manner an approximate directivity pattern as well as an accurate measure of acoustic intensity on the acoustic axis were obtained. All acoustic measurements were made using short pulses in order to avoid surface reflected path interference. These acoustic data were obtained with the center of the array submerged to a depth of 150 feet whereas all other data were taken with the array at a center depth of 400 feet.

A dc polarizing current of approximately ten amperes per element was used in all experiments. All the data in these experiments were obtained with an ac input to the transducer of 15 amperes with the exception of impedance measurements made in air and one run in which the voltage input to the amplifier was held constant. The constant current and constant voltage data are treated separately.

RESULTS

A. Impedance Measurements

The impedance of the submerged array was computed from the measured values of input current voltage and power. Meters of the portable standards type were used to measure these quantities. Figure 3 illustrates the impedance characteristics of the fifteen module array over the frequency range of 250 to 600 cycles per second. The impedance values shown are those measured at the input to the underwater cable supplying driving signal to the paralleled primaries of three identical transformers located in the underwater component tanks. Each transformer has five secondary windings each of which is connected to a transducer module through tuning and blocking capacitors. Thus, each of the fifteen transducer modules is energized from a separate secondary winding. The turns ratio between the primary winding and each of the secondary windings is 4.125 to 1. Each module is tuned with a 13.2 microfarad series capacitor. It can be seen from figure 3 that the maximum resistive component of impedance is 42.7 ohms. Considering the transformer turns ratio, this represents a single module resistance of 36 ohms. Previous

CONFIDENTIAL

tests with a two module array indicated a maximum resistive component of approximately twice this value for each module. The decreased module resistance in the enlarged array is indicative of better acoustic loading.

Figure 4 is a vector impedance locus plot for the fifteen module array. Resonance appears at approximately 422 cycles per second.

Prior to the underwater tests, the impedance of the five modules in the top row was measured in air. Time did not permit these measurements to be made on the entire array. The vector impedance locus diagram obtained from measurements in air is shown in figure 5. The signal current was held constant at 0.3 amperes at all frequencies except those between 461.9 and 470.2 cycles per second where it was reduced to 0.2 amperes. The small power amplifier used for these tests was not capable of supplying 0.3 amperes at all frequencies. Resonance appears at approximately 465 cycles per second. The maximum value of the resistive component of impedance agrees closely with the value obtained from previous measurements on a two module array when the shunting effect of the transformer primary reactance is considered. The coupling transformers have a primary reactance of approximately 40,000 ohms, being designed for use with a transducer having a water load. The higher impedance of the transducer when operating in air requires that the shunting effect of the primary reactance be taken into consideration.

B. Acoustic Measurements

A limited amount of acoustic response data was obtained. This was accomplished by suspending a hydrophone from a small boat in the region of the acoustic axis of the source. The output of the hydrophone was observed on a calibrated battery operated oscilloscope. The source was programmed for 50 millisecond pulses at twelve second intervals. Free field measurements were obtained by noting the amplitude of the received signal after the signal level had reached a steady value and before the first surface reflection. The small boat was tethered by lines to the bow and stern of the source ship and held at a range of approximately sixty yards. A wire connection was made between the small boat and the source ship to enable an acoustic range measurement.

The hydrophone was moved vertically and in azimuth until a maximum signal response was obtained. This point was assumed to be the acoustic

CONFIDENTIAL

axis of the source. The bearing of the small boat relative to the source ship was then measured and an acoustic range obtained. Response measurements were made at five frequencies in this position. The results are plotted in figure 6. For the five frequencies at which measurements were made, the maximum response occurred at 420 cycles per second. Time and sea conditions prevented more extensive measurements.

After measuring the response at the position yielding the maximum signal, the small boat was moved in azimuth to positions six, eleven, and fifteen degrees aft of the original location. Measurements at these positions yielded the directivity pattern illustrated in figure 7. This pattern is probably not precise since the starting point might not have been exactly on the acoustic axis and there is no assurance that the hydrophone traveled through the same arc as the supporting boat.

C. Displacement Amplitude

The drawing in figure 8 represents the positions of the elements and modules in the fifteen module array. The modules are numbered from six through twenty as shown. To identify any element position, a three part number is used. The first number identifies the module in which a position is located. The second number represents the row within that module with rows being numbered from one through twelve starting at the top. The third number represents column with the columns in each module being numbered from one through six starting at the left. Thus, element position number 7-1-1 is located in the upper lefthand corner of module seven. The positions marked with an "X" are those in which an external accelerometer had been attached to the element. They are the only positions in which element displacement data was obtained in this experiment. The positions in which the accelerations of the squashed tube reflectors were measured are similarly marked in figure 9. The accelerometers were attached to the center of the back face of the tubes directly behind the element position marked with an "X".

Figures 10 through 18 illustrate the manner in which the element displacement varied in two rows and one column. Row "18" is composed of the sixth row of elements in modules 11, 12 and 13. It lies along the horizontal center line of the left half of the array. Column "15" which is composed of the third column of module eight and part of the third column of module 13 lies along the vertical center line of the top half of the array. Row "1" is the uppermost row of elements in modules six, seven and eight. The positions in the array of these rows and columns can be seen

CONFIDENTIAL

in figure 8. Although data was obtained at each five cycle increment of frequency from 350 to 460 and at 2-1/2 cycle increments from 490 to 450 cycles per second, only 1-1/2 cycle increments from 400 to 440 cycles per second are shown here. It can be seen that large and random variations existed. This was true for all frequencies at which measurements were made. The incidence of exceptionally large amplitudes does have a marked frequency dependence, however. The frequency distribution of element displacement is illustrated in figure 19. The curve in the lower part of this figure represents the displacements required of a fully loaded and uniformly vibrating transducer to produce the same acoustic power as the actual transducer. From this curve it can be seen that ideally the transducer displacement should be approximately 0.15 thousandths of an inch peak to peak from 380 to 440 cycles per second, dropping to somewhat lower values above and below these frequencies.

The bar graphs in figure 19 indicate the number of sampled elements which displayed displacements equal to or greater than the values indicated above each graph. It is apparent that frequencies between approximately 375 and 460 cycles per second produce the most erratic behavior. The elements of this array resonate at approximately 450 cycles per second in the unloaded condition. The unusually high displacements apparently represent elements in various degrees of unloading.

The frequency dependence of displacement for four individual elements can be examined in figures 20 through 23. In general, several sharp peaks and nulls occur as frequency is varied with current maintained at a constant value. Element position 0-1 was sampled twice and the results of both instances are plotted in figure 20. This position is in the upper left-hand corner of the array. The results of the repeated measurements show reasonable agreement in general form. Element position 0-0-3, which is examined in figure 21, is in the center of the array. Despite efforts to do so, no recognizable pattern of displacement distribution could be found.

The frequency distribution of smallest measured displacements is shown in figure 24. In general, the smallest measured displacements were larger than measured displacements. No marked frequency dependence is evident in this case as it was in figure 19. The corresponding representation of element displacement. It is significant, however, that no measured displacements exceeding 1.5 mils were found at 402.5 and 405 cycles per second. These frequencies are also favorable in the element displacement distribution. These frequencies therefore represent the

CONFIDENTIAL

safest operating region for the array in its present condition. Four sample plots of squashed tube displacement as a function of frequency are shown in figures 24 through 28. Typically, these show many displacement peaks and nulls.

D. Displacement Phase

The phase of the elements in rows and columns is illustrated in figures 29 through 37. These elements are the same as those for which the displacements were depicted in figures 10 through 18. In a number of positions no value of phase angle is shown. In most cases, data was not obtained for these positions because the signal level from the accelerometers was very low due to small displacement amplitude, and phase jitter caused by noise made readings uncertain. As in the case of displacement amplitude, no spacial pattern of phase angle could be ascertained. Also, no strong correlation between phase angle and displacement amplitude could be found. By averaging the phase angles of all sampled elements at each frequency, the curve shown in figure 38 was obtained. These phase angles were measured with respect to the amplifier input voltage. At the bottom of figure 38, the average deviation from the mean phase angle is shown. Note that the deviation reaches a maximum at 450 cycles per second which is the resonant frequency of the elements in the unloaded condition. A sharp dip in the mean phase angle also occurs at that frequency. This would indicate that some of the elements are unloaded and therefore are experiencing large displacement amplitudes and impedances which are changing rapidly with frequency at the frequency of unloaded resonance. Figures 39 and 40 exemplify the manner in which the displacement phases of individual elements vary with frequency. Typically, these curves differ considerably at frequencies higher than the loaded resonant frequency.

E. Equivalent Loading

Previous tests with a two module array, on which the pressure release tubes had been removed, revealed an equivalent loading of 0.1 rho c. Equivalent loading was determined in the following manner. A root-mean-square value of displacement amplitude was computed for all sampled elements at each operating frequency. These values were compared with the values of displacement required of an equivalent uniform velocity transducer producing the same acoustic source levels.

CONFIDENTIAL

In the case of the two-module array, an acoustic loading of 0.1 rho c would have produced approximately the same source levels as the actual array. The same procedure was followed to find the equivalent loading of the 15 module array. The results are shown in figure 41. In this case it can be seen that the equivalent loading is not constant for all frequencies. However, an average value is approximately 0.4 rho c.

The two module array differed from the larger array in that it was not equipped with acoustic pressure release tubes and therefore was loaded on both the front and back faces. For this reason the loading effects on the two arrays cannot be directly compared. However, if it is considered that the only effect of the double loading on the smaller array was to double the radiating area, and the two arrays are compared on the basis of this assumption, then the larger array appears to be more fully loaded both from the standpoint of electrical impedance and mechanical displacement.

F. Especially Instrumented Element

The especially instrumented transducer element, having internally mounted accelerometers on both the inner and outer masses, was re-positioned to three locations in the array. In addition to the two internal accelerometers, a third accelerometer was attached externally in the tapped hole provided in the center of the radiating face. Since the mass ratio of outer to inner mass is 1.5 to 1.0, and the water loading is applied to the outer mass, it would be expected that the inner mass would have a considerably larger displacement amplitude than the outer mass. Also, if the transducer element experienced pure rectilinear motion, the two accelerometers attached to the outer mass should exhibit identical displacements in both amplitude and phase. The relative displacement phase of the inner and outer masses for the unloaded condition should be approximately 180 degrees. Water loading would cause the relative phase to depart from this value. Unity rho CA loading should result in a phase angle of approximately 135 degrees, varying only slightly with frequency over the frequency range of interest. In this report the three accelerometers on the special transducer element are referred to as "inner", "outer" and "external". The first two designations refer to the internally mounted accelerometers on the inner and outer mass respectively, and the last designation refers to the externally mounted unit. One internal accelerometer is mounted in a corner of the outer mass and the other is mounted on an edge of the inner mass.

CONFIDENTIAL

Figures 42, 43 and 44 illustrate the displacements of the special transducer element measured at positions 6-1-1, 13-6-3 and 8-11-3 respectively. It can be seen that the displacement ratio of the outer and inner masses is far from constant and the outer mass, in some frequency regions, has the larger amplitude. This might be explained, at least in part, by the interaction effects with the other elements of the array. At some frequencies, the special transducer could be driven by the acoustic field and would be absorbing energy. The displacements measured by the two accelerometers on the outer mass differ widely indicating a departure from rectilinear motion since these two accelerometers do not measure displacement at the same part of the radiating area. Figures 45, 46 and 47 show the corresponding phase angles for the special element accelerometers in the three array positions. The phase angles of the inner and external displacements are shown relative to the outer displacement. The phase of the externally measured displacement is generally within 90 degrees of the internally measured displacement. The phase of the inner mass takes on all possible values. The cause of this anomaly is not clearly understood.

G. Alternating Current Measurements

The current sensors, which measure the alternating current in the series connected rows of elements within a module, were used to measure the current into each row of module number six in one experiment and into each row of module number 13 in another experiment. The current is plotted as a function of row number with frequency as a parameter in figures 48 and 49. There are well-formed patterns which progress smoothly as frequency is increased. Since an identical driving voltage is applied to all rows within a module, the current variations must be the result of impedance differences among the rows. The close manufacturing tolerances on the individual elements would not permit variations of this magnitude among the individual elements due to their inherent characteristics. It is most probable, therefore, that the impedance differences are caused by acoustic interaction effects among the elements which cause non-uniform loading of the elements depending on their positions in the array and the wave length of the sound waves in water. Additional indications of this nature are evidenced by the module current data. Current sensors located in the underwater component tanks measured the alternating current into each of the fifteen modules. The results of these measurements for

CONFIDENTIAL

one experiment are plotted in figure 50. In this illustration, each curve is a plot of the module current in a row of five modules. Curves for the three rows are grouped vertically. Frequency progresses from left to right in three lines. For most frequencies within the pass band, the current is a maximum in the center module and decreases more or less symmetrically toward each side of the array. In general, the current distribution in the top and bottom rows of modules differs considerably. This might be caused by lack of mechanical symmetry of the array structure in the vertical direction. The oil-filled component tanks and junction boxes are located at the base of the structure behind the bottom row of modules, and the nitrogen bottles are mounted near the top of the structure just above and to the rear of the top row of modules.

H Waveforms

Figures 51 through 54 exemplify the waveforms existing in various circuits during this set of experiments. Figures 51 through 53 show for three frequencies the waveforms experienced with pulsed operation for the total transducer current, accelerometer output, and monitor hydrophone voltage. Figure 54 illustrates the waveform of the input signal to the amplifier. The left side of each illustration shows the waveform when the input signal is passed through a 350 to 450 cycle per second band-pass filter. The right side shows the waveform when no filter is used. Pulsed operation, as illustrated here, was used only in the experiment in which acoustic response was obtained. In all other experiments a steady state signal was used. The photograph of component tank acceleration waveform was obtained from the output of an accelerometer attached to a vertical surface of the pressure compensation tank atop one of the component tanks. During the course of these experiments several accelerometers were attached at various positions on the component tanks and junction boxes. These measurements indicated only very small amplitude of vibration with the exception of the position illustrated. At some frequencies, this position experienced vibration amplitudes as high as the transducer amplitude.

I. Constant Voltage Drive

All of the preceding data, with the exception of air impedance, was obtained with a constant current input to the amplifier of 15 amperes. One additional run was made in order to obtain system response data.

CONFIDENTIAL

In this run the voltage input to the driving amplifier was held constant. The input voltage was adjusted to a value such that the current did not exceed 15 amperes at any frequency in the band from 350 to 450 cycles per second. Figure 55 illustrates the amplitude and phase of the current into the transducer. The phase is referenced to signal voltage input to the amplifier. If a linear response with respect to input current is assumed, the voltage response of the system can be computed making use of the measured current response which is plotted in figure 6. The resulting system voltage response is shown in figure 56. The phase of the acoustic pressure at the face of the transducer can be measured in either of two ways. One method utilizes the measured phase of the accelerometer outputs. Since the pressure is in phase with displacement and displacement is 180 degrees out of phase with the acceleration, the accelerometer output voltage is 180 degrees out of phase with the pressure at the face of the transducer. The preamplifier used with the accelerometers reversed the signal phase such that displacement or pressure phase was measured directly. The pressure phase, as obtained by this method, relative to the input signal voltage, is plotted in figure 57. To obtain this curve, the phase of 23 accelerometers was averaged. These accelerometers were located principally on elements in the upper left hand section of the array as shown in figure 58. A measure of the pressure phase can also be obtained from the output of the monitoring hydrophone. This hydrophone was located on the acoustic axis 34-1/3 feet in front of the center of the face of the array. Phase measurements obtained with this hydrophone, when referred to the face of the array, yield results which are similar to those obtained from the accelerometer outputs with the exception that they are displaced by approximately 100 degrees leading. Since the hydrophone range is insufficient for far-field measurements, the data obtained by this method are not considered as reliable as those obtained with the accelerometers. On the other hand, no phase data can be very meaningful considering the widely varying phase distribution over the face of the array.

CONCLUSIONS

Tests with the 15 module ARTEMIS source have indicated probable improved acoustic loading as compared with initial tests with a two module array. The improved loading is evidenced by both a reduction in the electrical impedance and by a higher ratio of radiated power to transducer displacement. However, a fundamental difference in the mode of operation restricts a direct comparison of the two arrays.

CONFIDENTIAL

The current response at 420 cycles per second was measured at 103.1 decibels relative to one dyne/cm²/ampere at one yard, and there is evidence that the directivity pattern is similar to that which would be predicted for an idealized array.

The velocity distribution over the face of the array, while less erratic than in the two module array, drastically restricts the permissible power level. The designed maximum displacement limitation of the transducer elements and the element in the array having maximum displacement determine the upper limit of electrical power input. Since the incidence of abnormally high element velocity is related to frequency, the allowable power level is greater at some frequencies than at others. A small frequency range in the vicinity of 405 cycles per second is the most favorable from the standpoint of maximum permissible power output.

The variation in acoustic loading, as manifested by aberrations of relative electrical impedance among rows of elements and from module to module, supports the theory that the velocity anomalies are caused by acoustic interaction effects. Operation at high power levels is contingent on discovery of a practical means of minimizing the effects of acoustic interactions among elements of the array.

The current variation between the electrically parallel connected rows of elements and parallel connected modules provide further evidence that electrical parallel connection of all elements as opposed to the present series-parallel connection will lead to reduced velocity anomalies. This, as well as other means of reducing the interaction effect, will be investigated.

CONFIDENTIAL

LIST OF ILLUSTRATIONS

<u>Title</u>	<u>Figure Number</u>
Photograph of array with 15 modules	1
Dead-reckoning tracks for operations in Exuma Sound	2
Transducer impedance characteristics	3
Vector impedance locus diagram for submerged transducer	4
Vector impedance locus diagram for transducer in air - one row of modules	5
Current response - 15 module array	6
Horizontal directivity pattern - 15 module array	7
Element and module positions in the 15 module array. The crosses indicate those elements to which accelerometers had been attached.	8
Front view of array with crosses indicating locations in which accelerometers had been attached to squashed tube reflectors	9
Amplitude of transducer element displacement	
400 cps	10
405 cps	11
410 cps	12
415 cps	13
420 cps	14
425 cps	15
430 cps	16
435 cps	17
440 cps	18
Frequency distribution of transducer element displacement	19
Transducer element displacement	
6-1-1	20
13-6-3	21
6-9-1	22
11-6-1	23

CONFIDENTIAL

<u>Title</u>	<u>Figure Number</u>
Frequency distribution of squashed tube displacement	24
Squashed tube displacement amplitude	
6-1-1	25
13-6-3	26
6-9-1	27
11-6-1	28
Transducer element displacement phase relative to amplifier input voltage	
400 cps	29
405 cps	30
410 cps	31
415 cps	32
420 cps	33
425 cps	34
430 cps	35
435 cps	36
440 cps	37
Average characteristics of transducer element displacement phase	38
Frequency characteristics of transducer element displacement phase	39
Frequency characteristics of transducer element displacement phase	40
Transducer loading characteristics	41
Element displacement characteristics for especially instrumented element in position	
6-1-1	42
13-6-3	43
8-11-3	44
Phase characteristics for especially instrumented element in position:	
6-1-1	45
13-6-3	46
8-11-3	47
Phase is plotted relative to phase of internal sensor or outer mass.	

CONFIDENTIAL

<u>Title</u>	<u>Figure Number</u>
Current distribution for rows of elements in module number:	
6	48
13	49
Current distribution in the 15 modules of the transducer array	50
Typical waveforms for 30 millisecond pulses with and without a 100 cps bandpass filter in the signal input	51, 52, 53
Waveform of pulsed signal input to amplifier with and without a 100 cps bandpass filter	54
Transducer current amplitude and phase for operation with constant voltage input to amplifier	55
Relative response for constant voltage input to amplifier, normalized to value of voltage producing one ampere into transducer at 400 cps	56
Pressure phase at face of array relative to amplifier input voltage for constant voltage input	57
Location of accelerometers for constant voltage experiment	58

CONFIDENTIAL

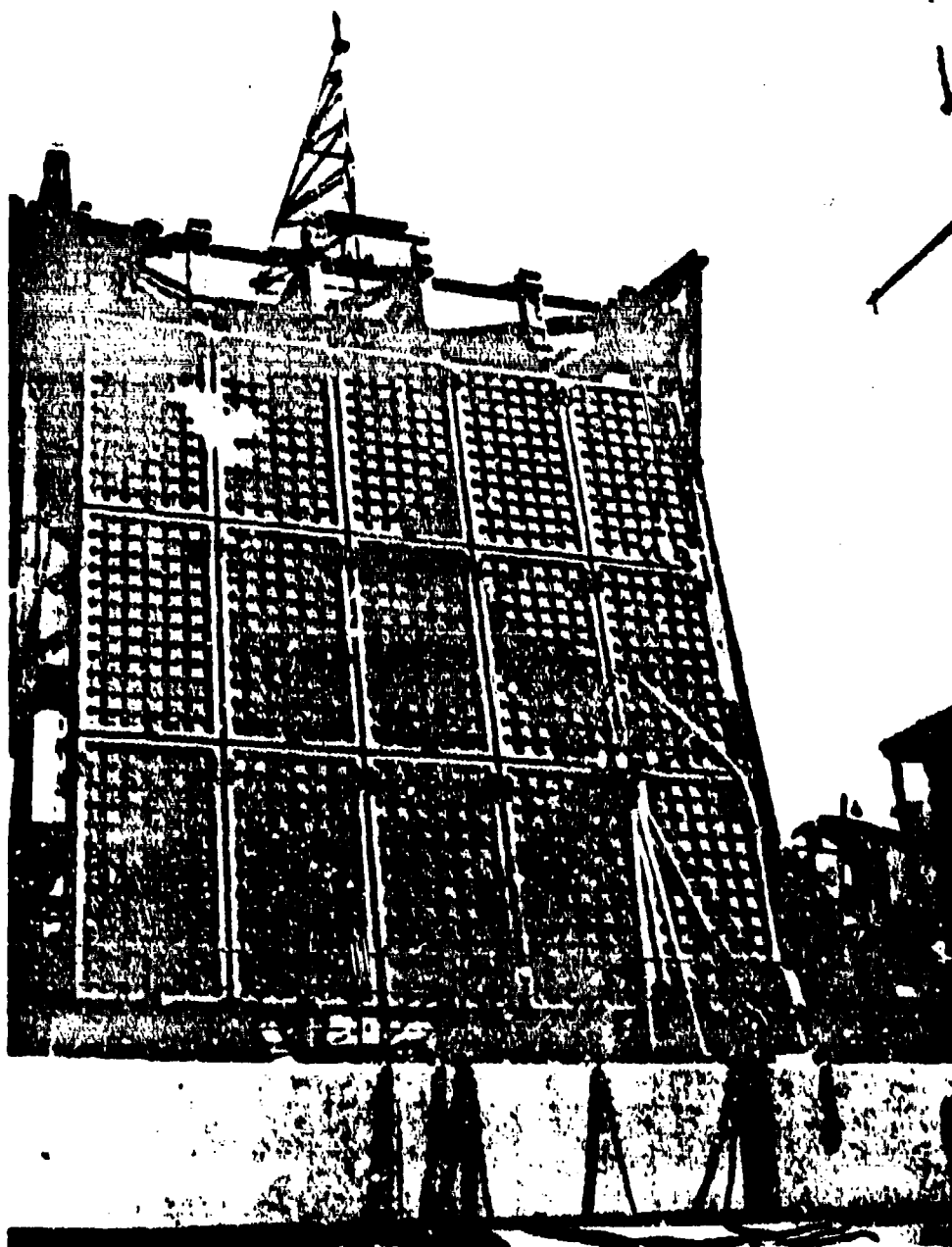


Figure 1 - Photograph of Array with 15 Modules

CONFIDENTIAL

CONFIDENTIAL

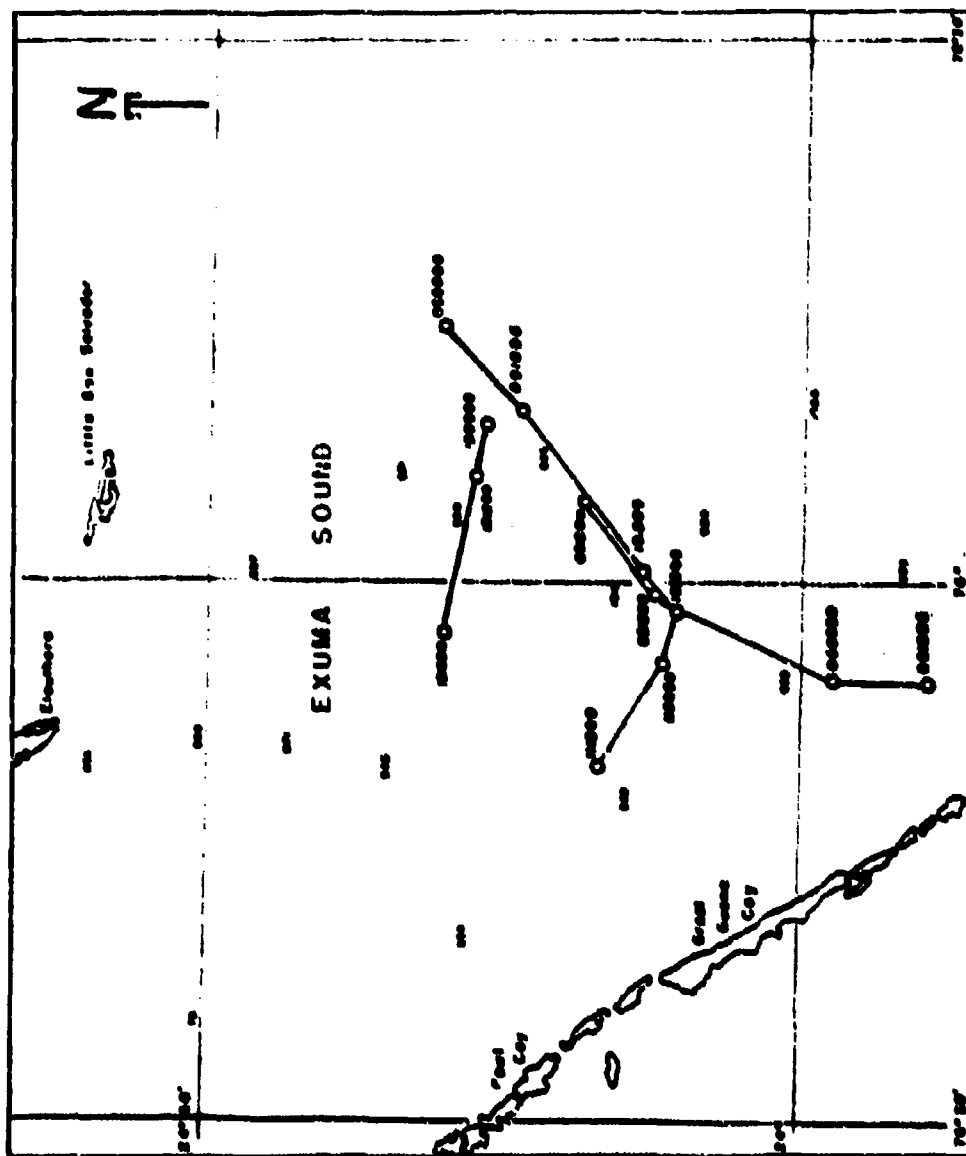


Figure 2 - Dead-reckoning Tracks for Operations in Exuma Sound

CONFIDENTIAL

CONFIDENTIAL

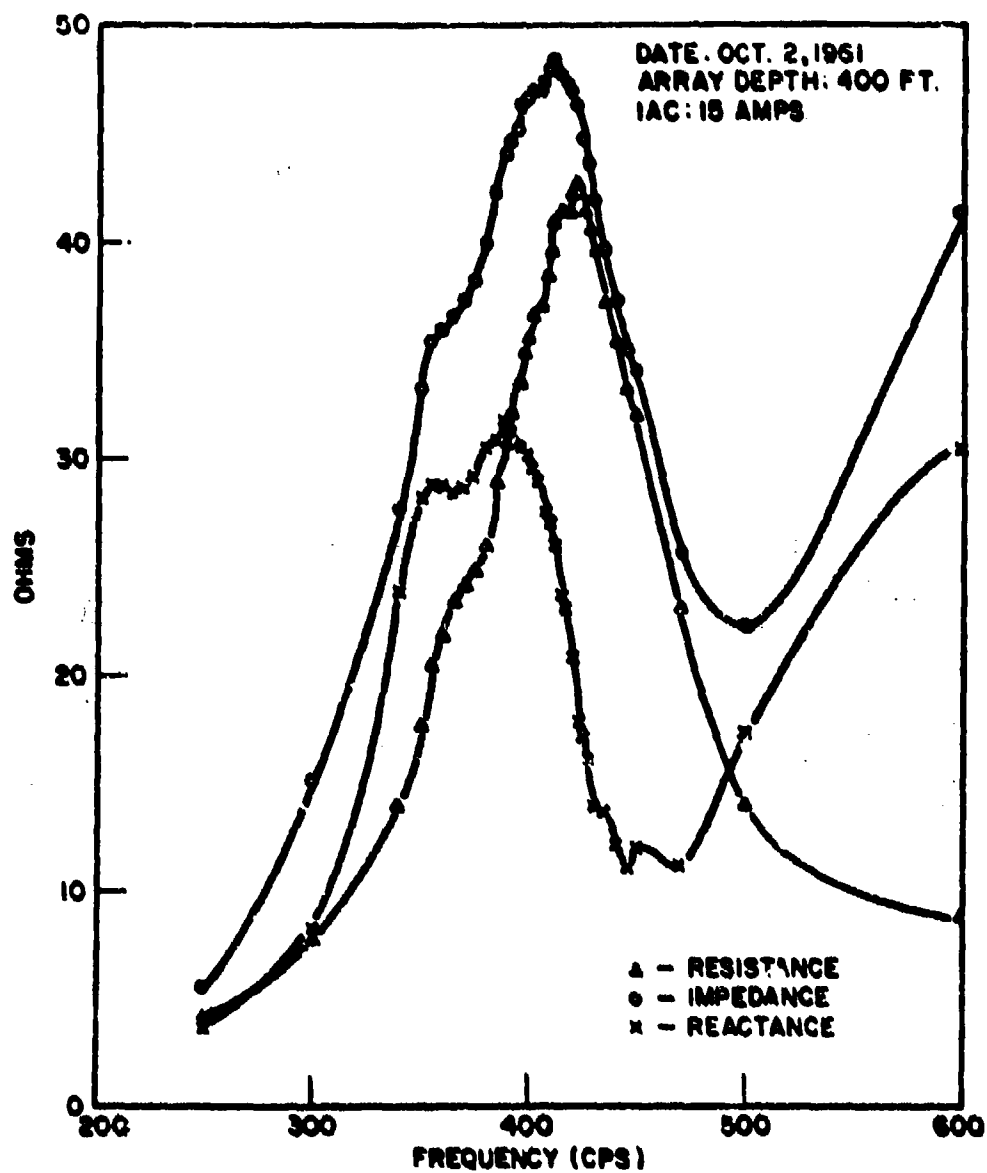


Figure 3 - Transducer Impedance Characteristics

CONFIDENTIAL

CONFIDENTIAL

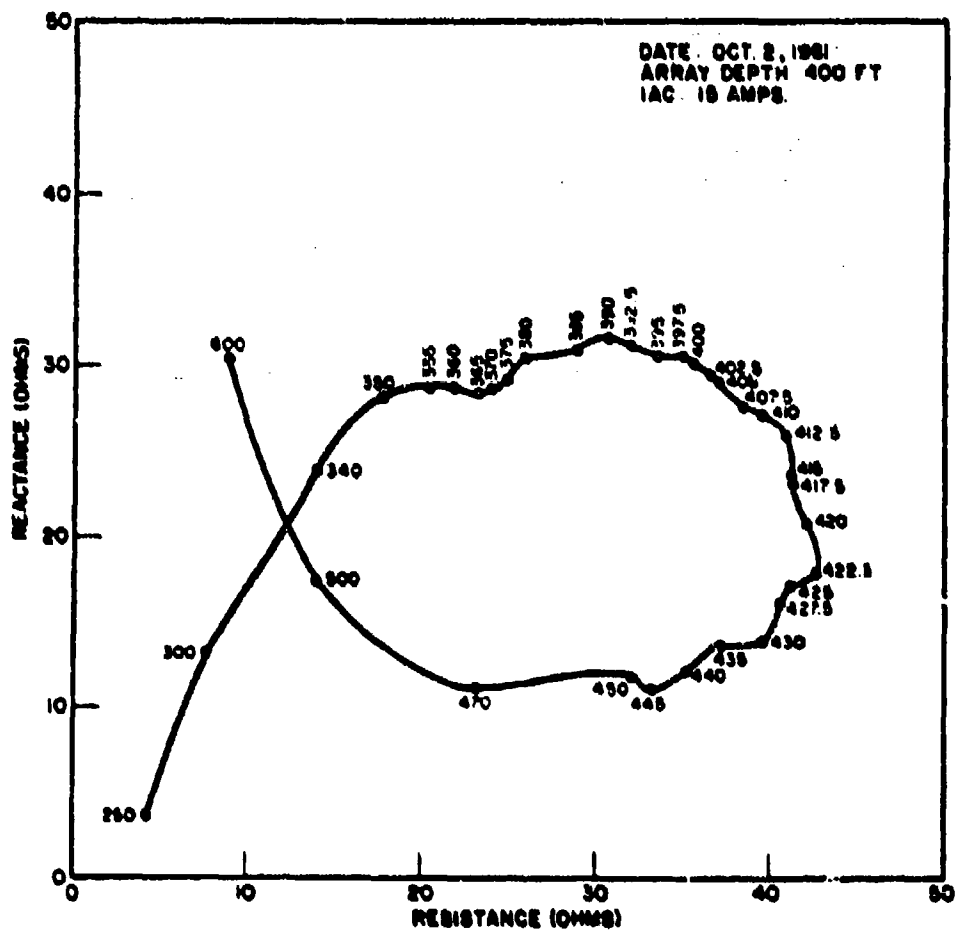


Figure 4 - Vector Impedance Locus Diagram for Submerged Transducer

CONFIDENTIAL

CONFIDENTIAL

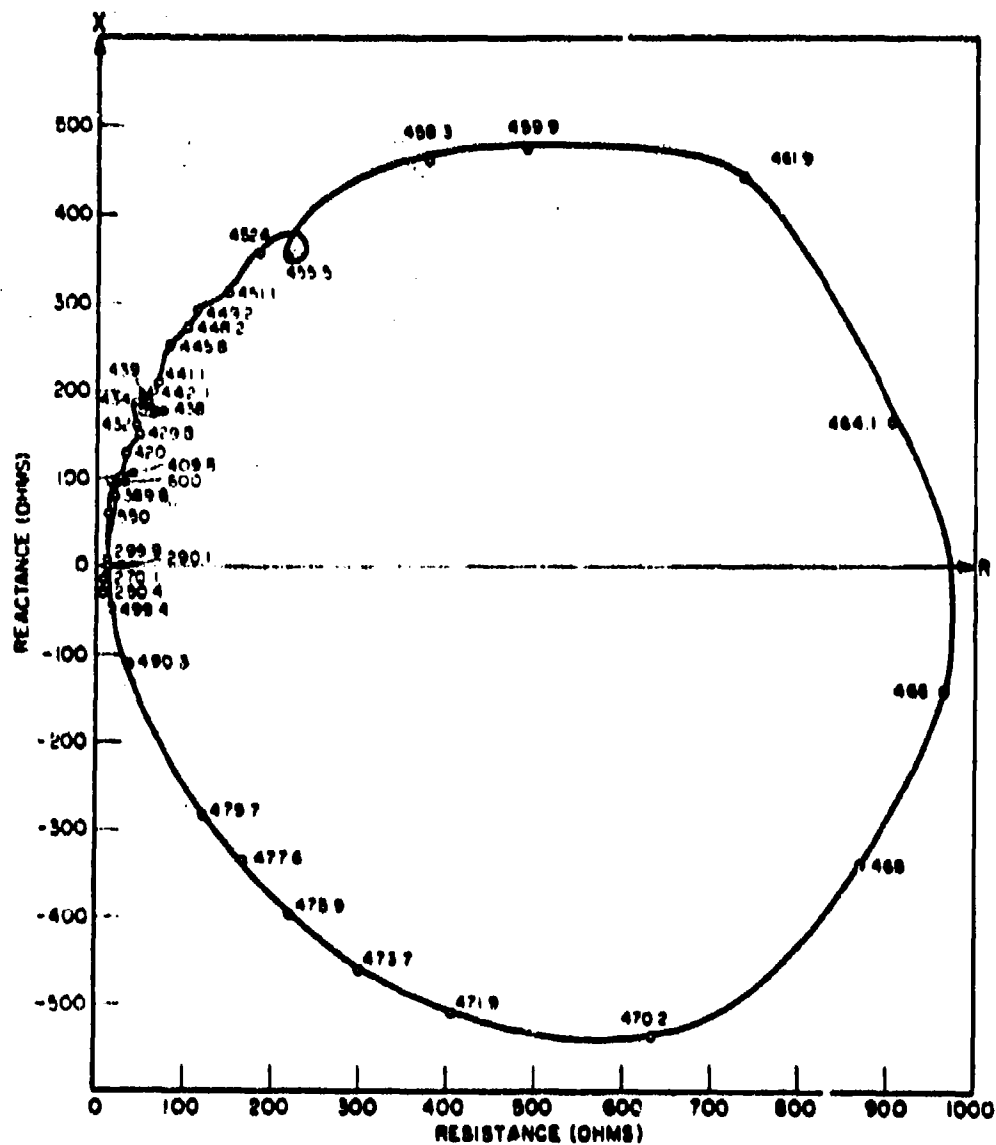


Figure 5 - Vector Impedance Locus Diagram for Transducer in Air-One Row of Modules

CONFIDENTIAL

CONFIDENTIAL

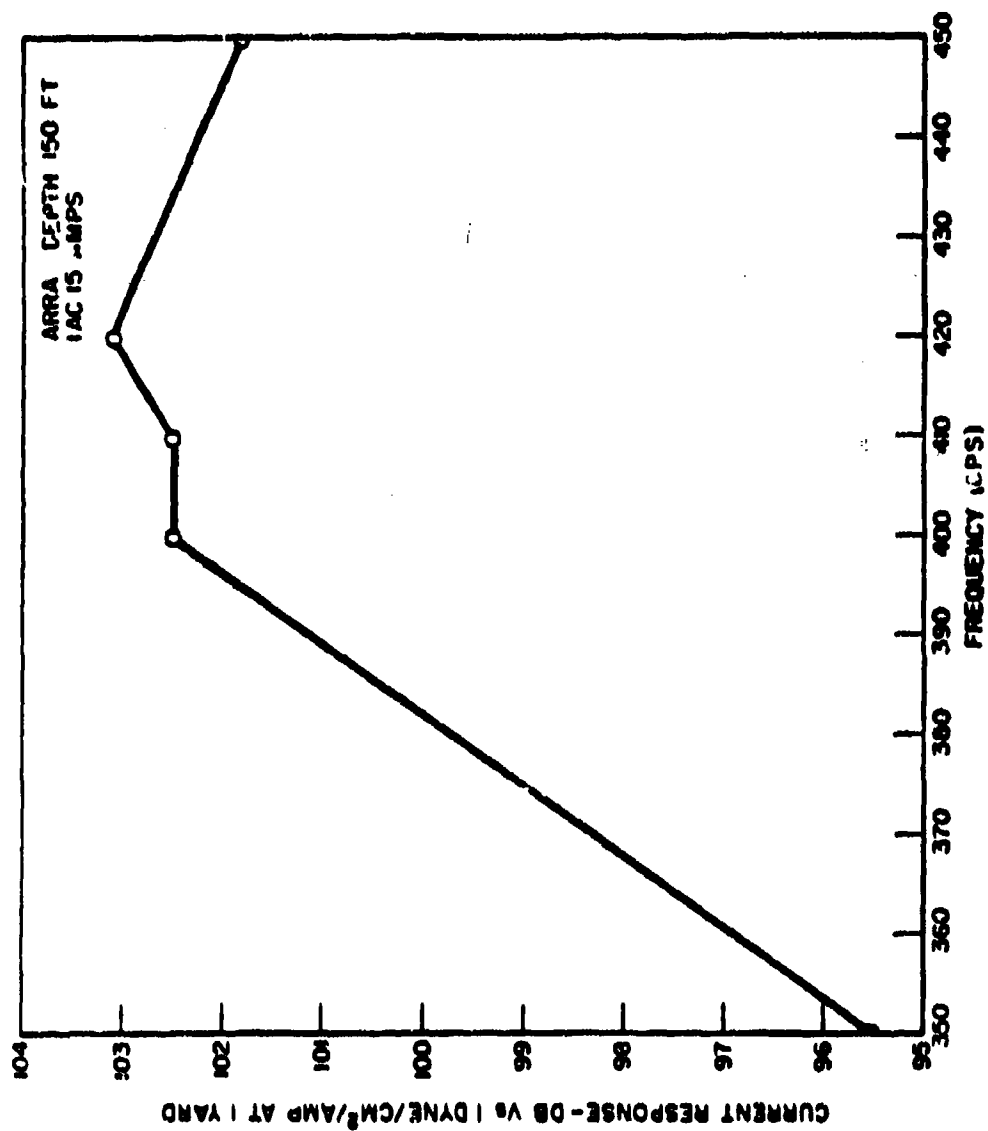


Figure 6 - Current Response - 15 Module Array

CONFIDENTIAL

CONFIDENTIAL

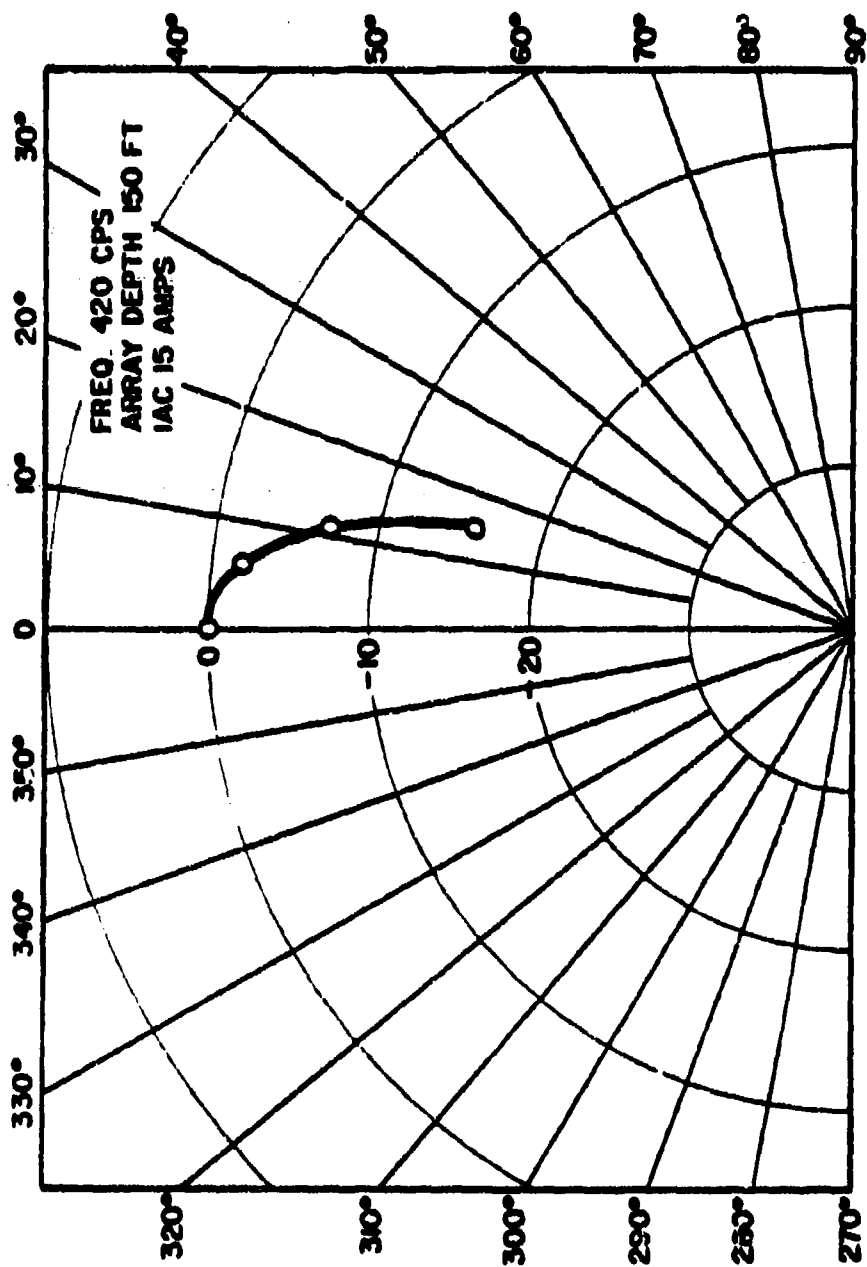
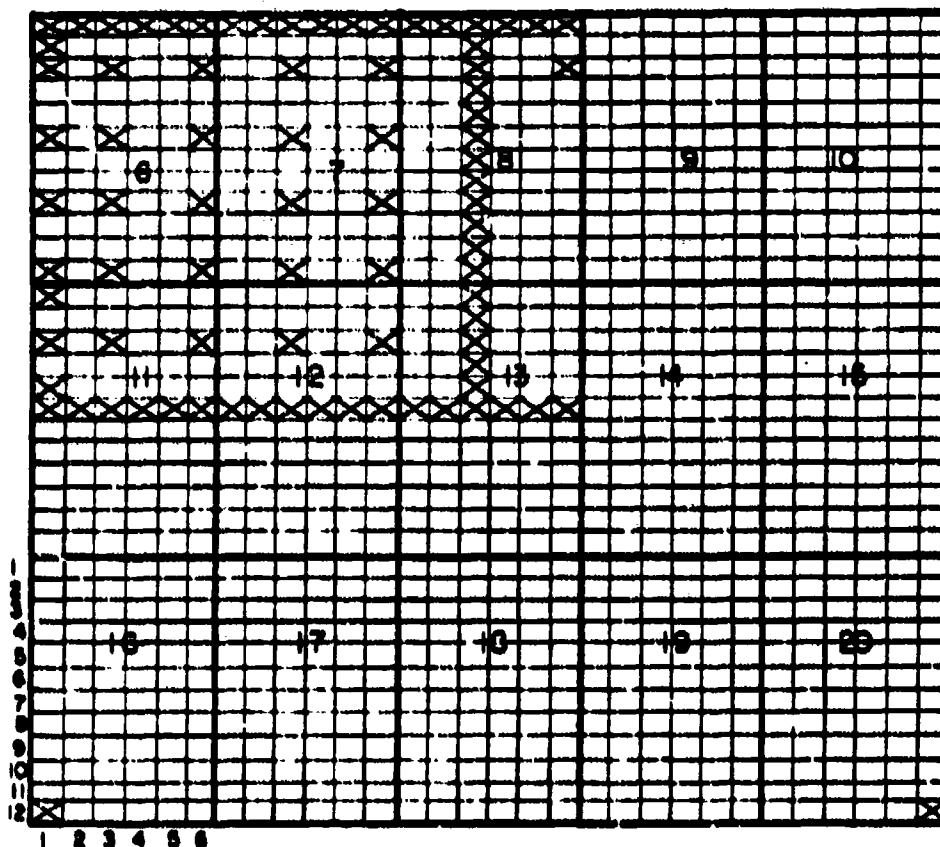


Figure 7 - Horizontal Directivity Pattern - 15 Module Array

CONFIDENTIAL

CONFIDENTIAL



CONFIDENTIAL

CONFIDENTIAL

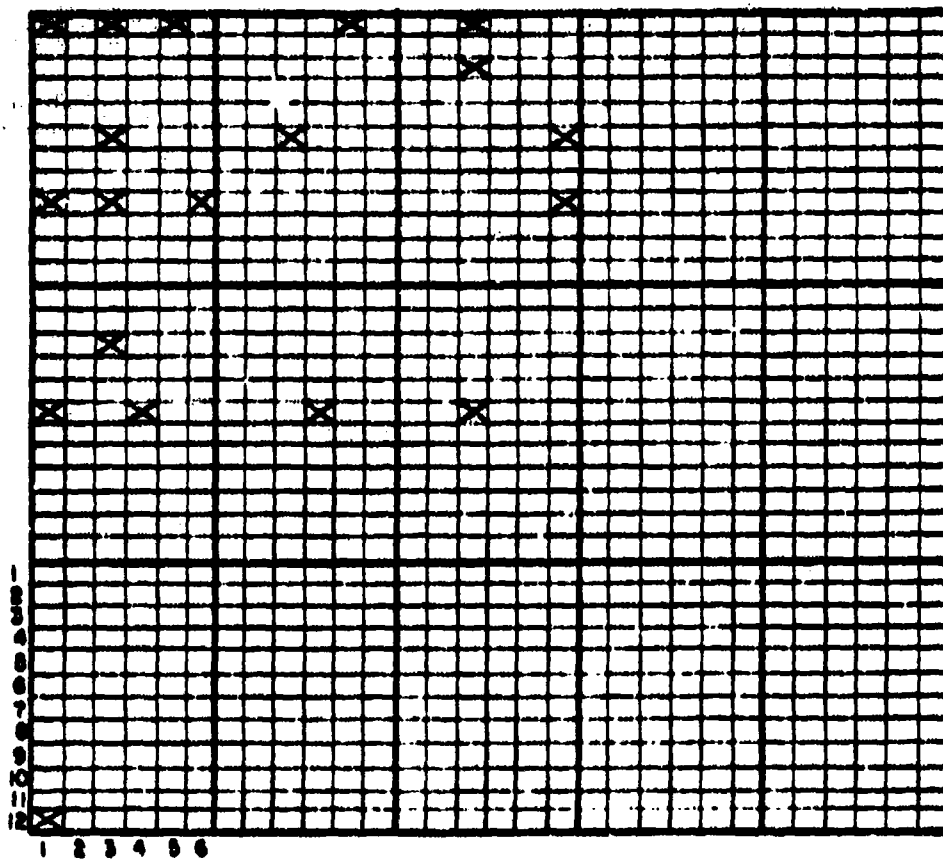


Figure 9 - Front View of Array with Crosses Indicating Locations in which Accelerometers had been Attached to Squashed Tube Reflectors

CONFIDENTIAL

CONFIDENTIAL

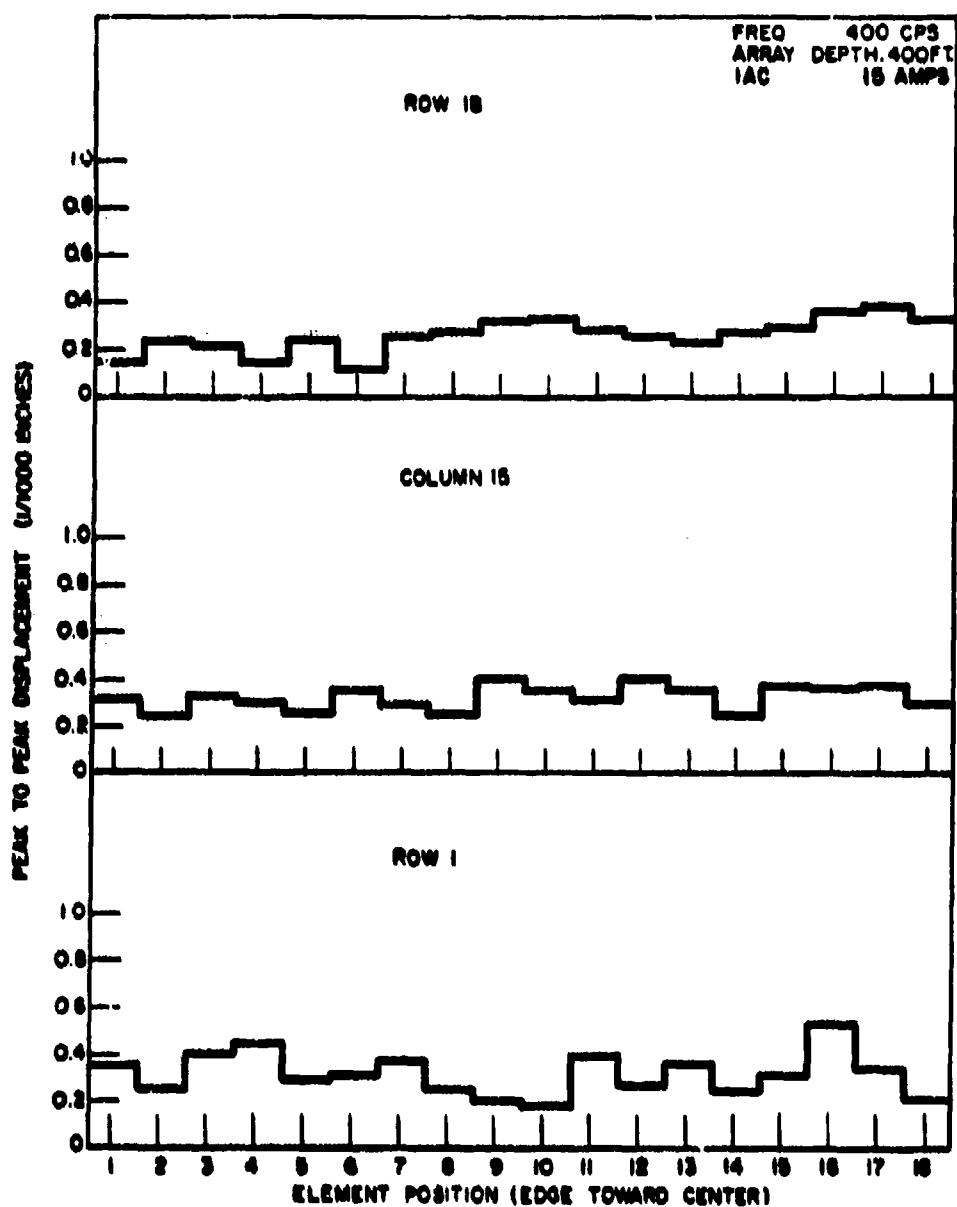


Figure 10 - Amplitude of Transducer Element Displacement

CONFIDENTIAL

CONFIDENTIAL

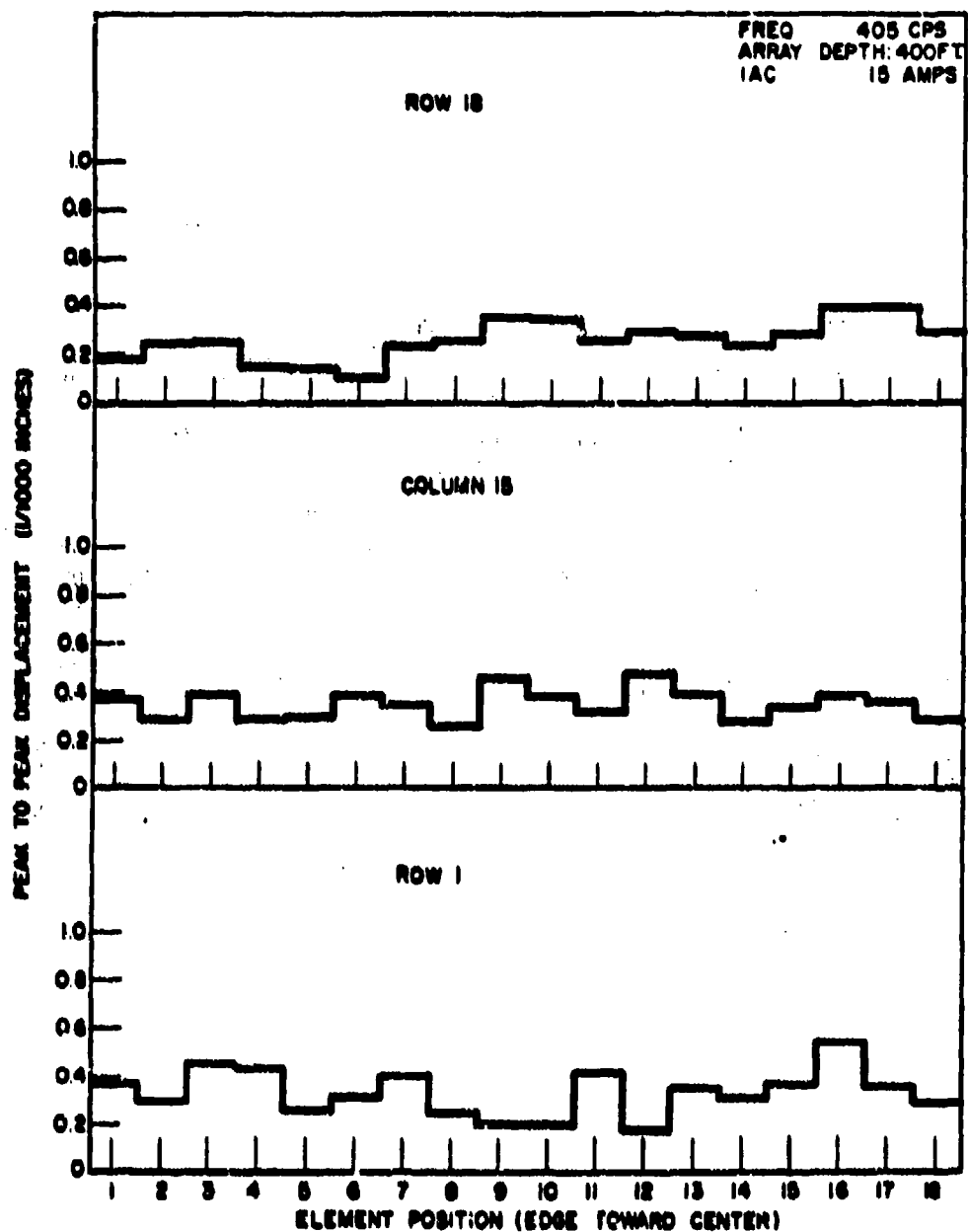


Figure 11 - Amplitude of Transducer Element Displacement

CONFIDENTIAL

CONFIDENTIAL

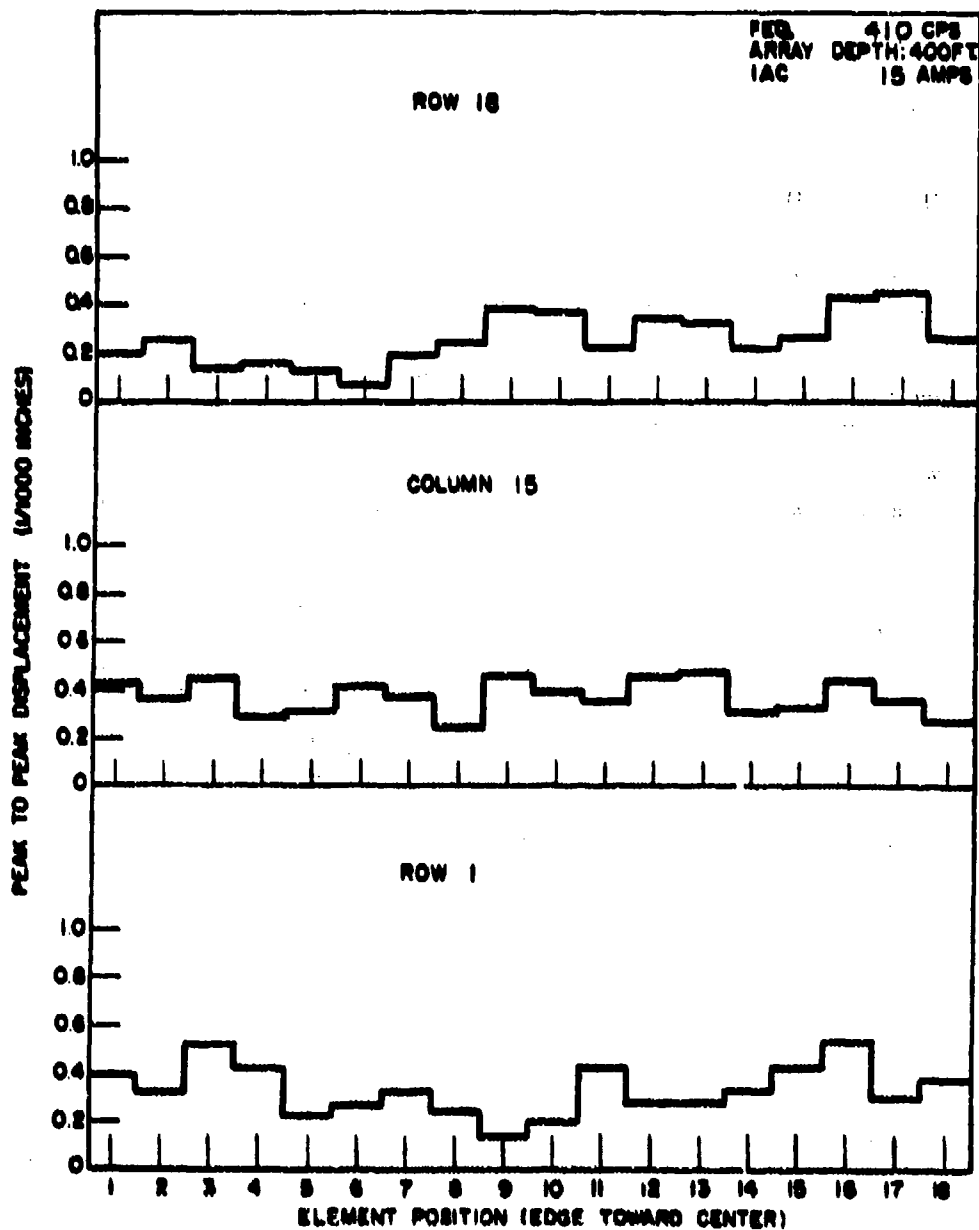


Figure 12 - Amplitude of Transducer Element Displacement

CONFIDENTIAL

CONFIDENTIAL

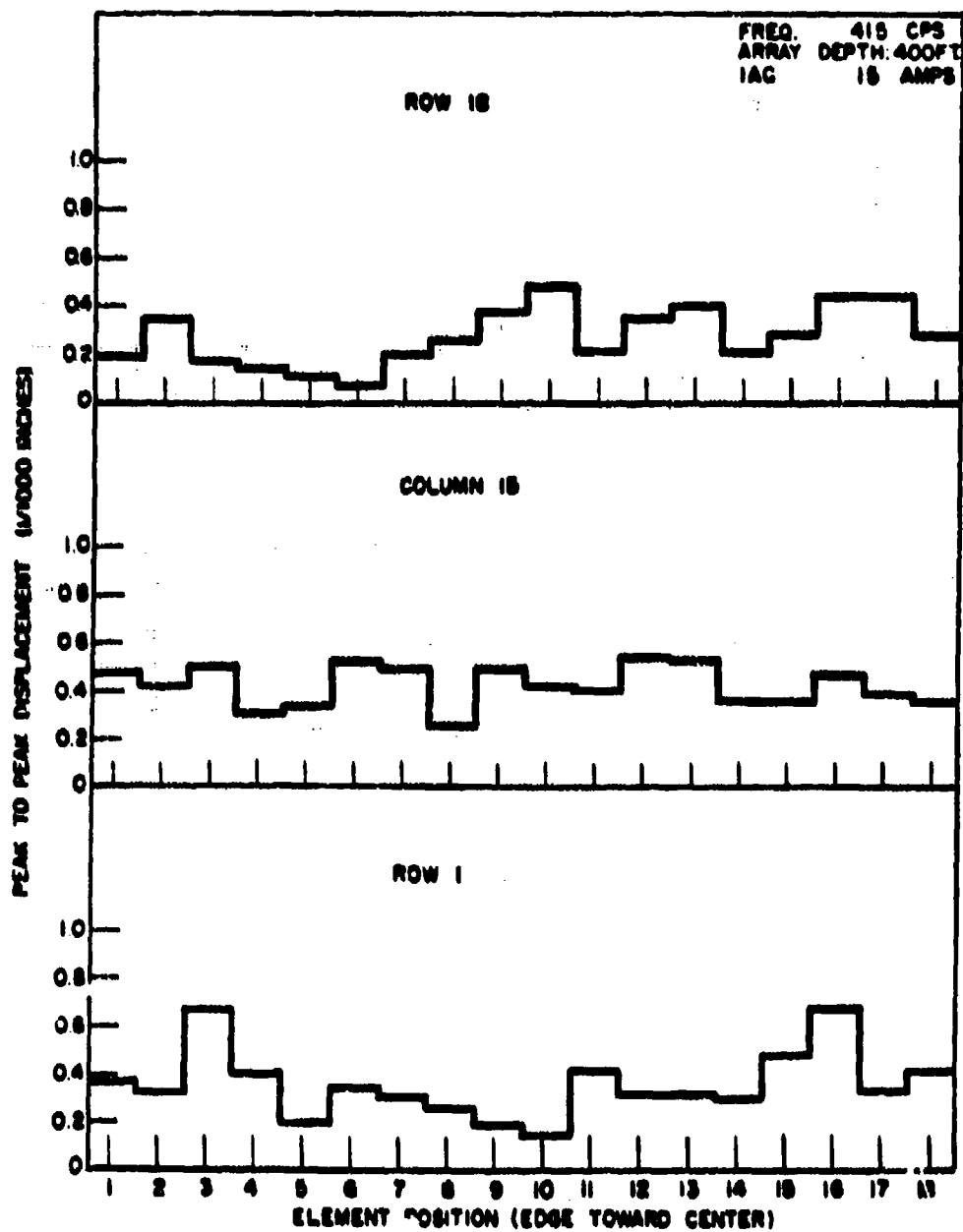


Figure 13 - Amplitude of Transducer Element Displacement

CONFIDENTIAL

CONFIDENTIAL

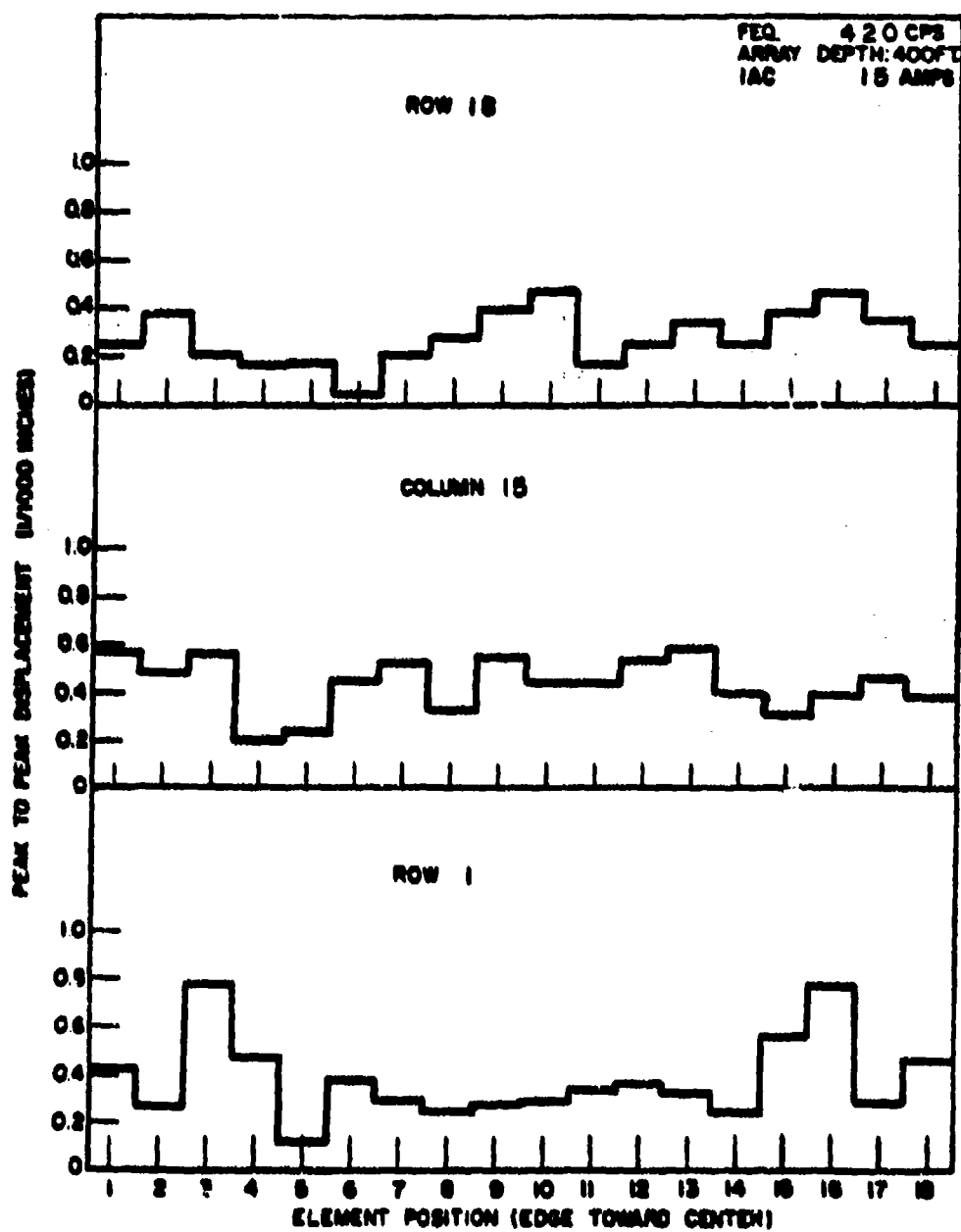


Figure 14 - Amplitude of Transducer Element Displacement

CONFIDENTIAL

CONFIDENTIAL

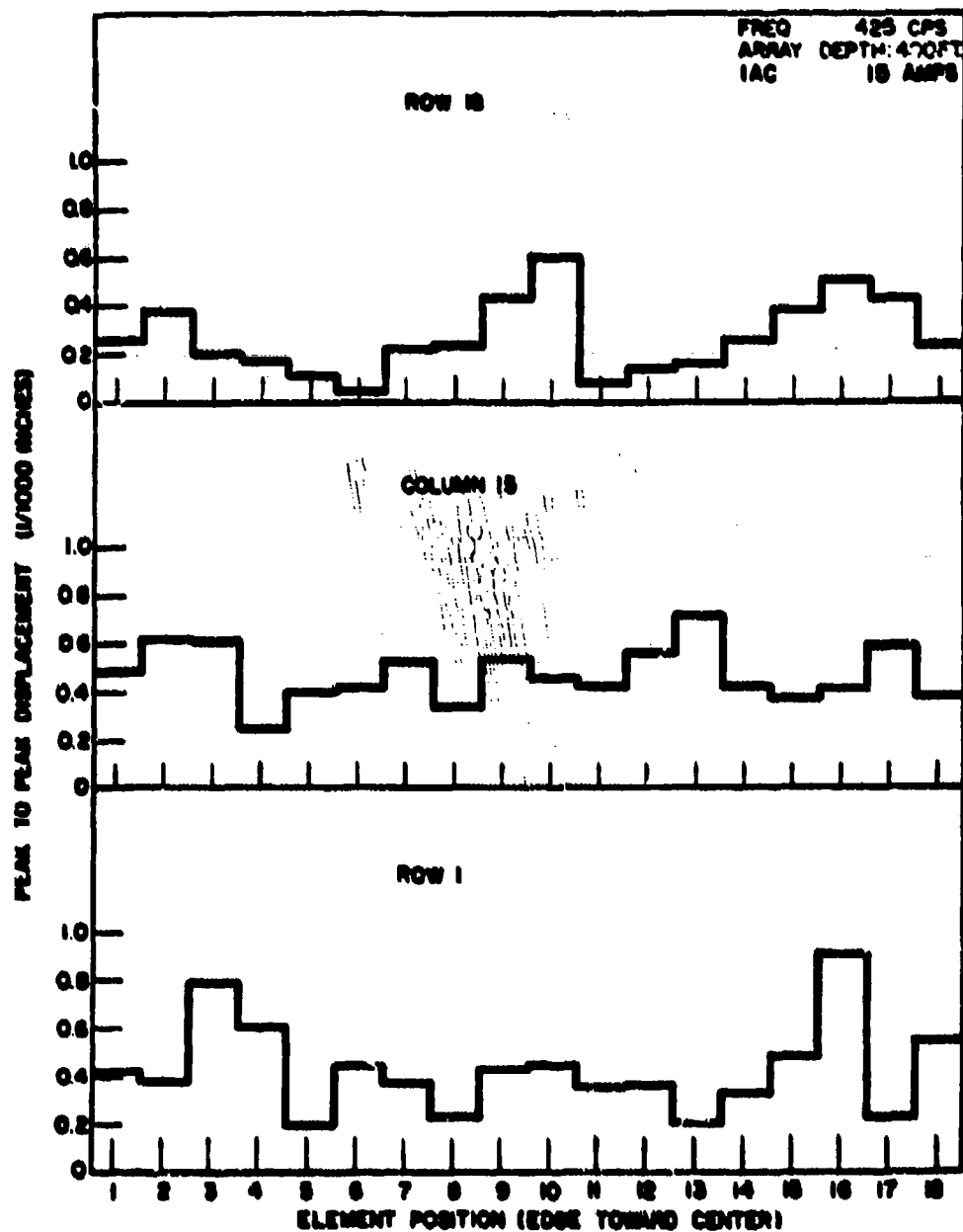


Figure 15 - Amplitude of Transducer Element Displacement

CONFIDENTIAL

CONFIDENTIAL

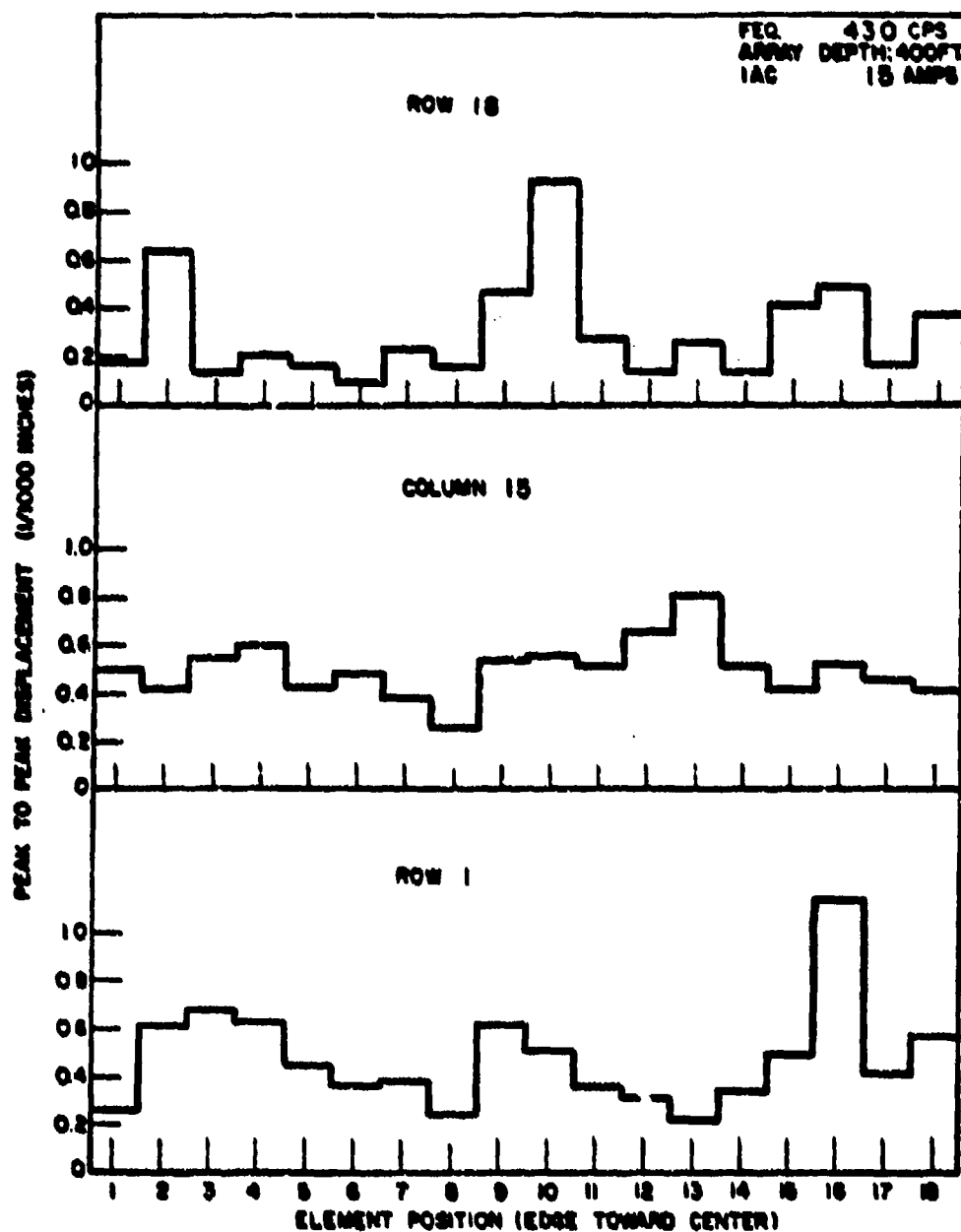


Figure 16 - Amplitude of Transducer Element Displacement

CONFIDENTIAL

CONFIDENTIAL

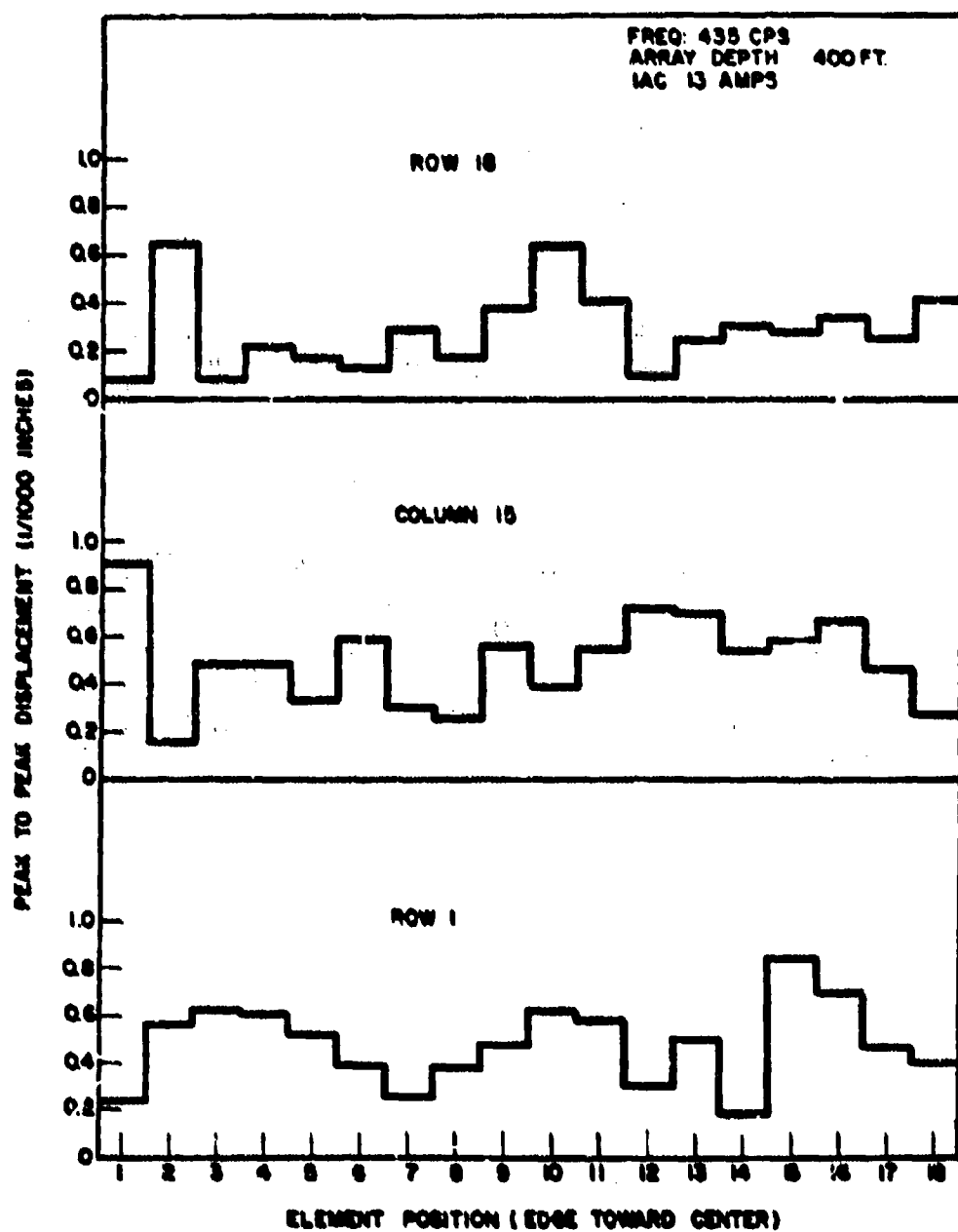


Figure 17 - Amplitude of Transducer Element Displacement

CONFIDENTIAL

CONFIDENTIAL

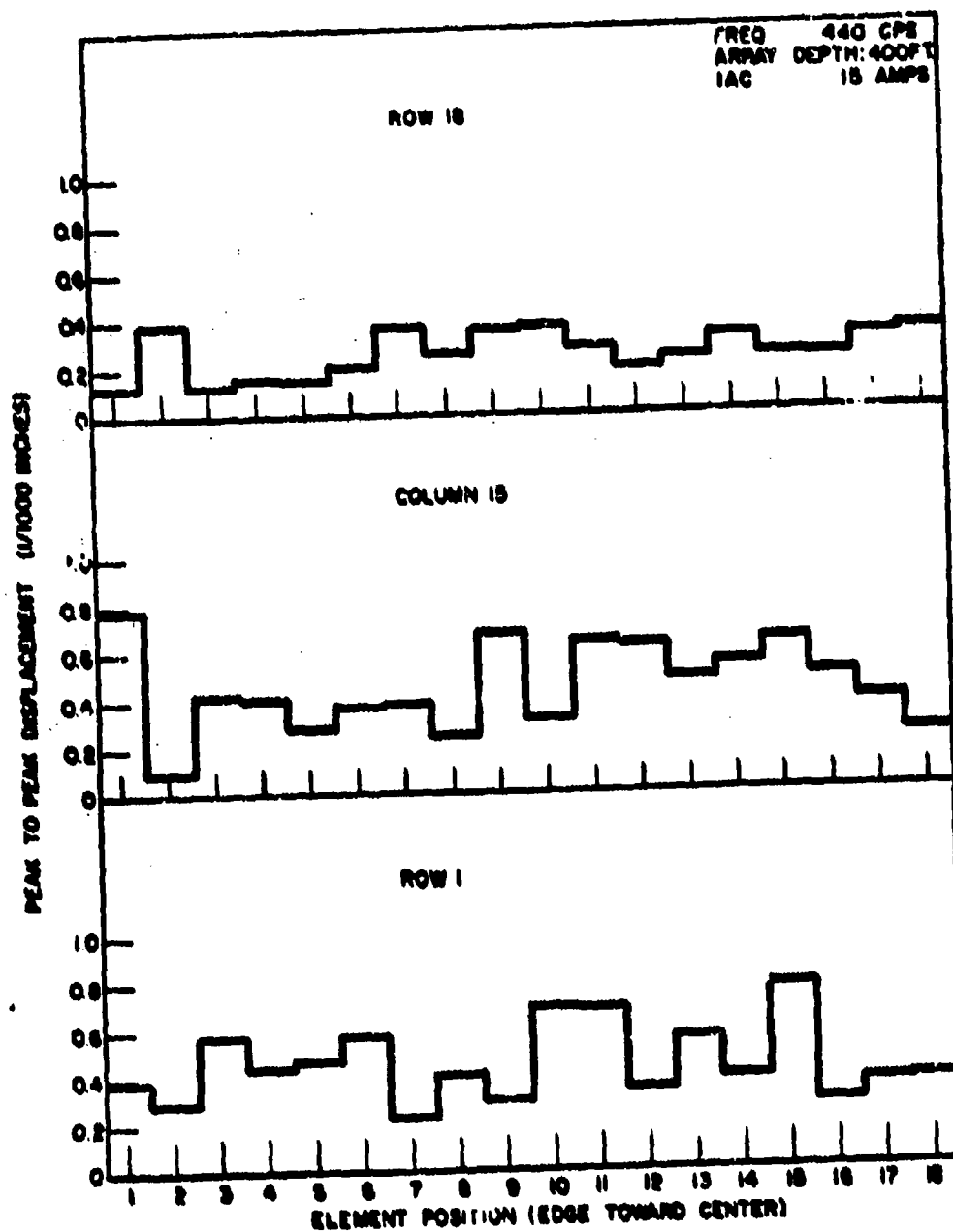


Figure 18 - Amplitude of Transducer Element Displacement

CONFIDENTIAL

CONFIDENTIAL

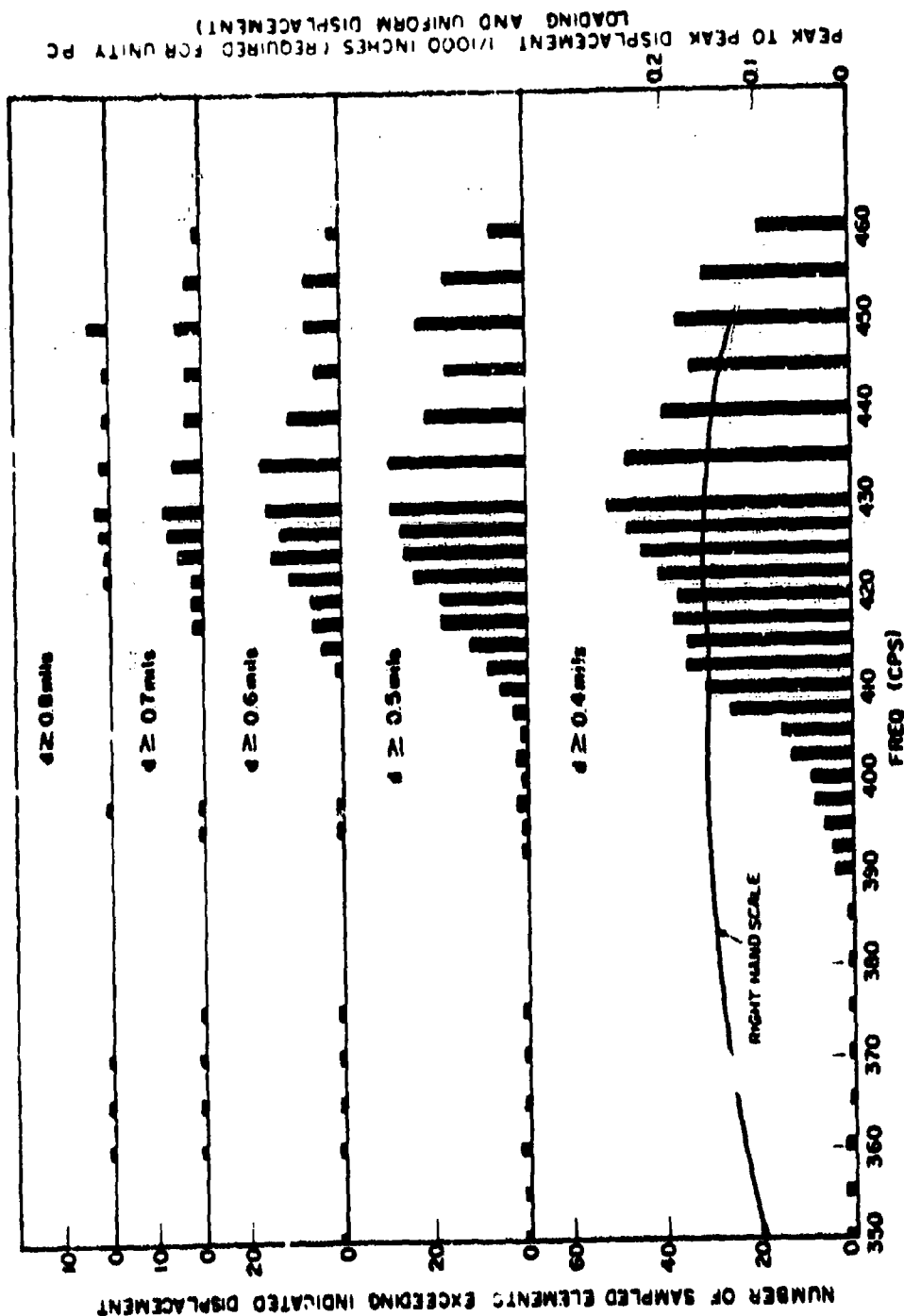


Figure 19 - Frequency Distribution of Transducer Element Displacement

CONFIDENTIAL

CONFIDENTIAL

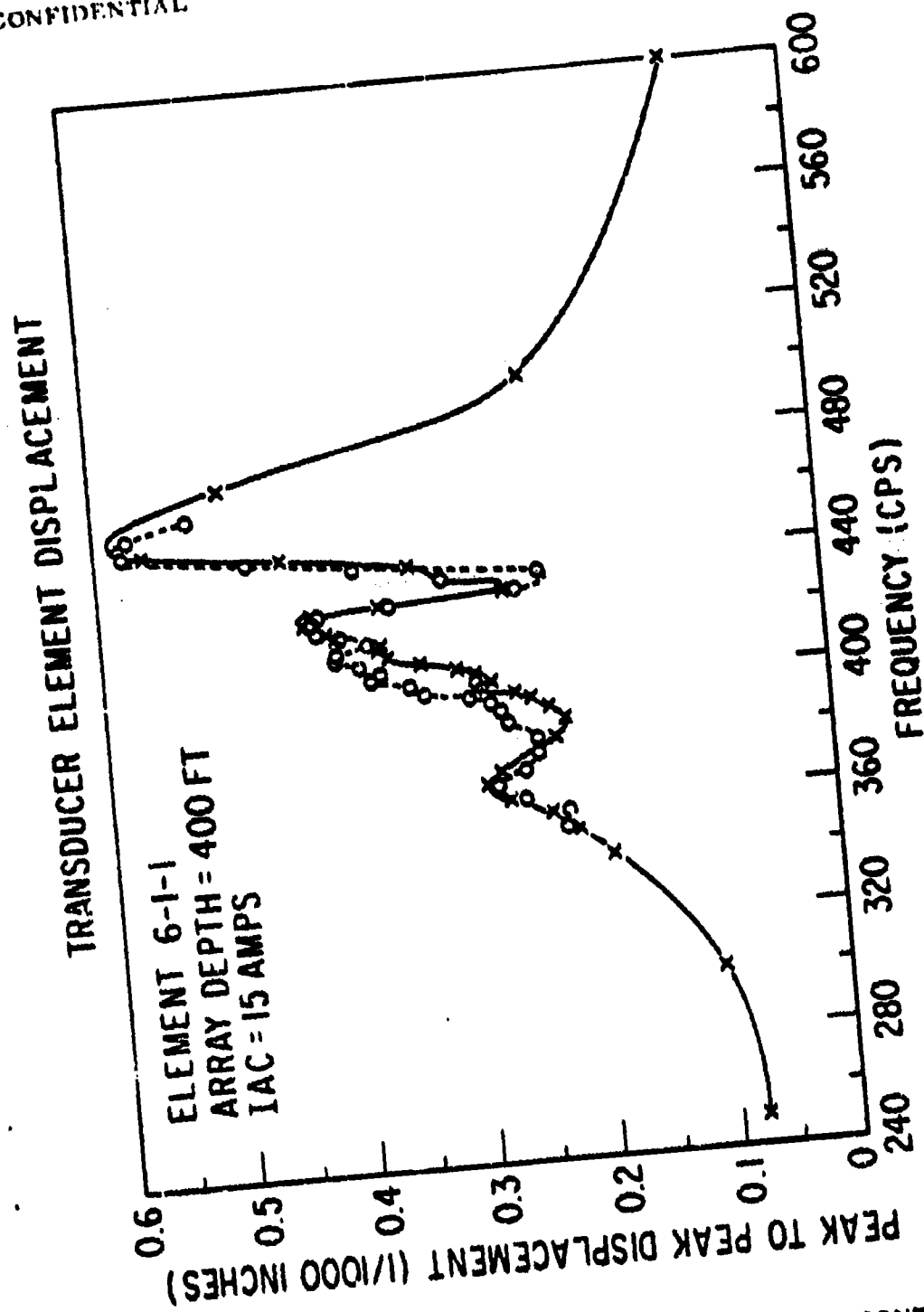


Figure 20 - Transducer Element Displacement (6-1-1)

CONFIDENTIAL

CONFIDENTIAL

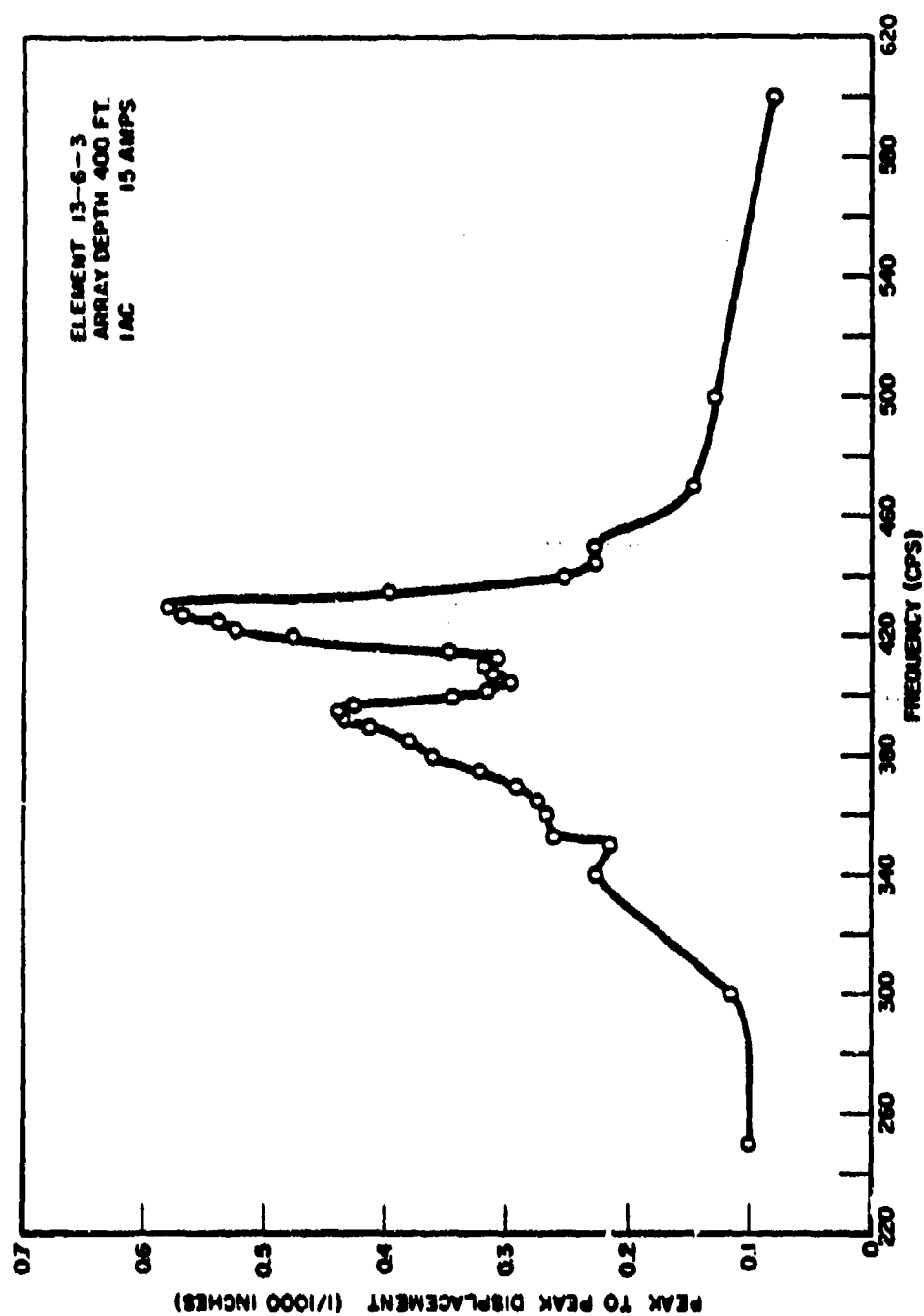


Figure 21 - Transducer Element Displacement

CONFIDENTIAL

CONFIDENTIAL

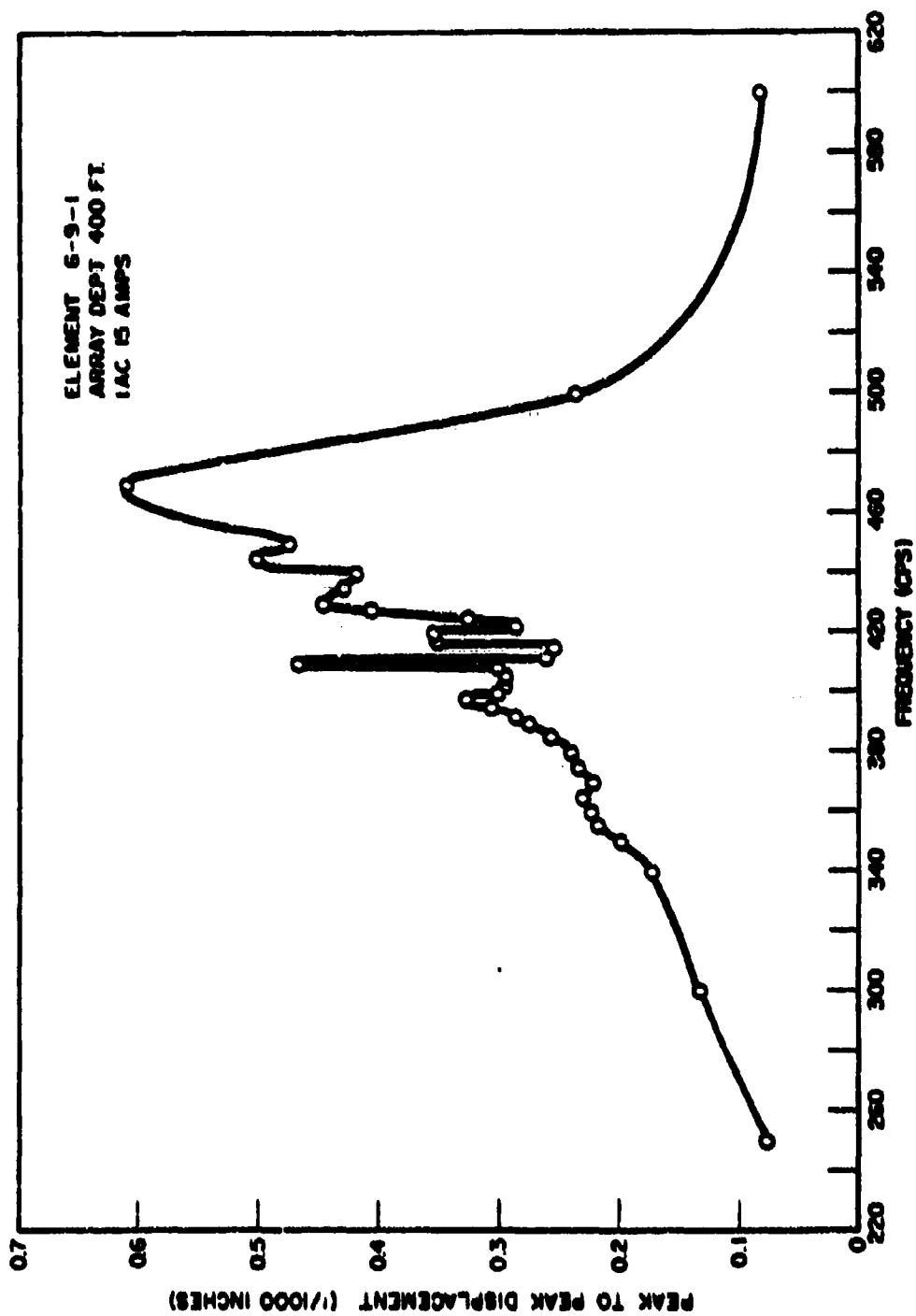


Figure 22 - Transducer Element Displacement

CONFIDENTIAL

CONFIDENTIAL

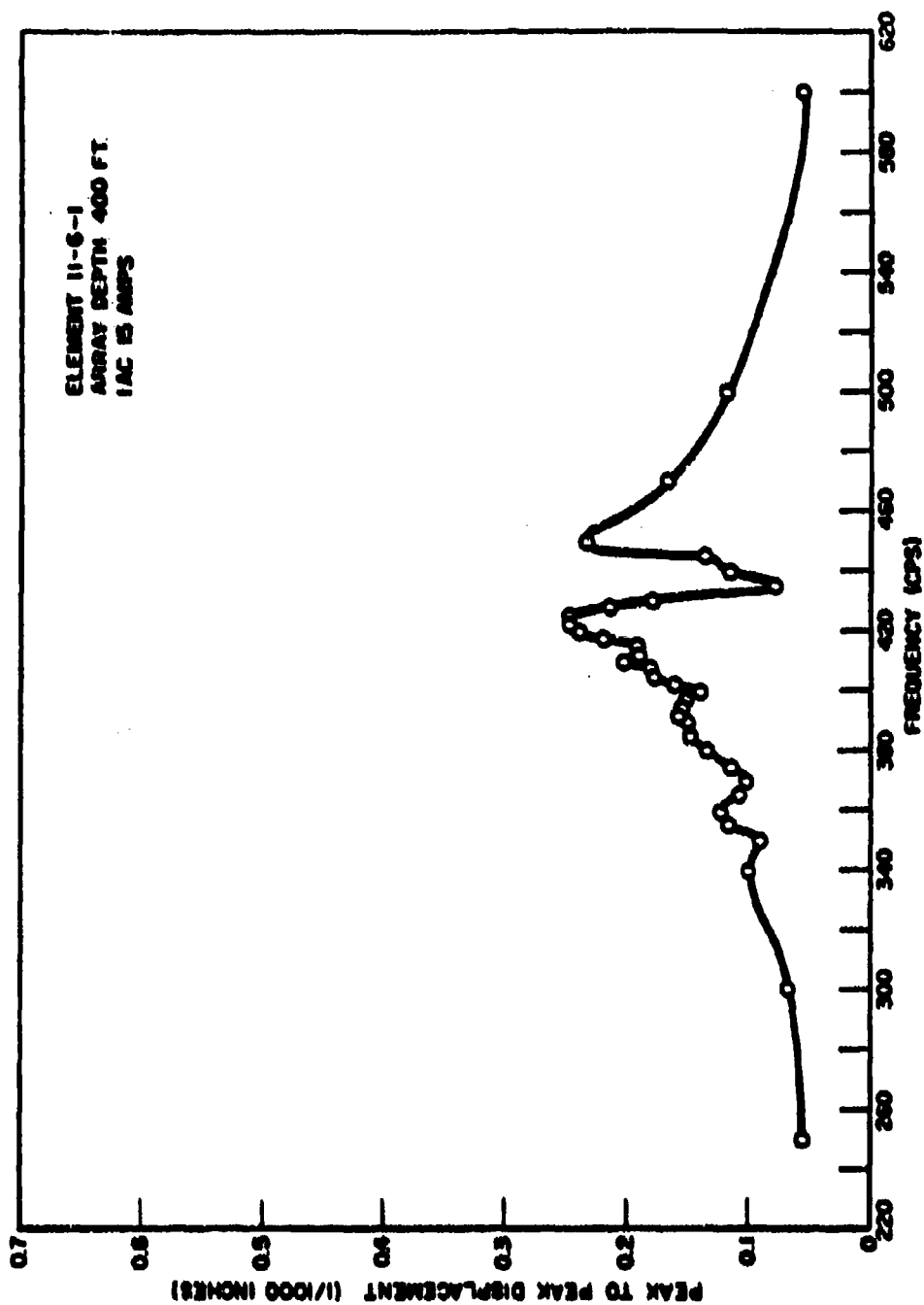


Figure 23 - Transducer Element Displacement

CONFIDENTIAL

CONFIDENTIAL

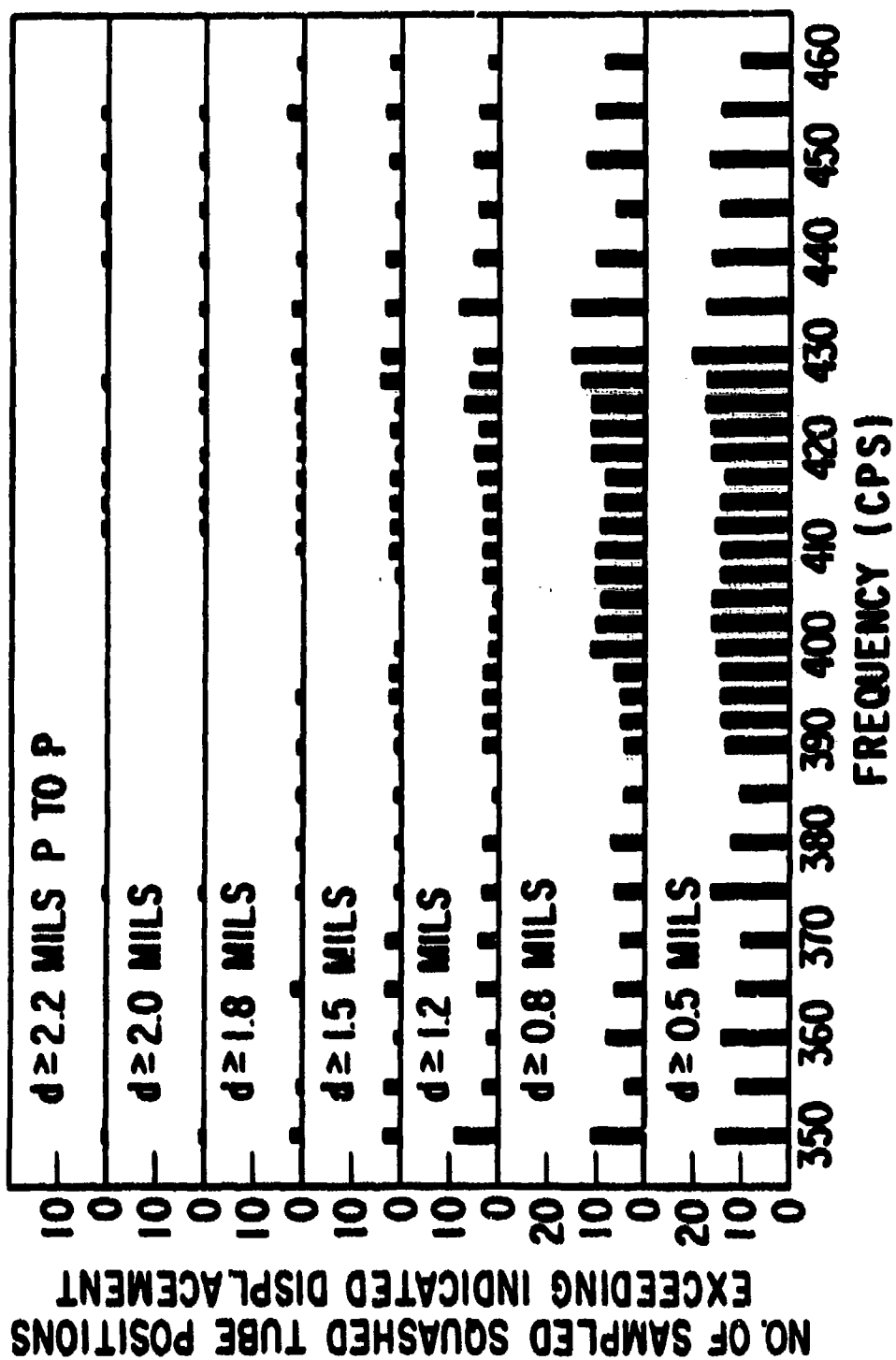


Figure 24 - Frequency Maximum in Squashed Tube Displacement

CONFIDENTIAL

CONFIDENTIAL

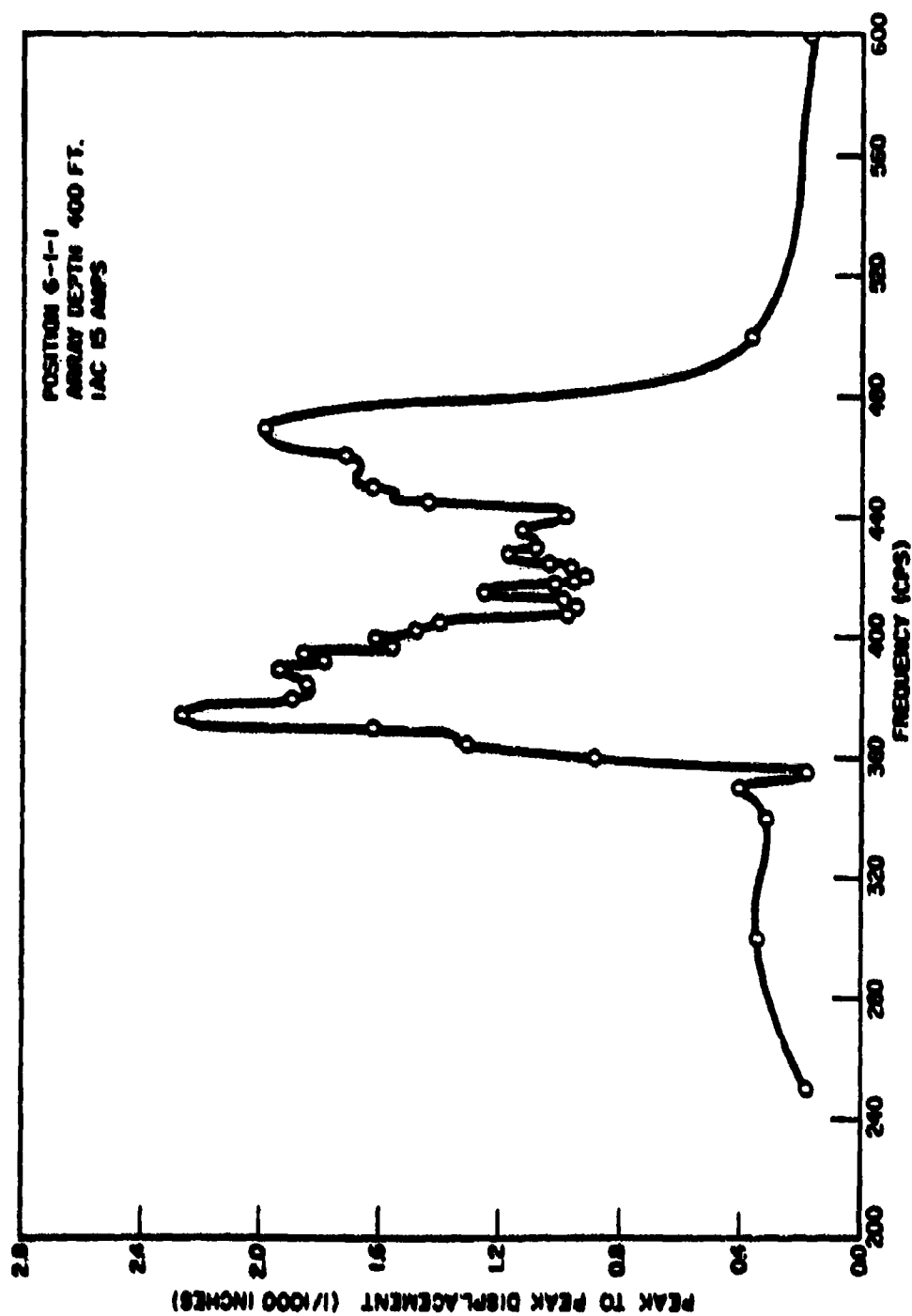


Figure 25 - Squashed Tube Displacement Amplitude

CONFIDENTIAL

CONFIDENTIAL

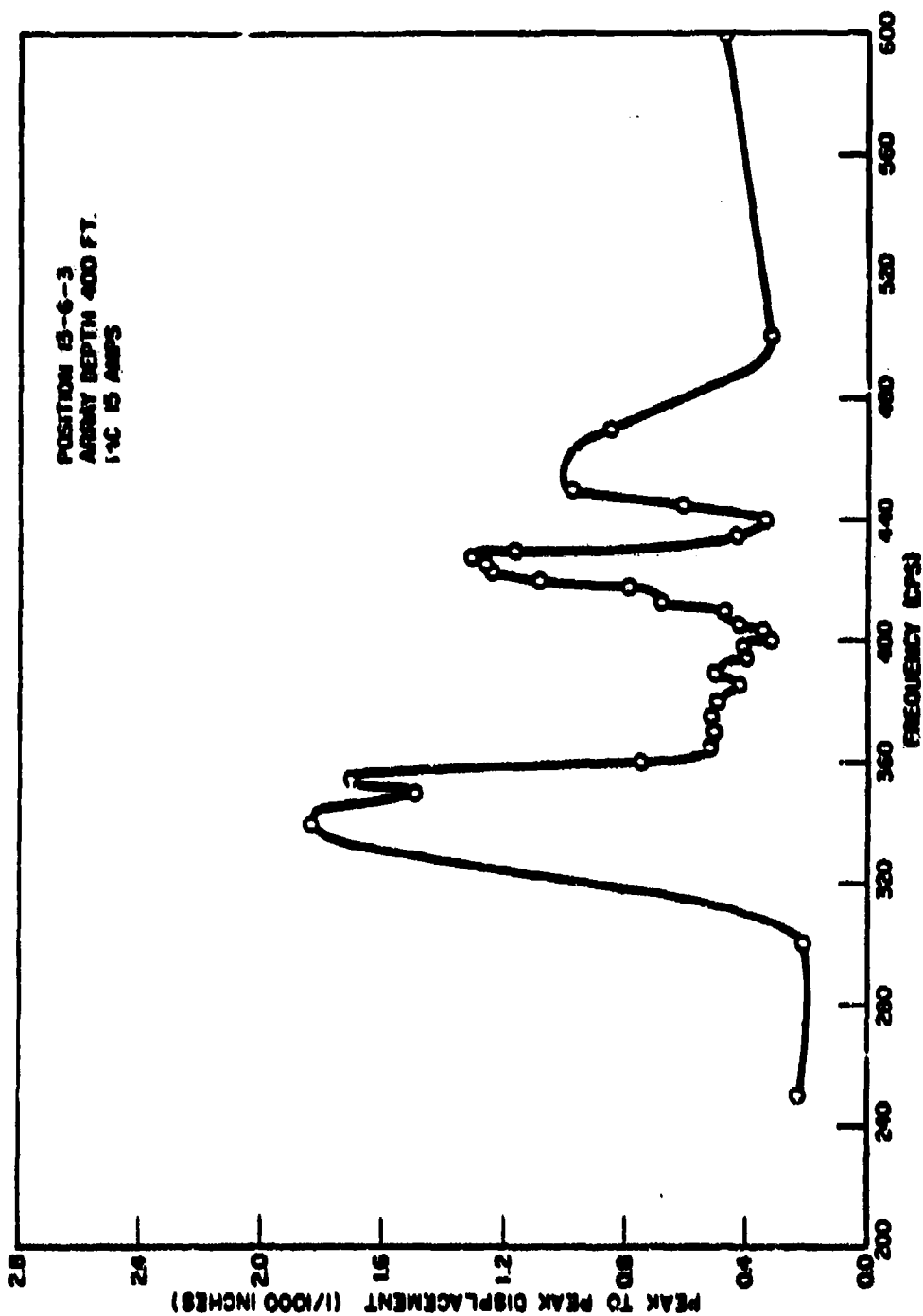


Figure 26 - Squashed Tube Displacement Amplitude

CONFIDENTIAL

CONFIDENTIAL

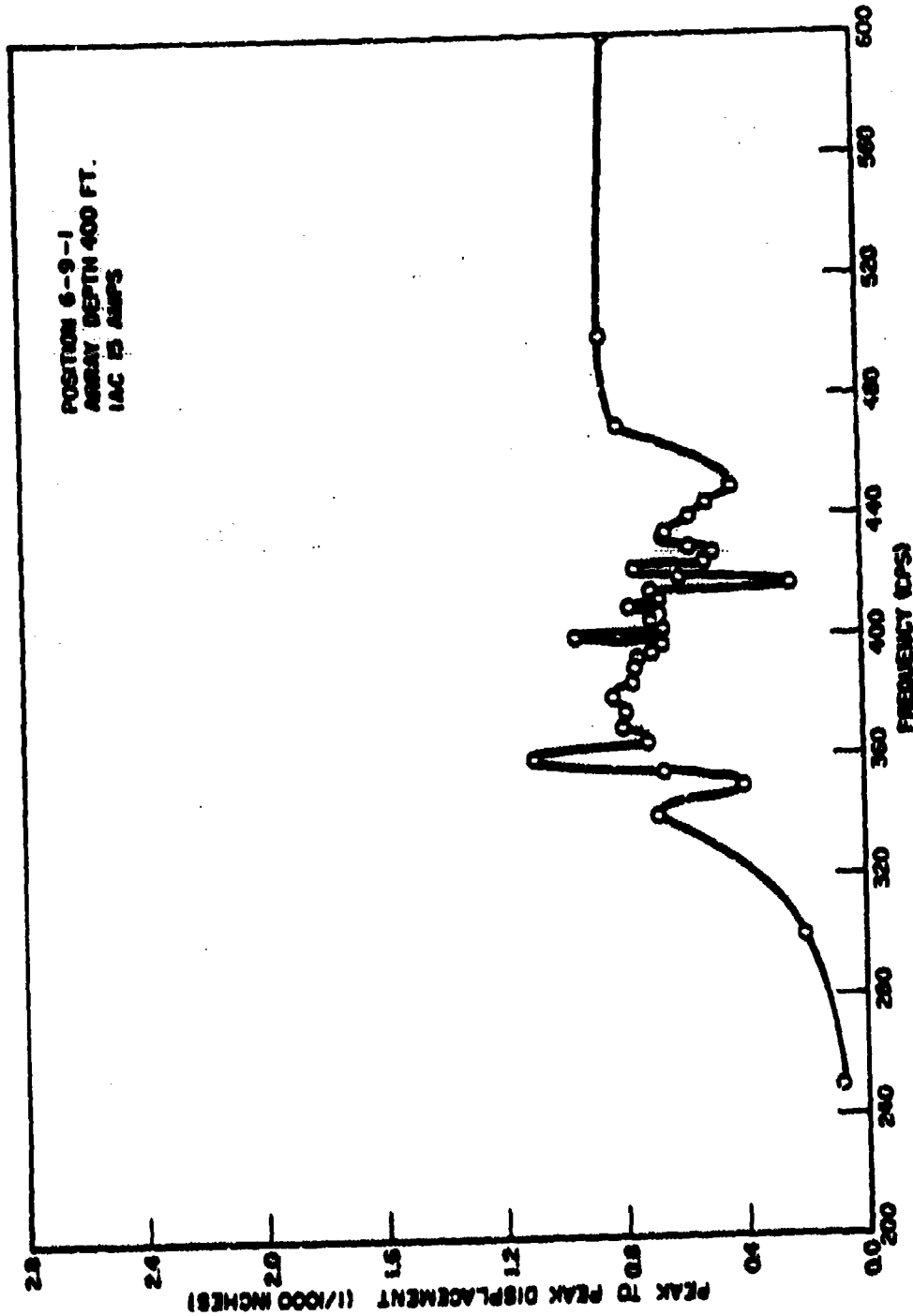


Figure 27 - Squashed Tube Displacement Amplitude

CONFIDENTIAL

CONFIDENTIAL

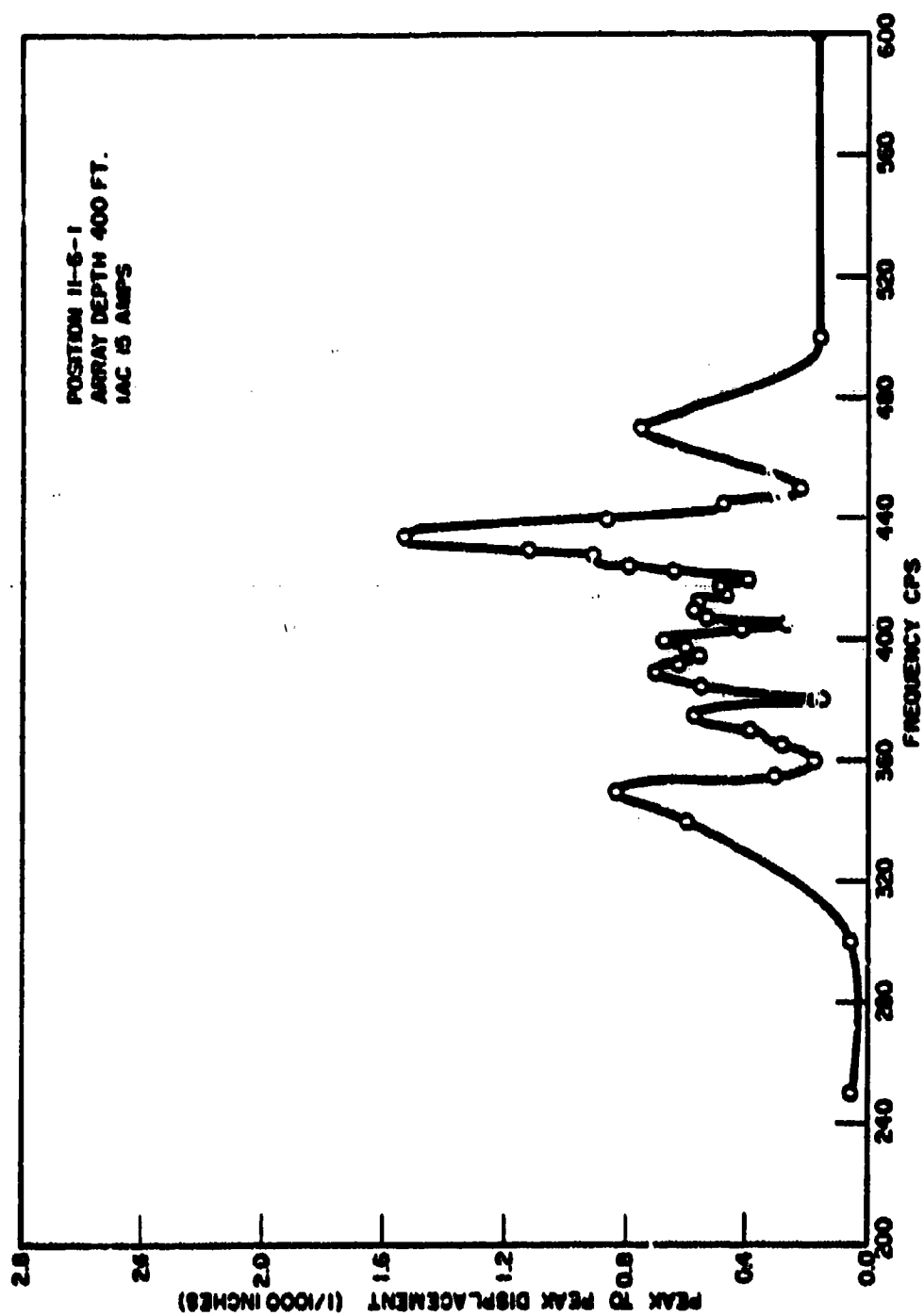


Figure 28 - Squashed Tube Displacement Amplitude

CONFIDENTIAL

CONFIDENTIAL

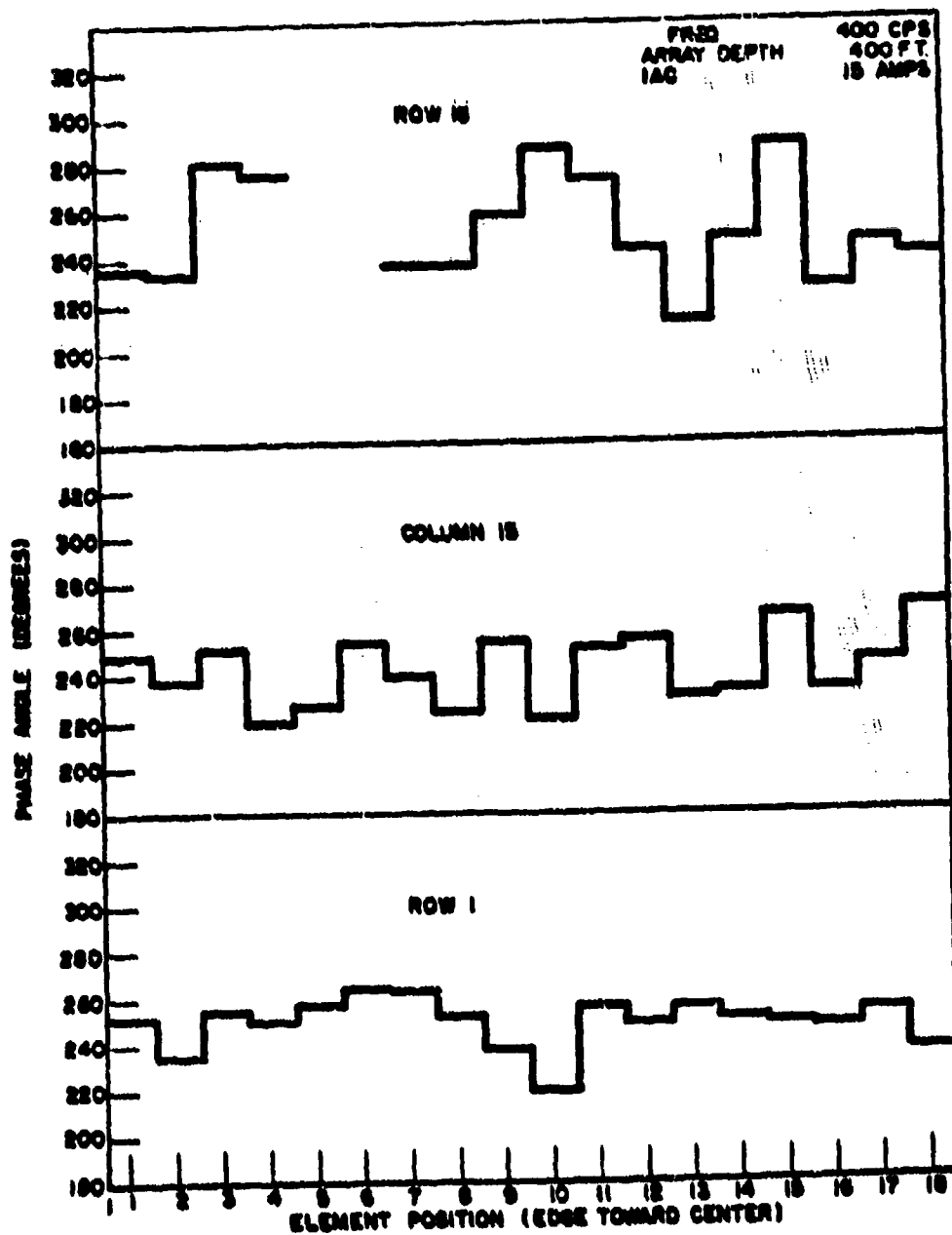


Figure 29 - Transducer Element Displacement Phase Relative to Amplifier Input Voltage

CONFIDENTIAL

CONFIDENTIAL

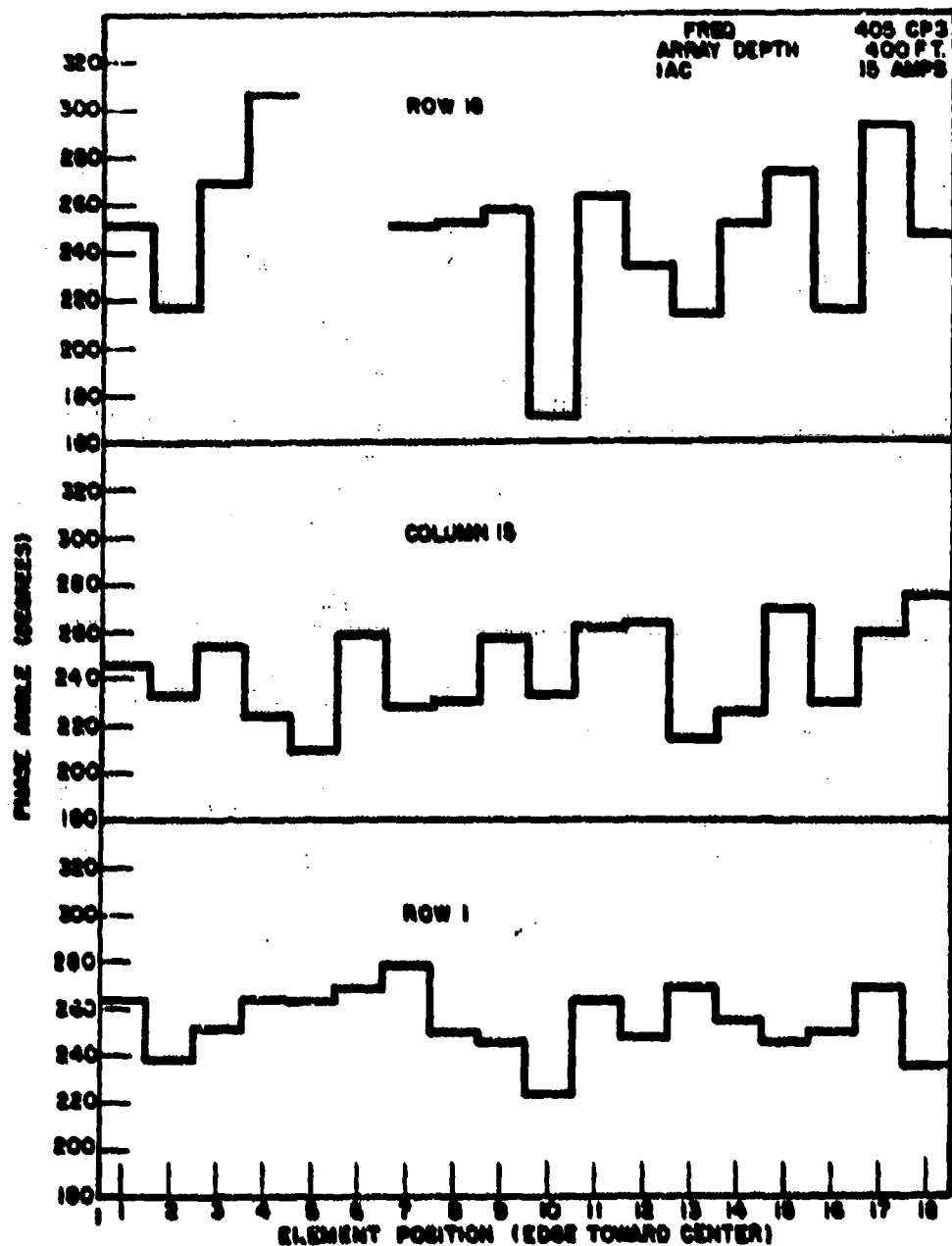


Figure 30 - Transducer Element Displacement Phase Relative to Amplifier Input Voltage

CONFIDENTIAL

CONFIDENTIAL

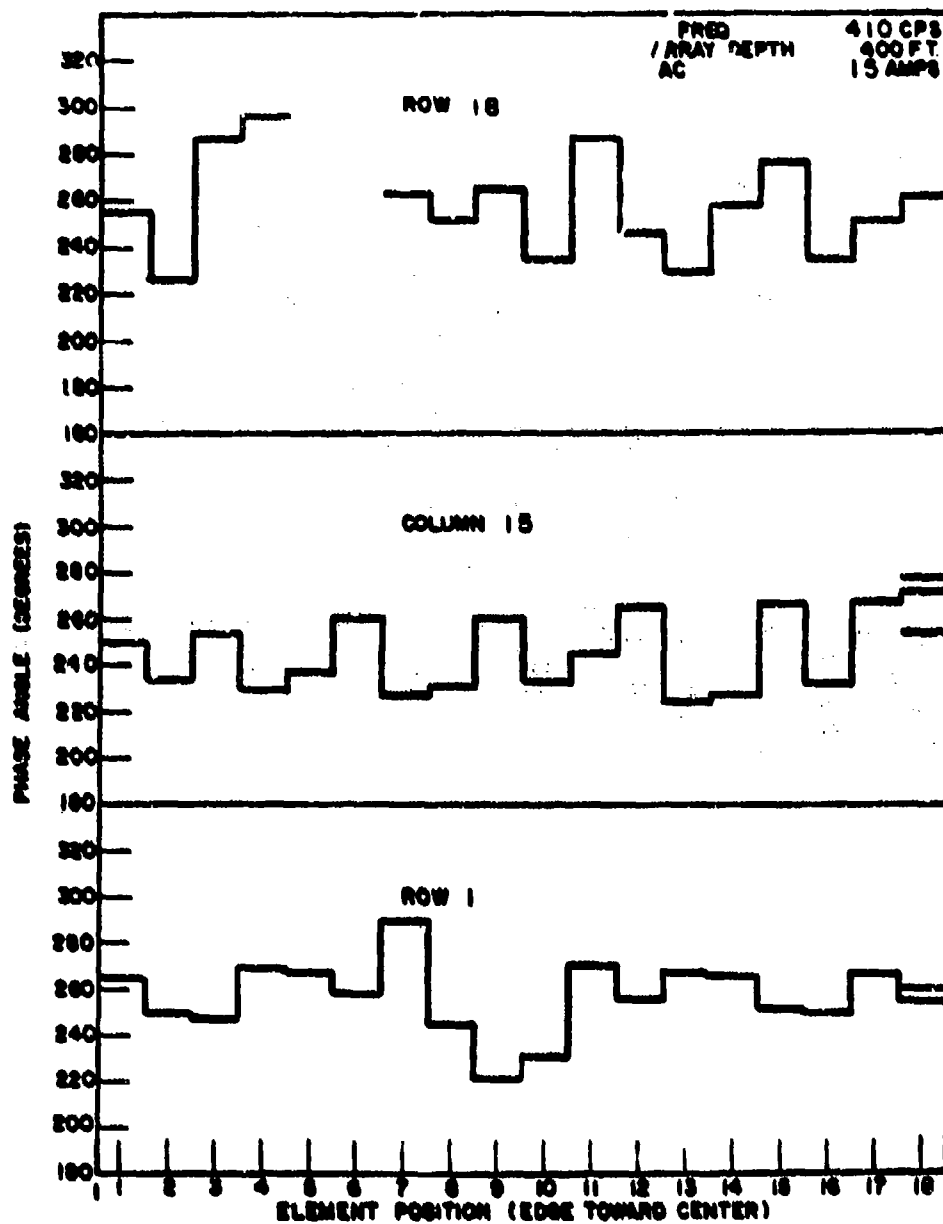


Figure 31 - Transducer Element Displacement Phase Relative to Amplifier Input Voltage

CONFIDENTIAL

CONFIDENTIAL

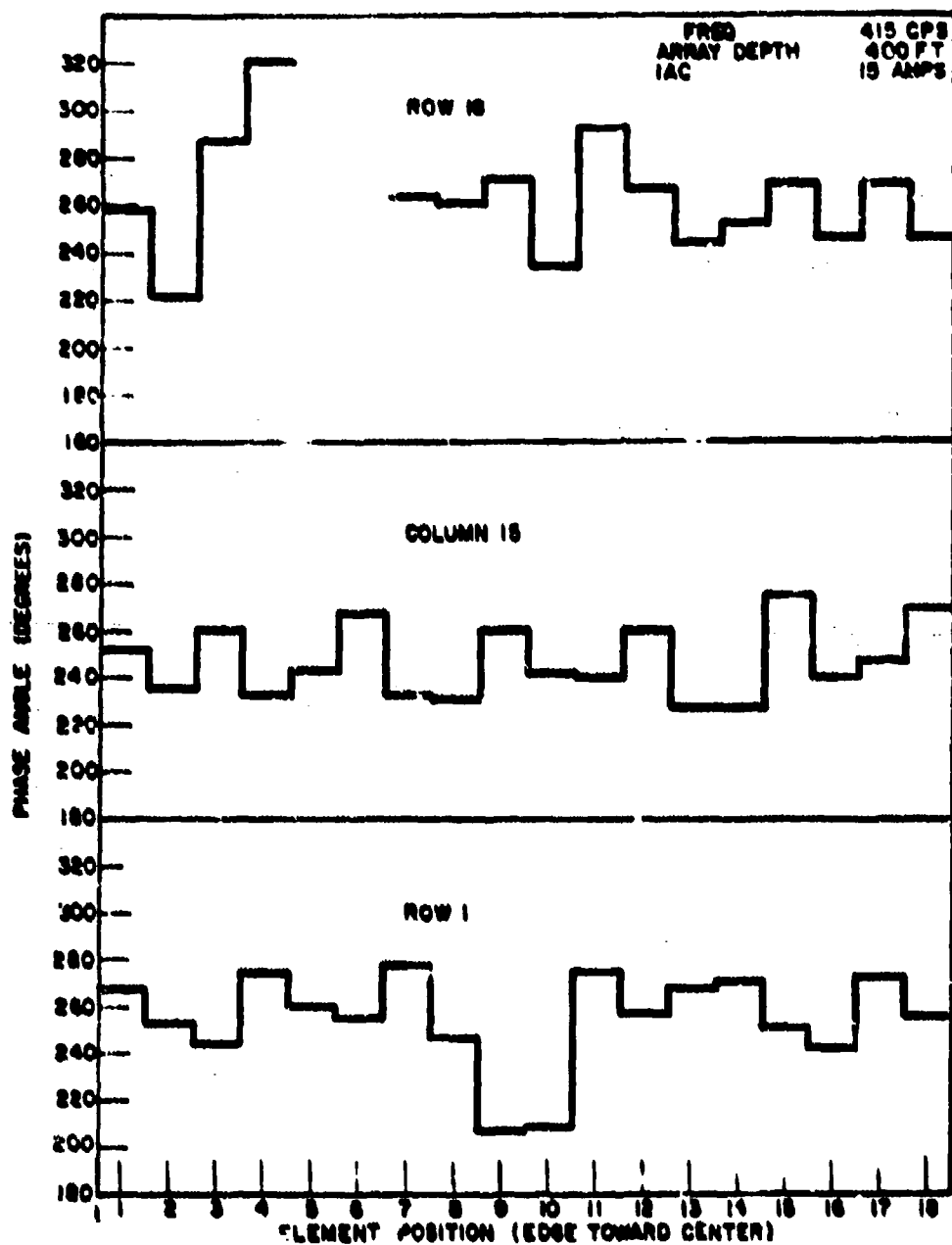


Figure 32 - Transducer Element Displacement Phase Relative to Amplifier Input Voltage

CONFIDENTIAL

CONFIDENTIAL

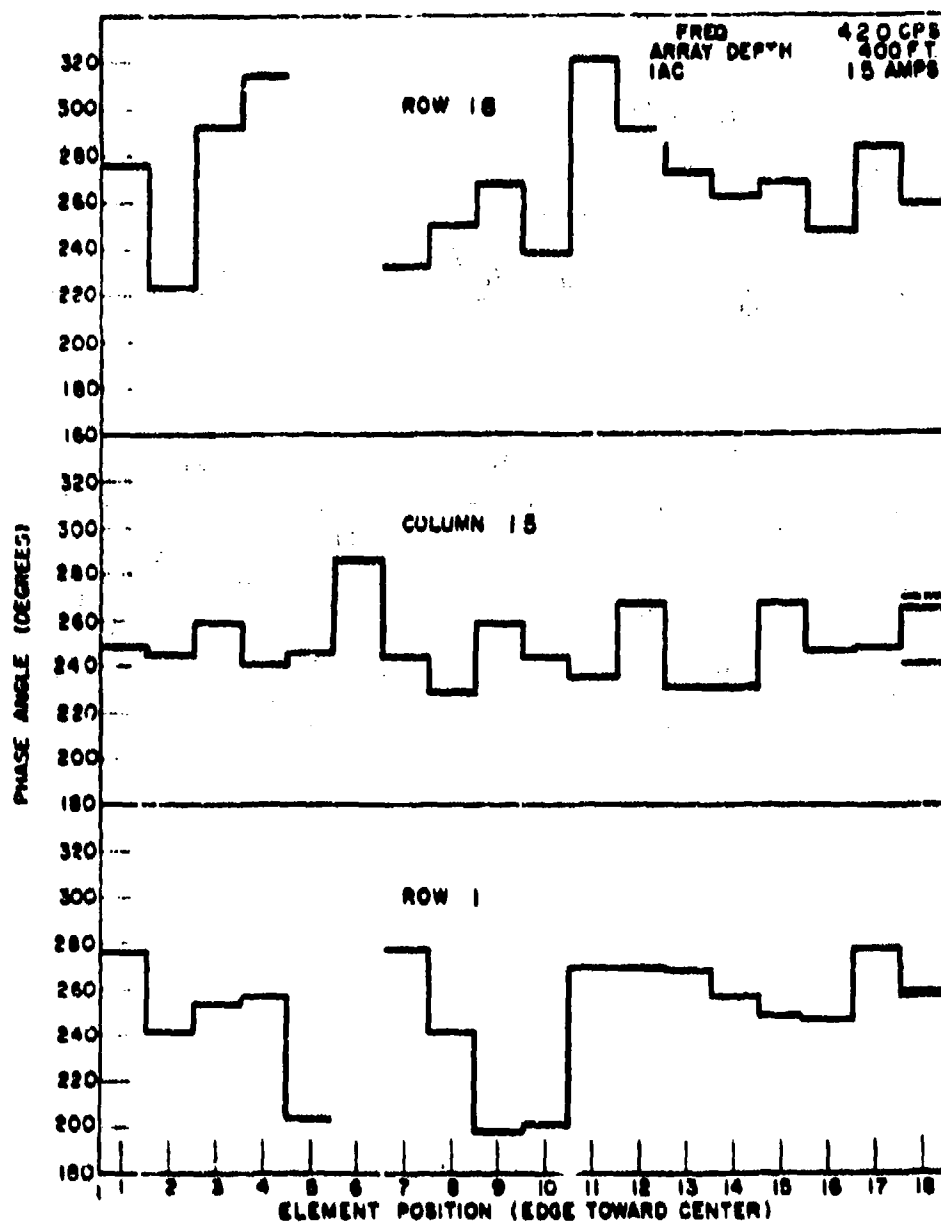


Figure 13 - Transducer Element Displacement Phase Relative to Amplifier Input Voltage

CONFIDENTIAL

CONFIDENTIAL

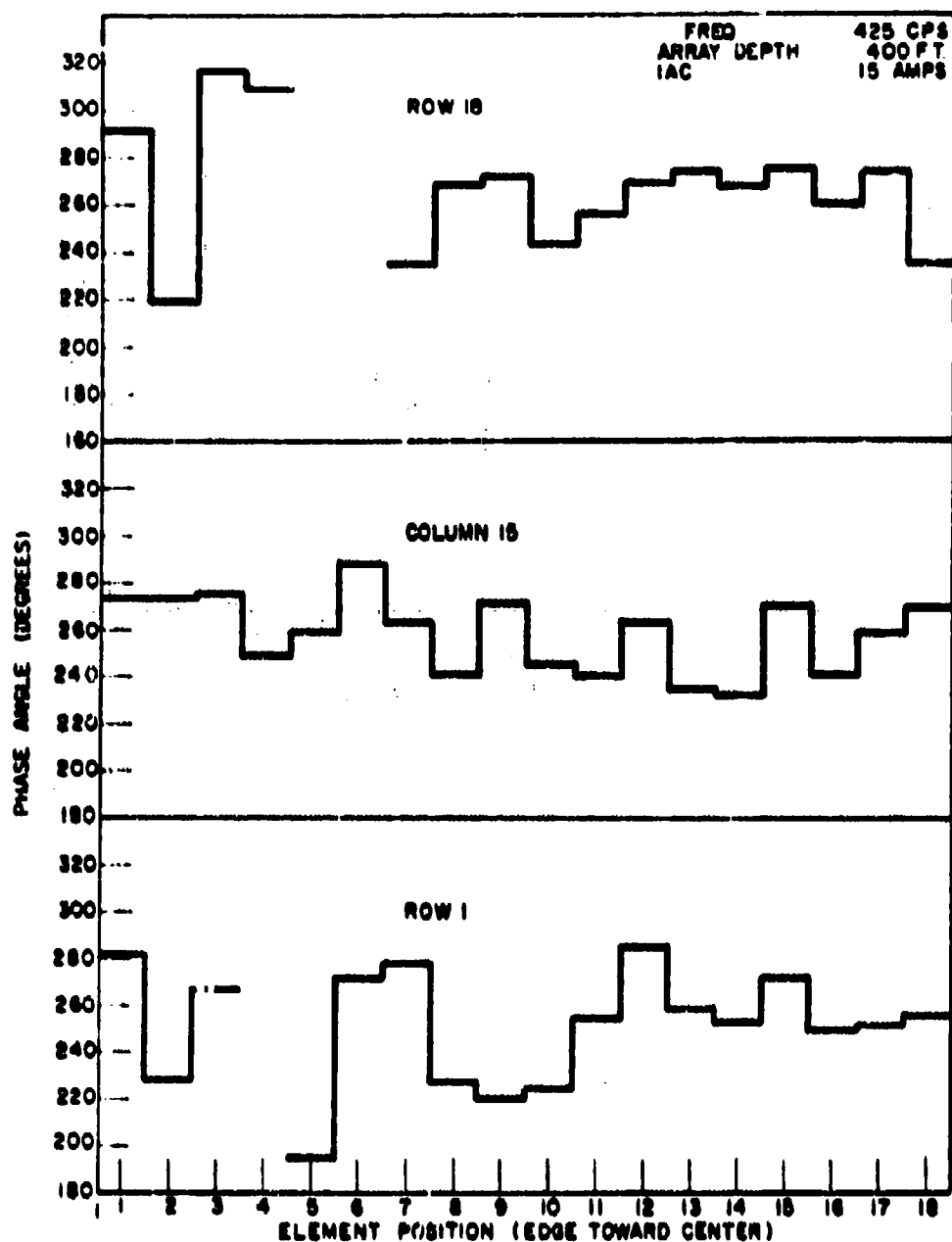


Figure 34 - Transducer Element Displacement Phase Relative to Amplifier Input Voltage

CONFIDENTIAL

CONFIDENTIAL

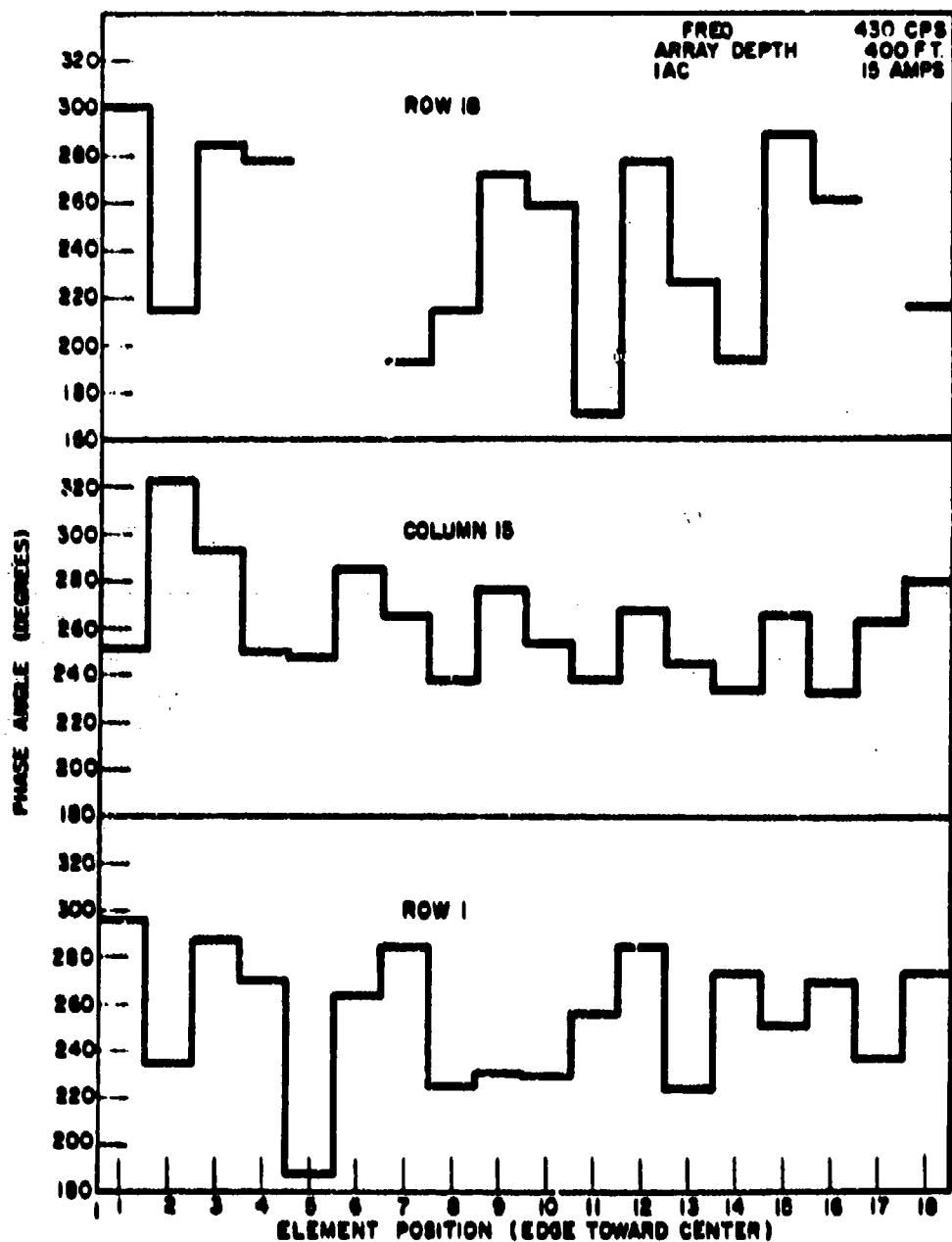


Figure 35 - Transducer Element Displacement Phase Relative to Amplifier Input Voltage

CONFIDENTIAL

CONFIDENTIAL

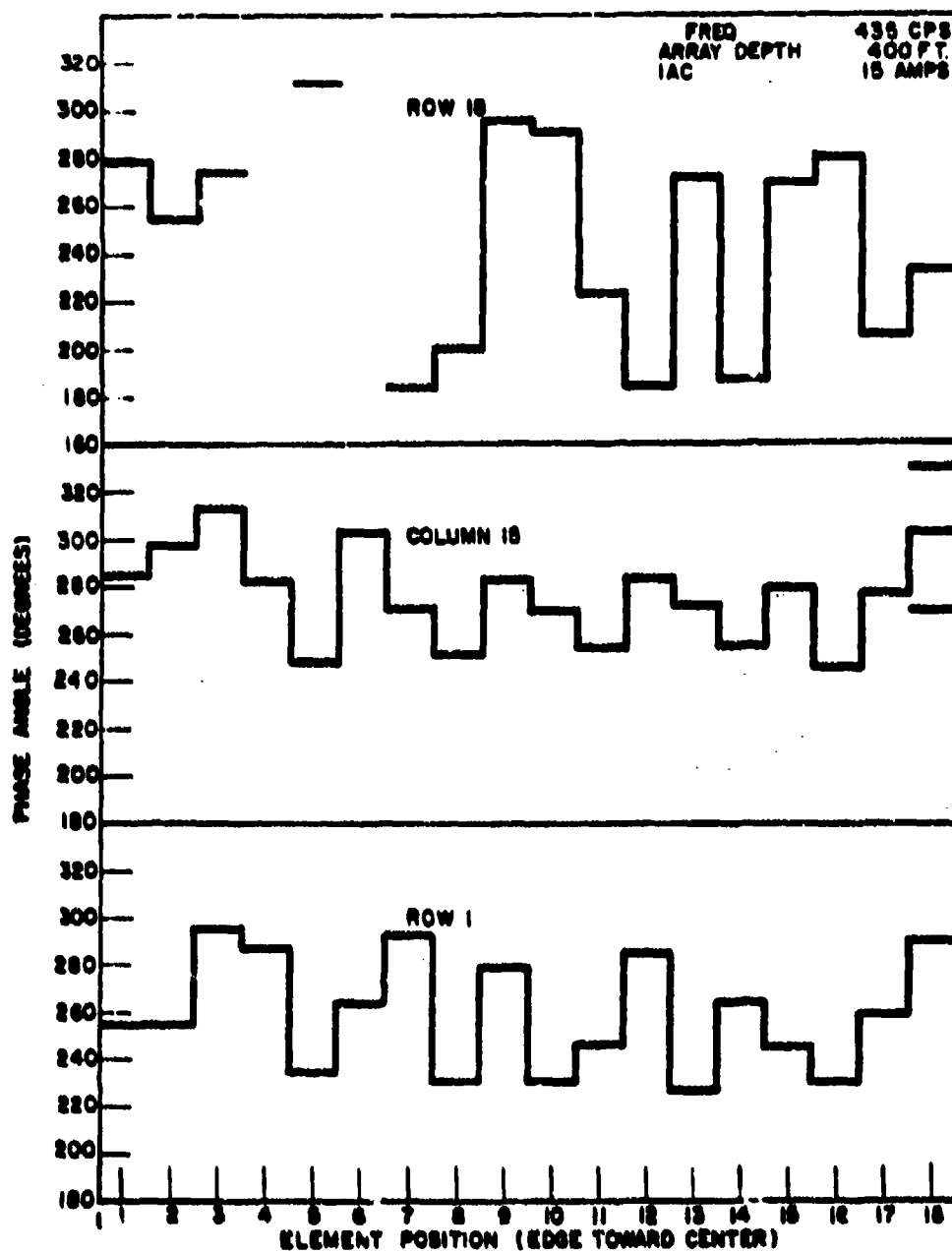


Figure 36 - Transducer Element Displacement Phase Relative to Amplifier Input Voltage

CONFIDENTIAL

CONFIDENTIAL

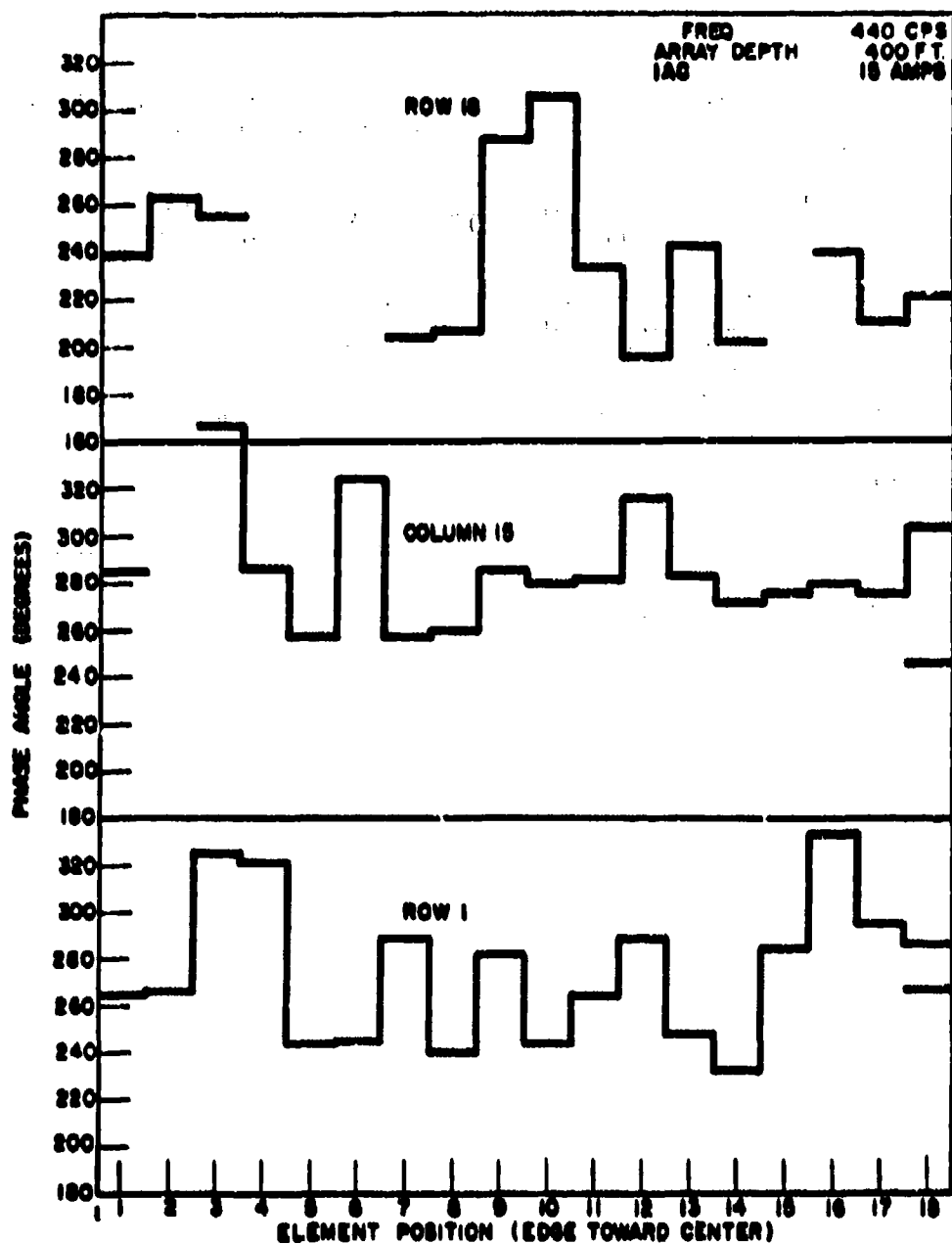


Figure 37 - Transducer Element Displacement Phase Relative to Amplifier Input Voltage

CONFIDENTIAL

CONFIDENTIAL

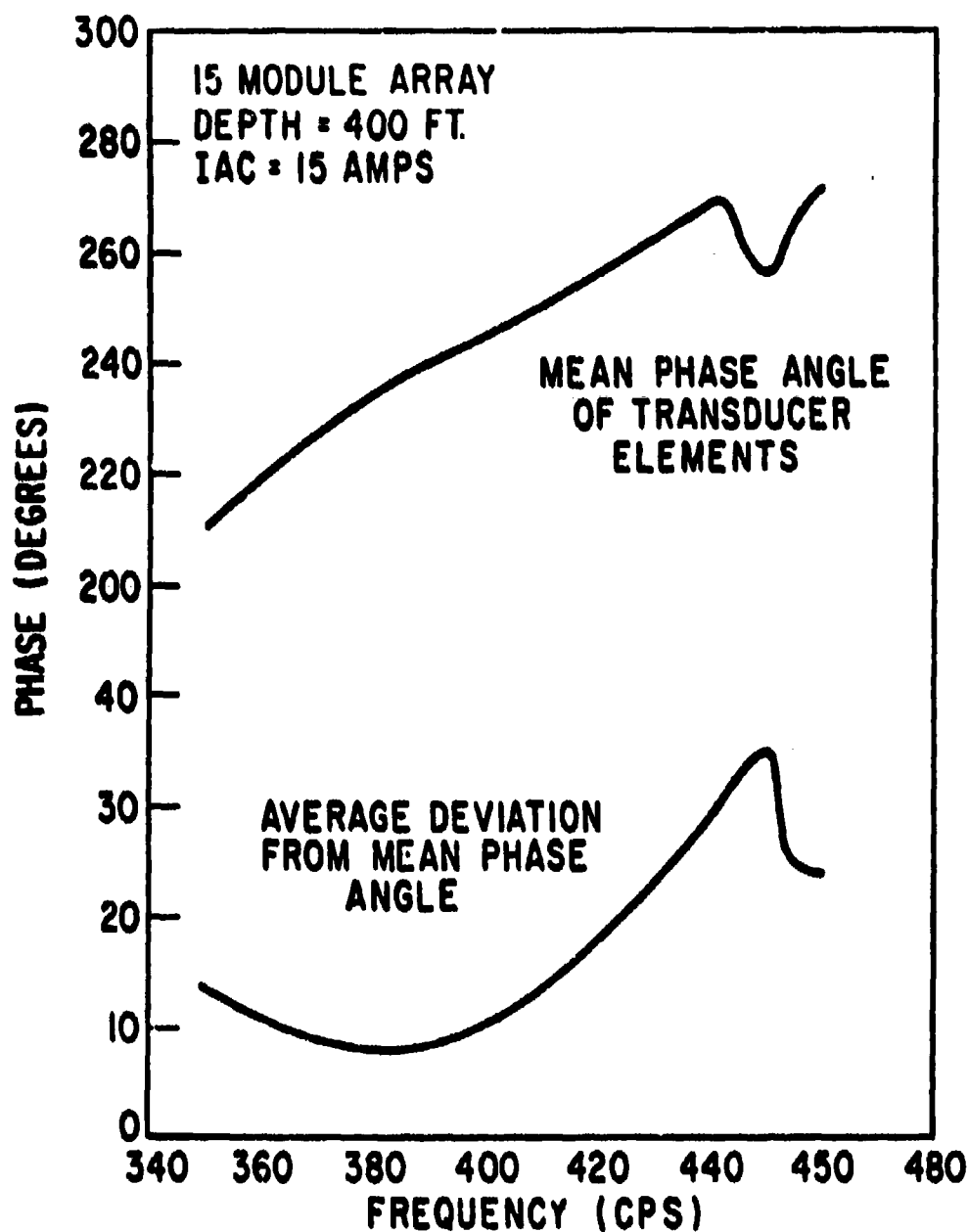


Figure 38 - Average Characteristics of Transducer Element Displacement Phase

CONFIDENTIAL

CONFIDENTIAL

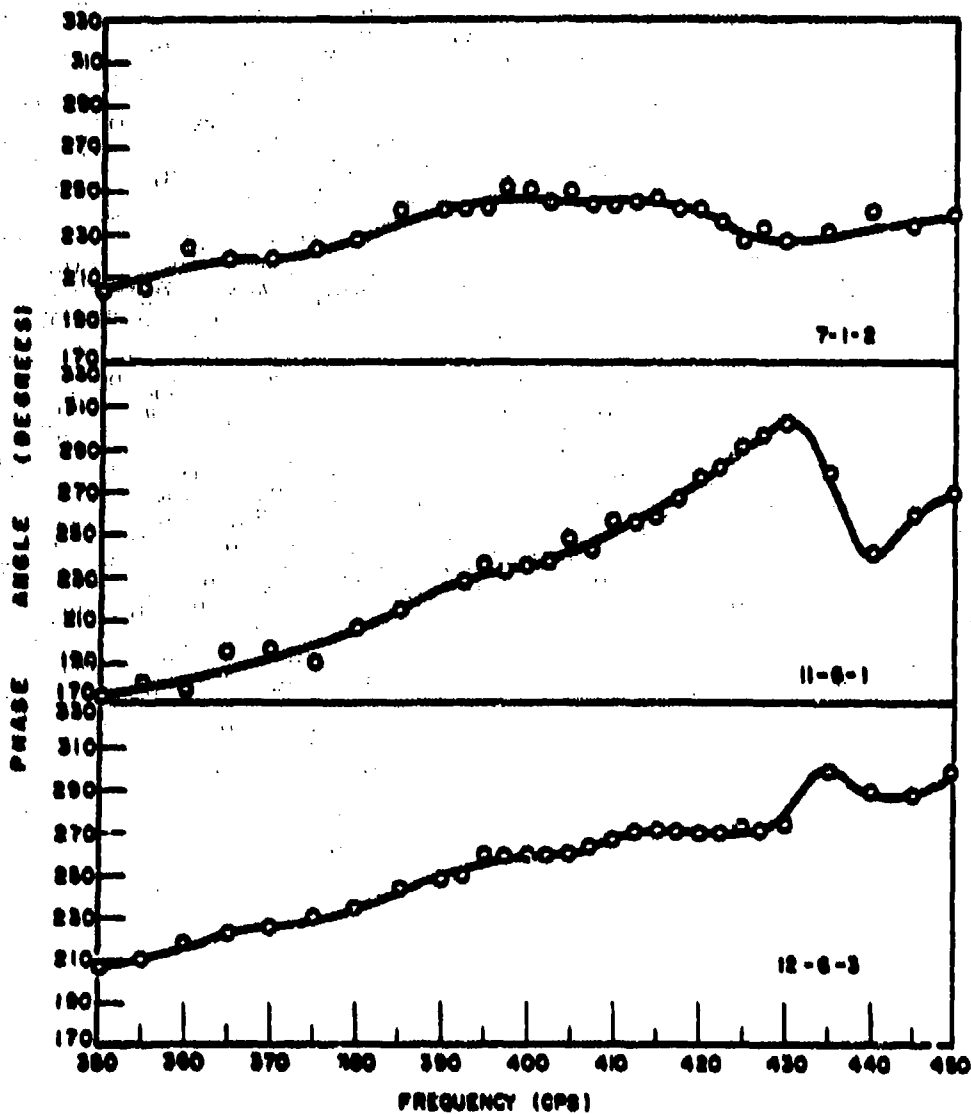


Figure 39 - Frequency Characteristics of Transducer Element Displacement Phase

CONFIDENTIAL

CONFIDENTIAL

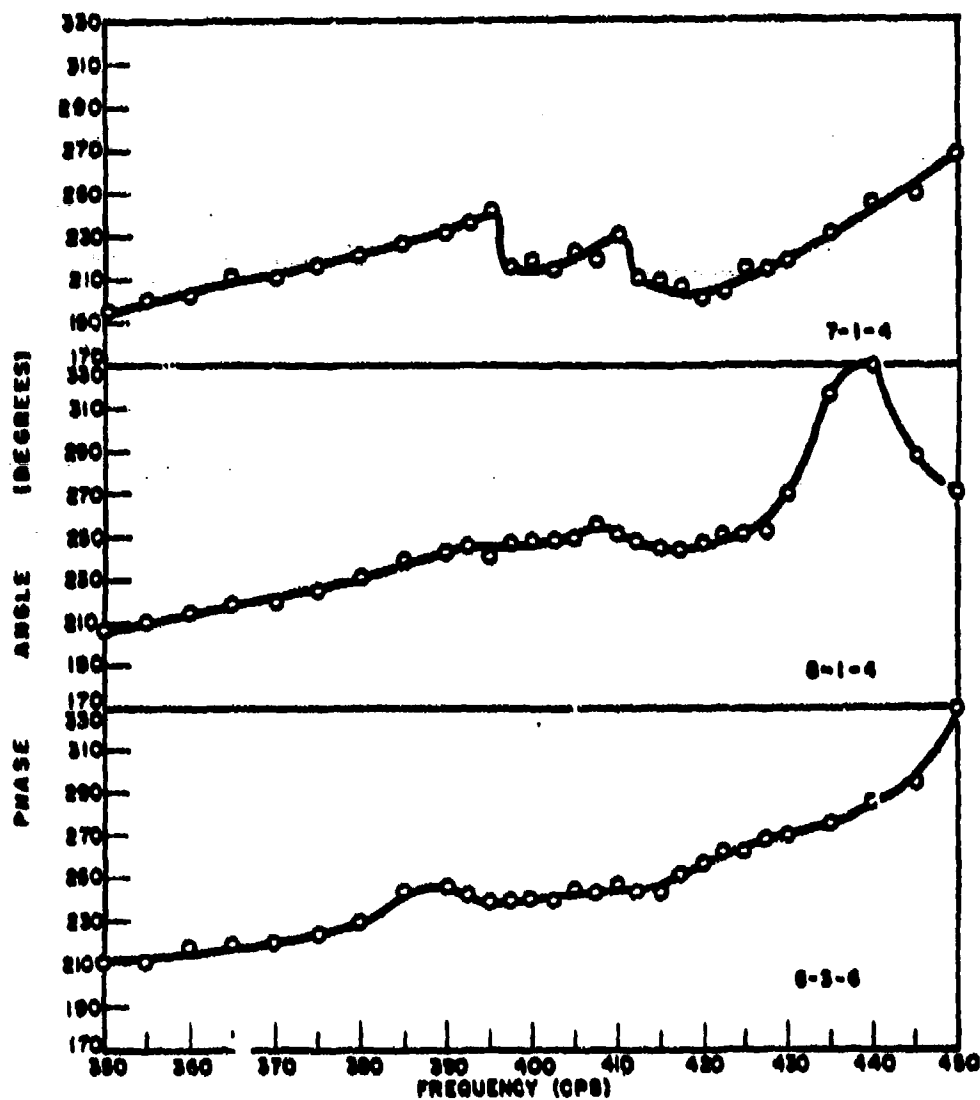


Figure 40 - Frequency Characteristics of Transducer Element Displacement Phase

CONFIDENTIAL

CONFIDENTIAL

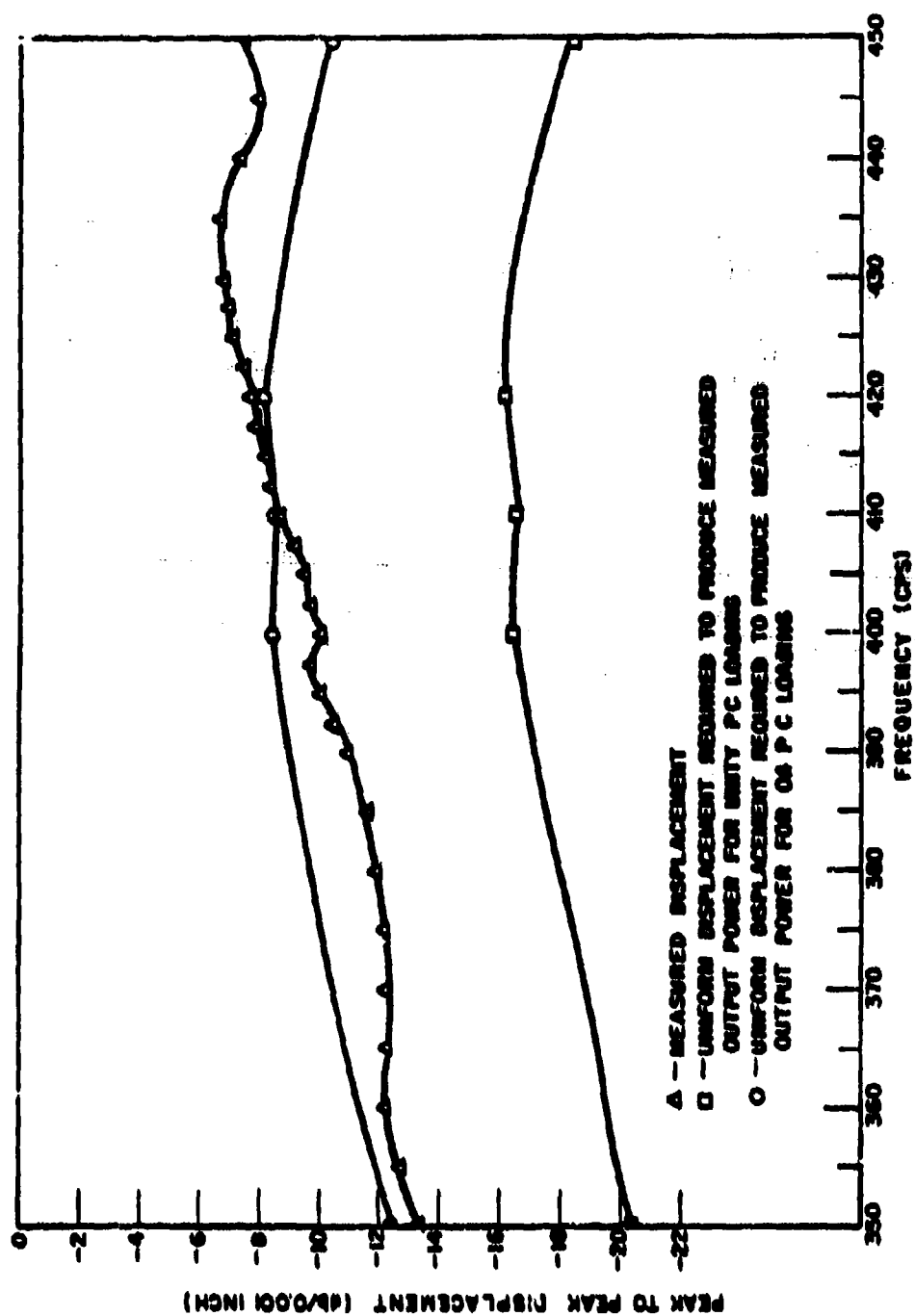


Figure 41 - Transducer Loading Characteristics

CONFIDENTIAL

CONFIDENTIAL

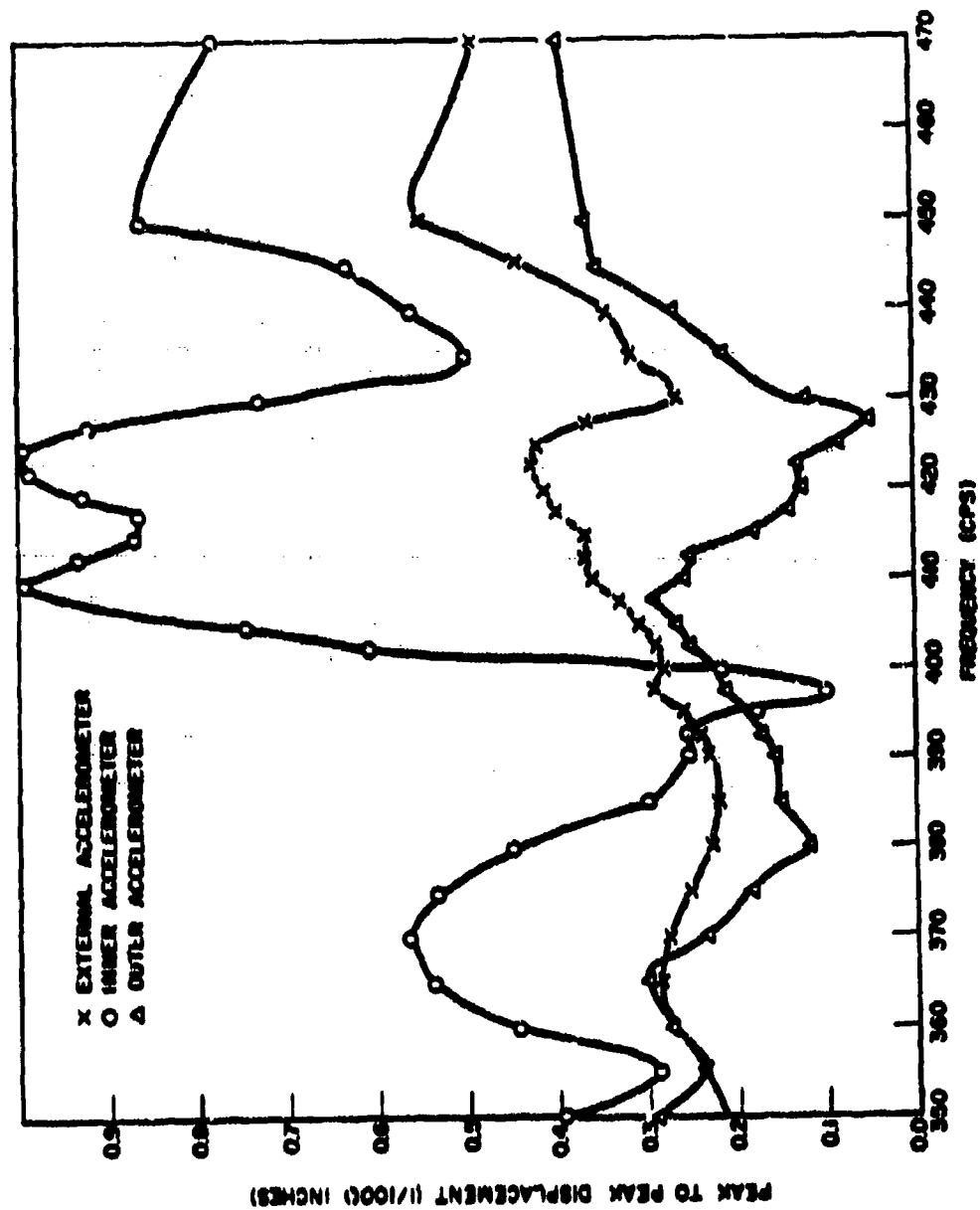


Figure 42 - Element Displacement Characteristics for Specially Instrumented Element in Position 6-1-1

CONFIDENTIAL

CONFIDENTIAL

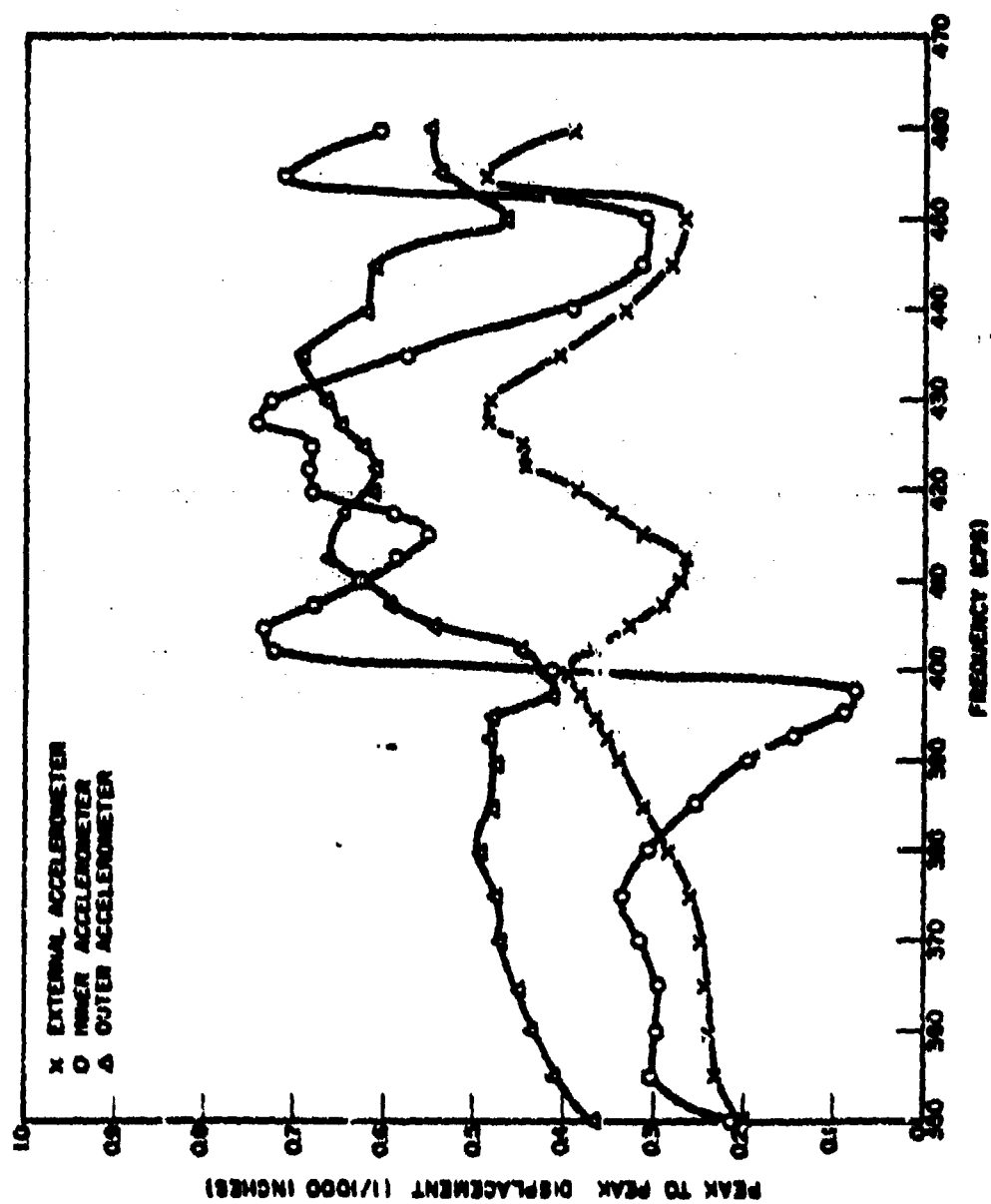


Figure 43 - Element Displacement Characteristics for Specially Instrumented Element in Position 13-6-3

CONFIDENTIAL

CONFIDENTIAL

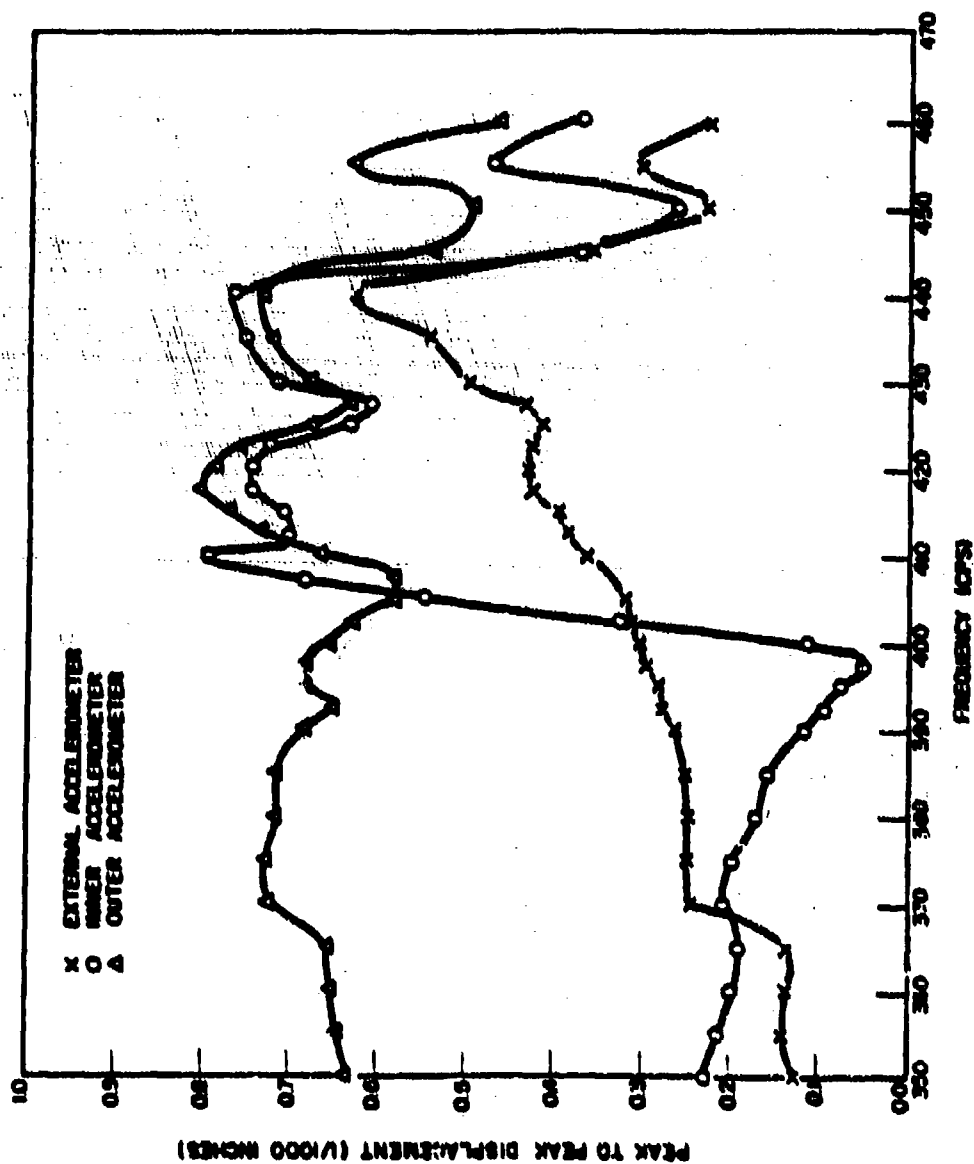


Figure 44 - Element Displacement Characteristics for Specially Instrumented Element in Position 8-11-3

CONFIDENTIAL

CONFIDENTIAL

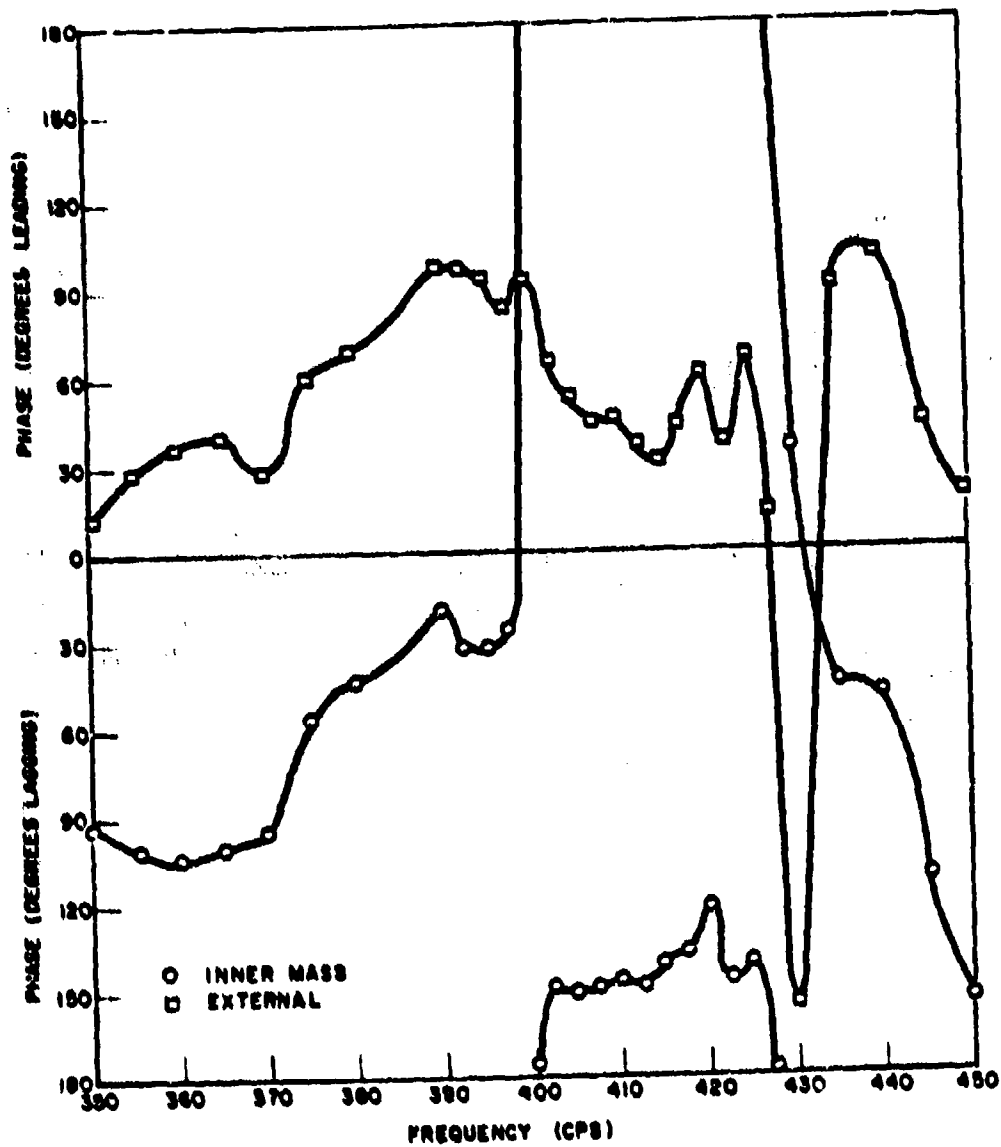


Figure 45 - Phase Characteristics for Specially Instrumented Element in Position 6-1-1. Phase is plotted Relative to Phase of Internal Sensor on Outer Mass.

CONFIDENTIAL

CONFIDENTIAL

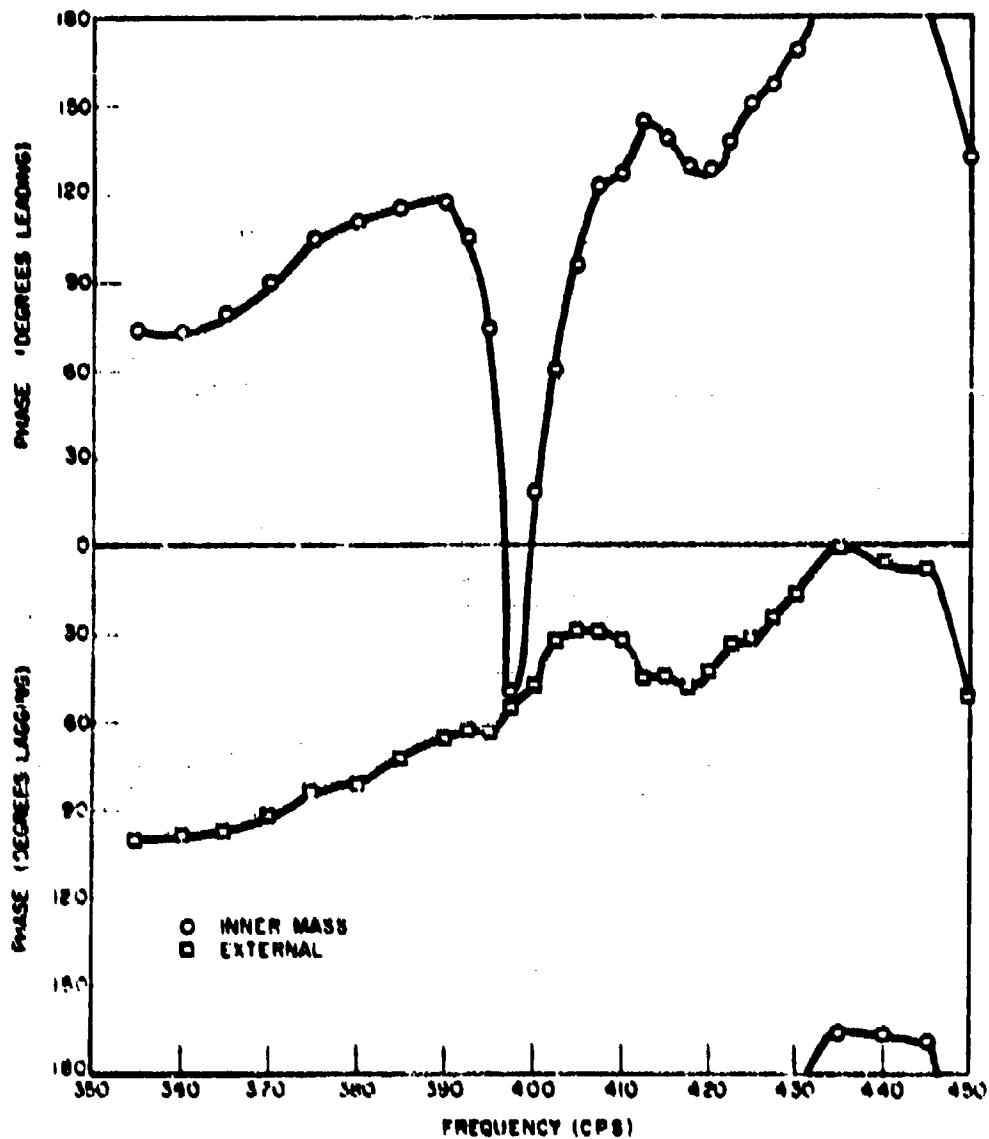


Figure 46 - Phase Characteristics for Specially Instrumented Element in Position 13-6-3. Phase is Plotted Relative to Phase of Internal Sensor on Outer Mass.

CONFIDENTIAL

CONFIDENTIAL

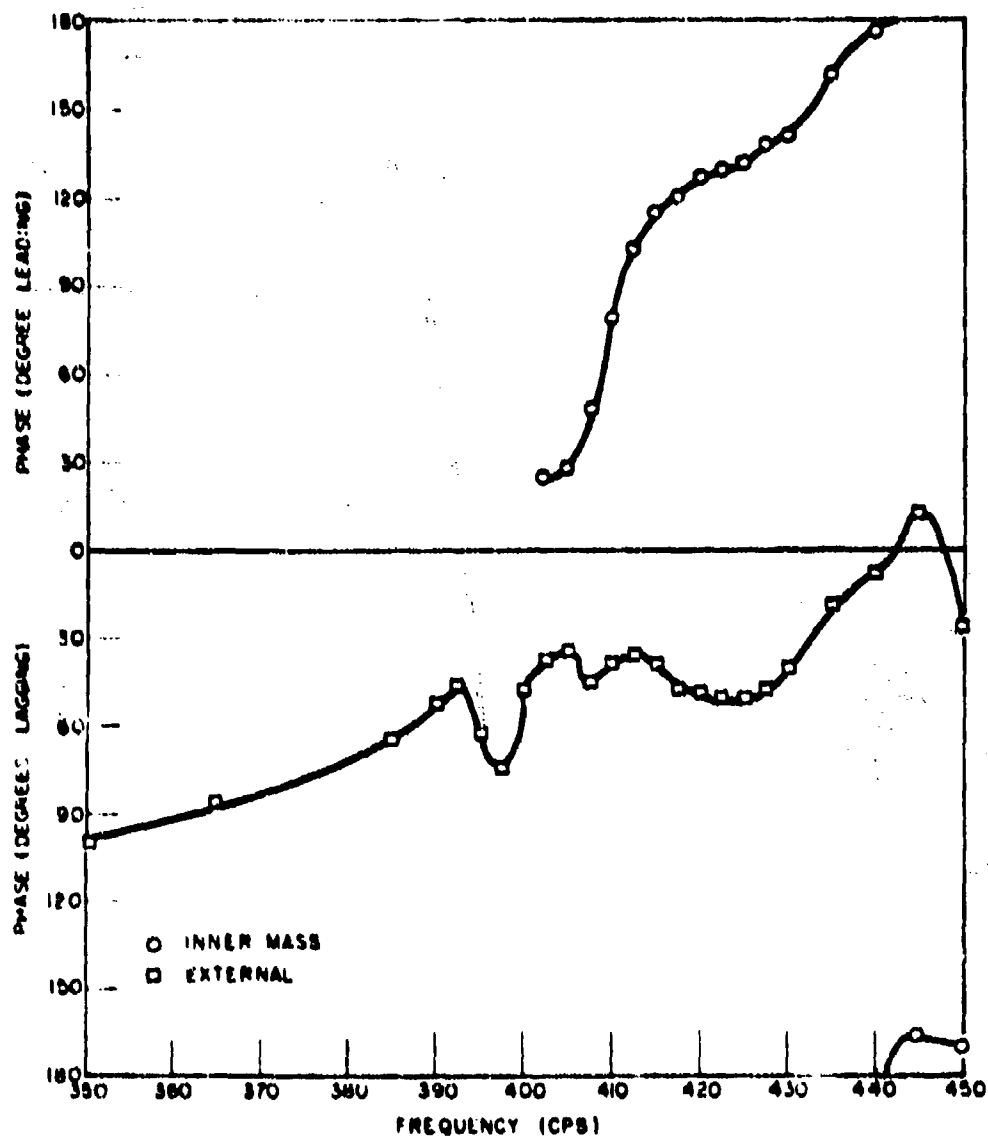


Figure 47 - Phase Characteristics for Specially Instrumented Element in Position 8-11-3. Phase is Plotted Relative to Phase of Internal Sensor or Outer Mass.

CONFIDENTIAL

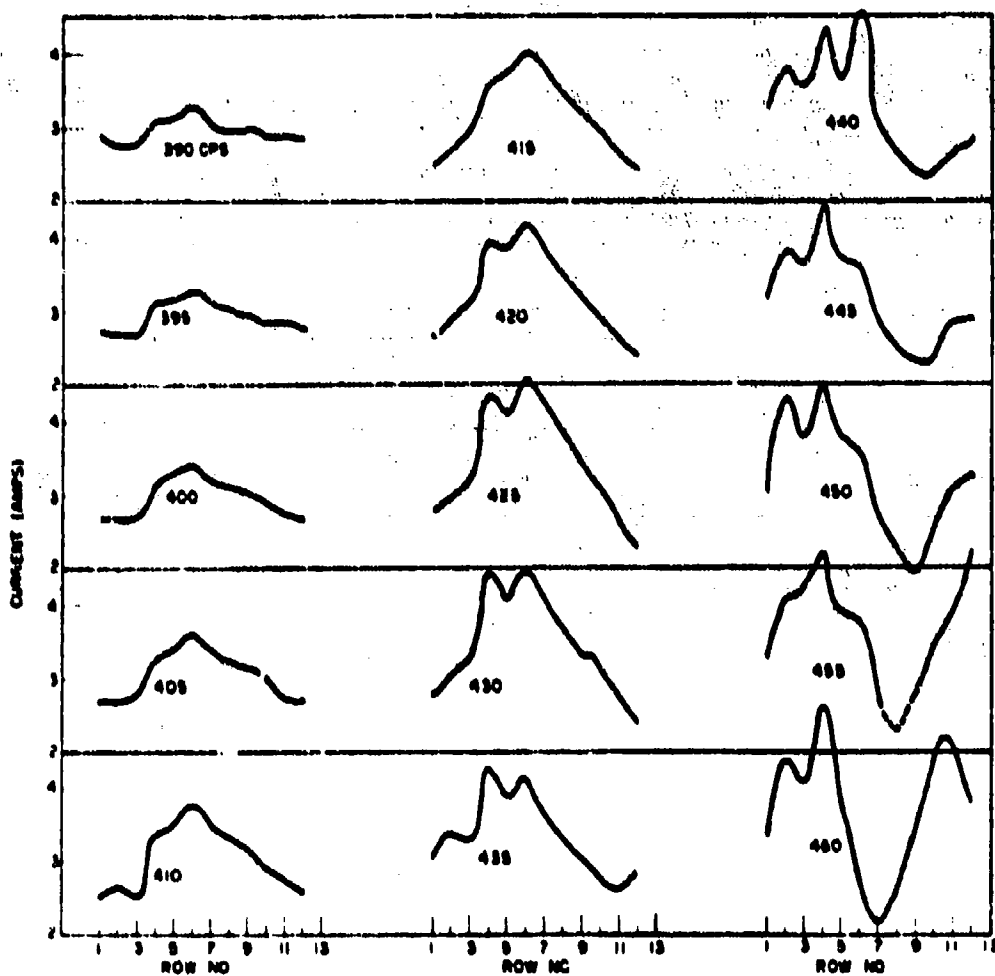


Figure 48 - Current Distribution for Rows of Elements in Module Number Six

CONFIDENTIAL

CONFIDENTIAL

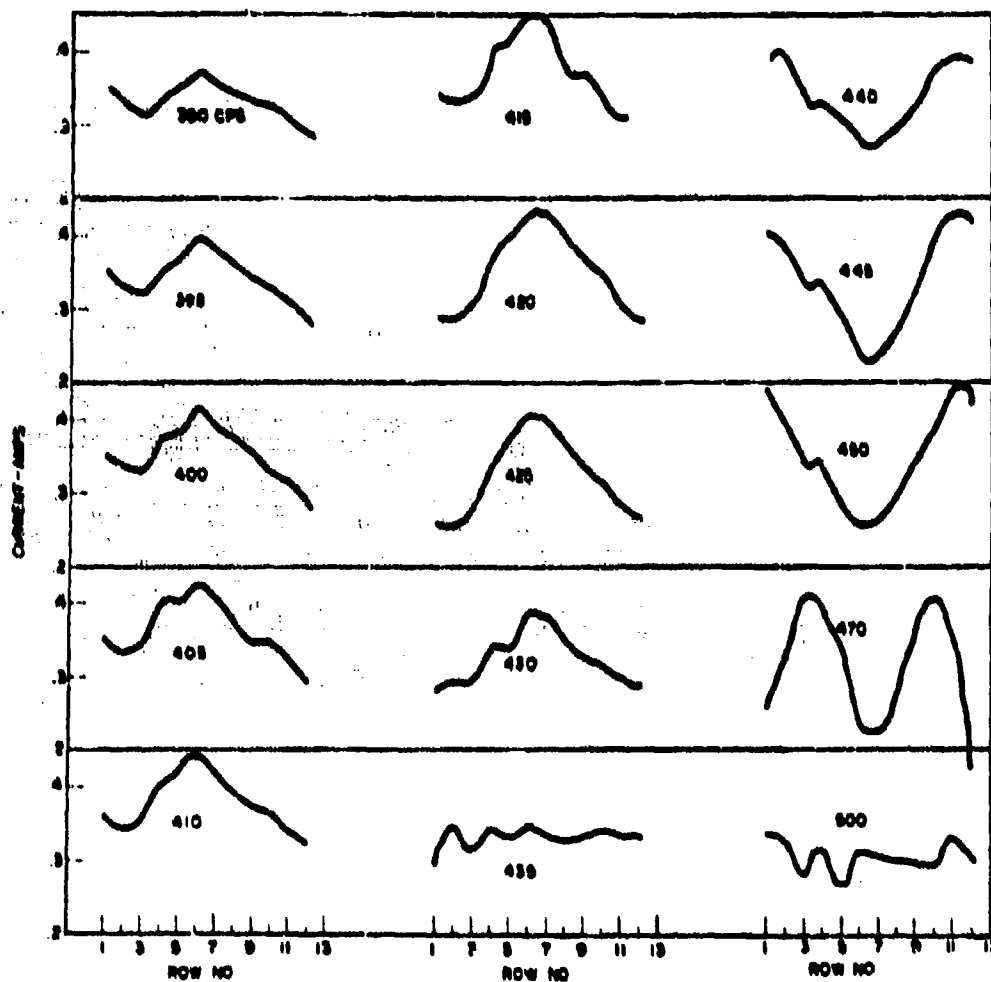


Figure 49 - Current Distribution for Rows of Elements in Module Number 13

CONFIDENTIAL

CONFIDENTIAL

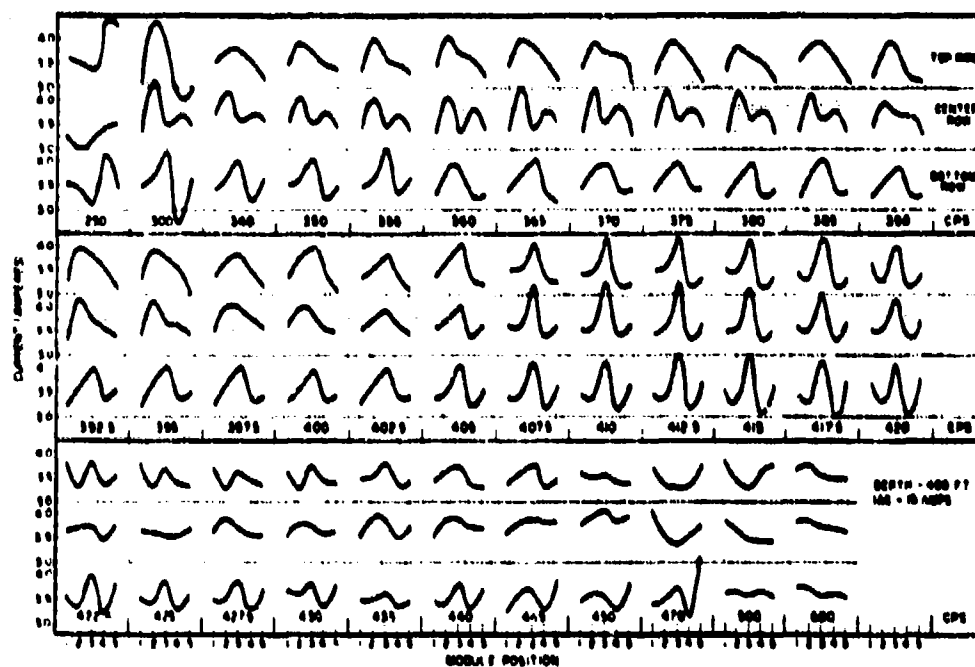


Figure 50 - Current Distribution in the 15 Modules of the Transducer Array

CONFIDENTIAL

CONFIDENTIAL

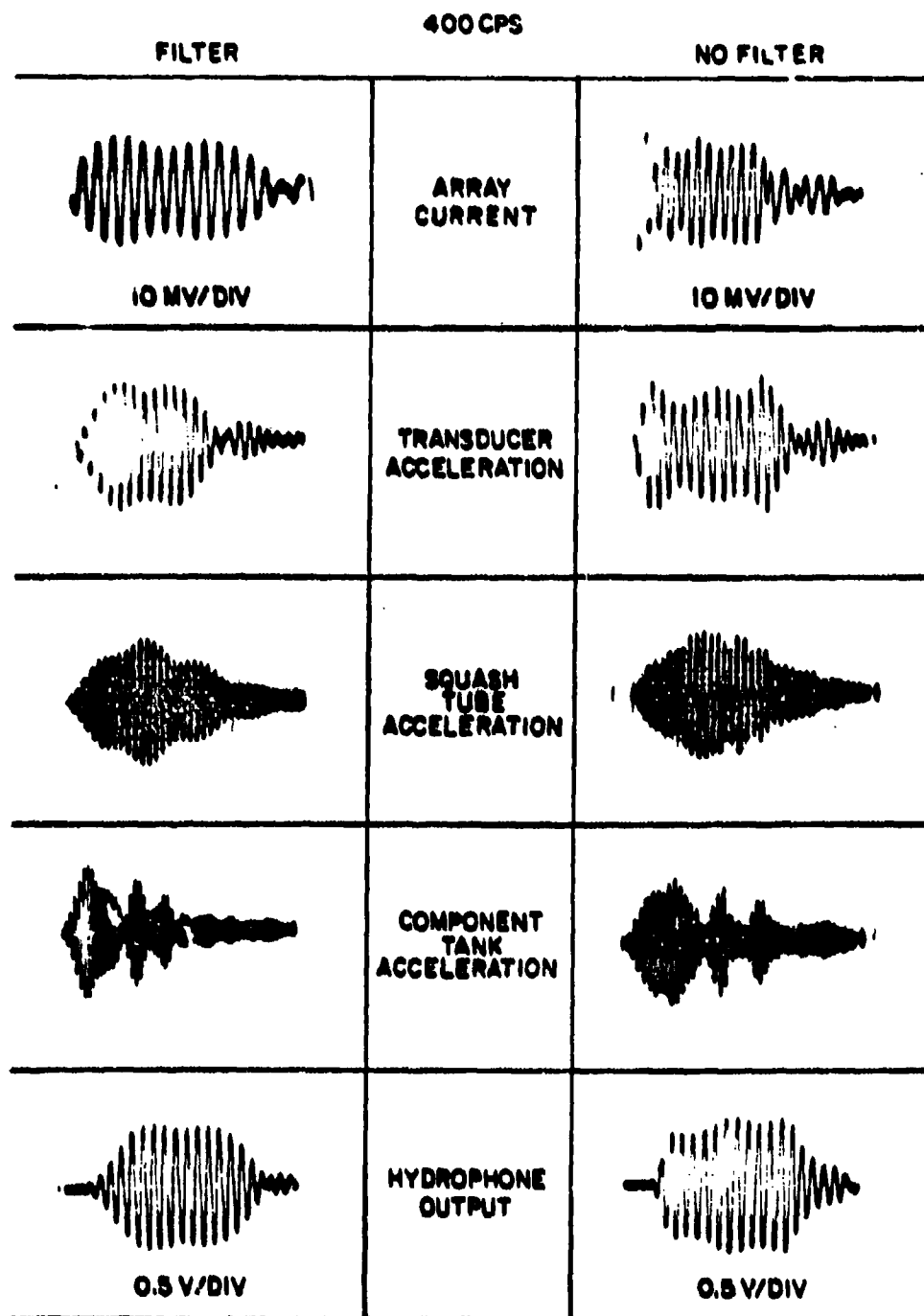


Figure 51 - Typical Waveforms for 30 millisecond Pulses With
and Without a 100cps Band Pass Filter in the Signal Input

CONFIDENTIAL

CONFIDENTIAL

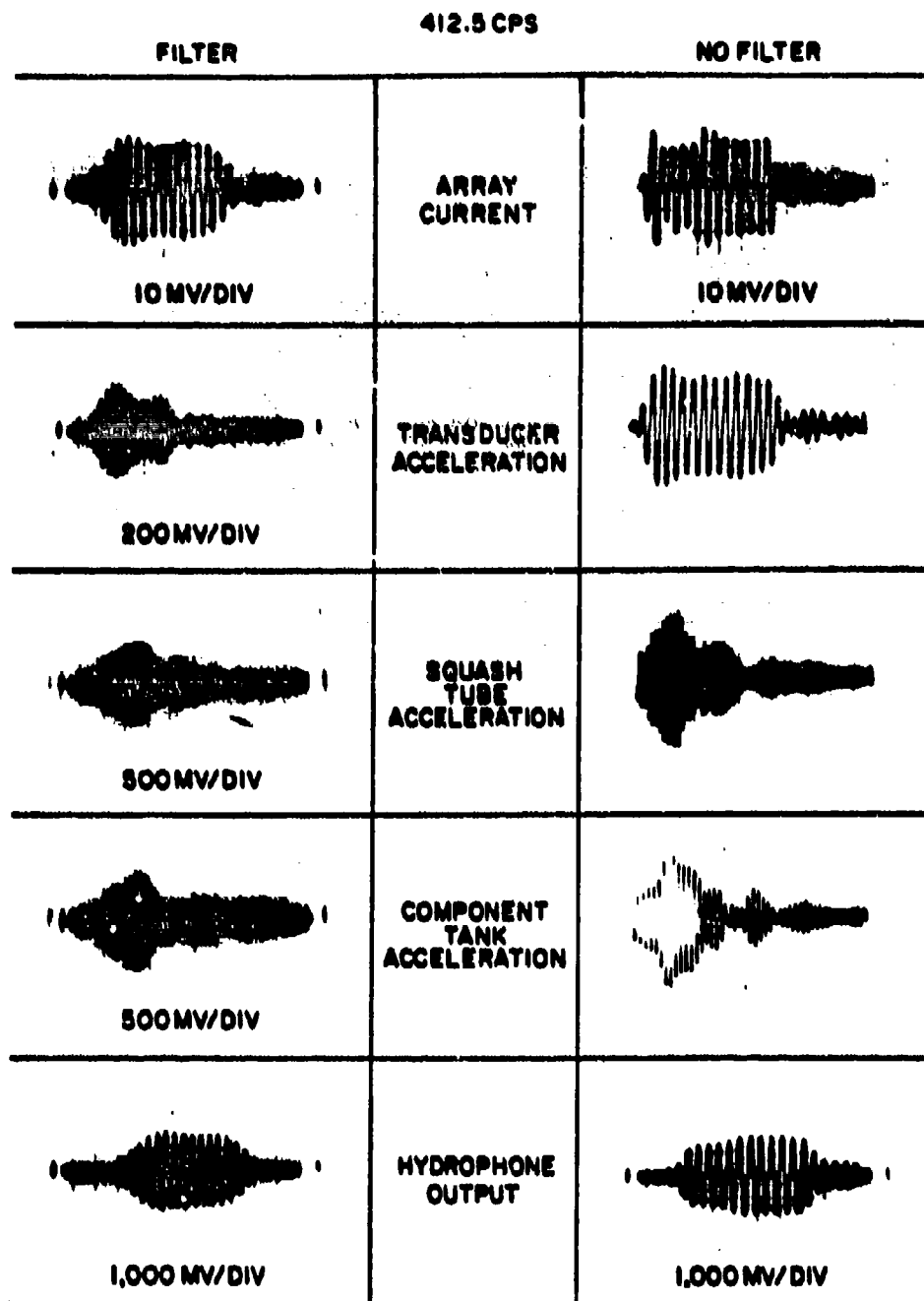


Figure 52 - Typical Waveforms for 30 millisecond Pulses With
and Without a 100cps Band Pass Filter in the Signal Input

CONFIDENTIAL

CONFIDENTIAL

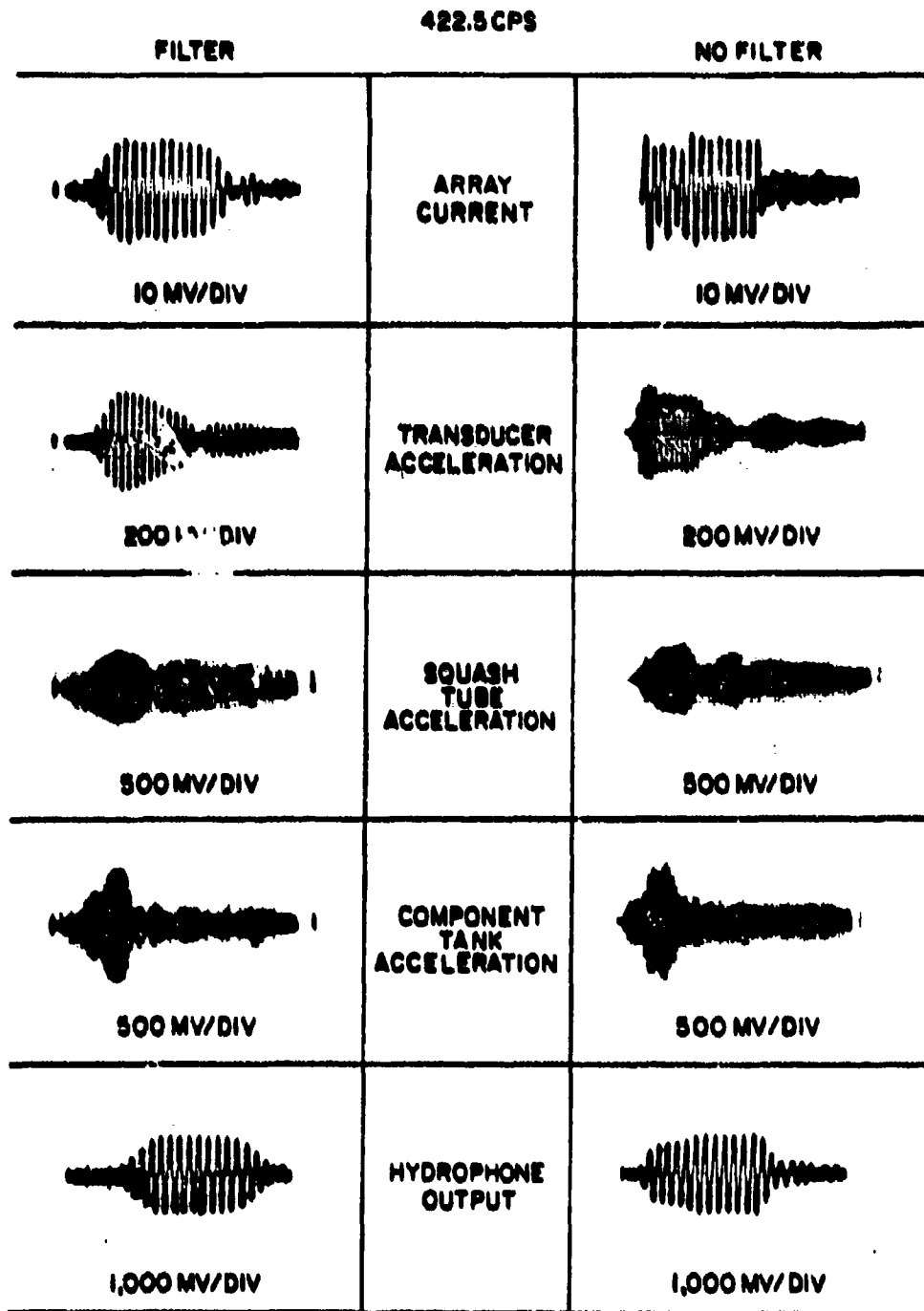
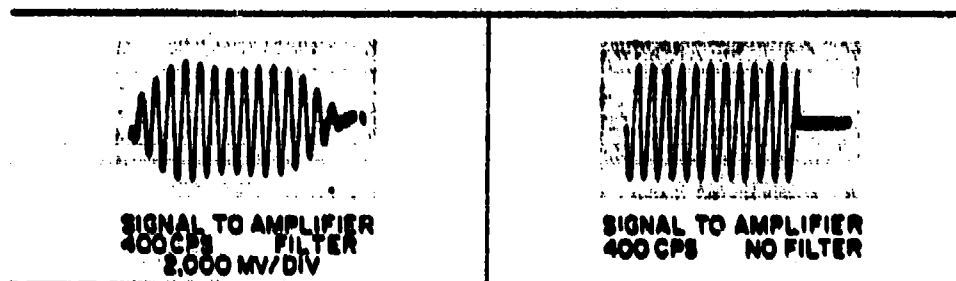


Figure 53 - Typical Waveforms for 30 millisecond Pulses With
and Without a 100cps Band Pass Filter in the Signal Input

CONFIDENTIAL

CONFIDENTIAL



**Figure 54 - Waveform of Pulsed Signal Input to Amplifier With
and Without a 100cps Band Pass Filter**

CONFIDENTIAL

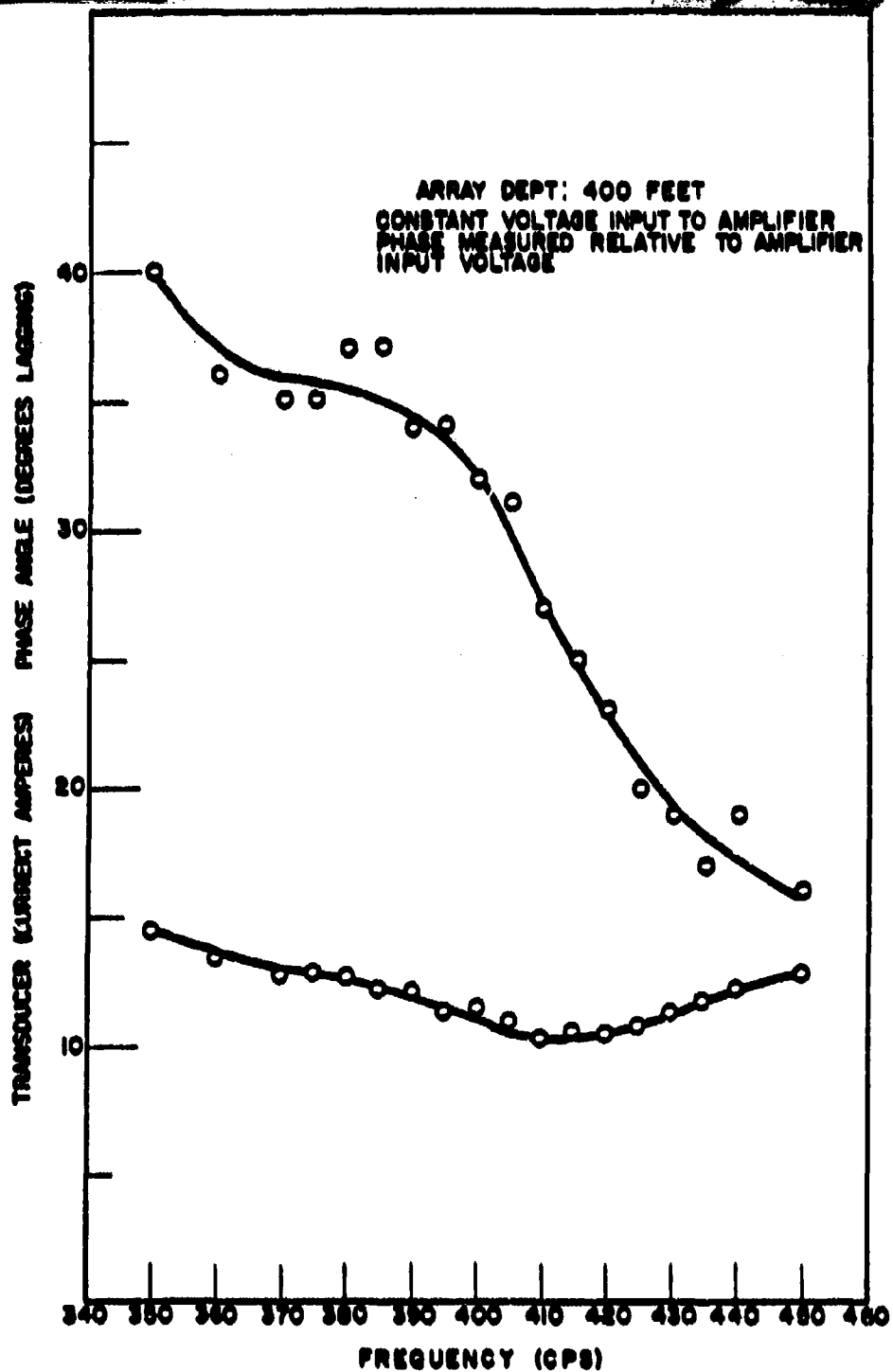


Figure 55 - Transducer Current Amplitude and Phase for Operation
With Constant Voltage Input to Amplifier

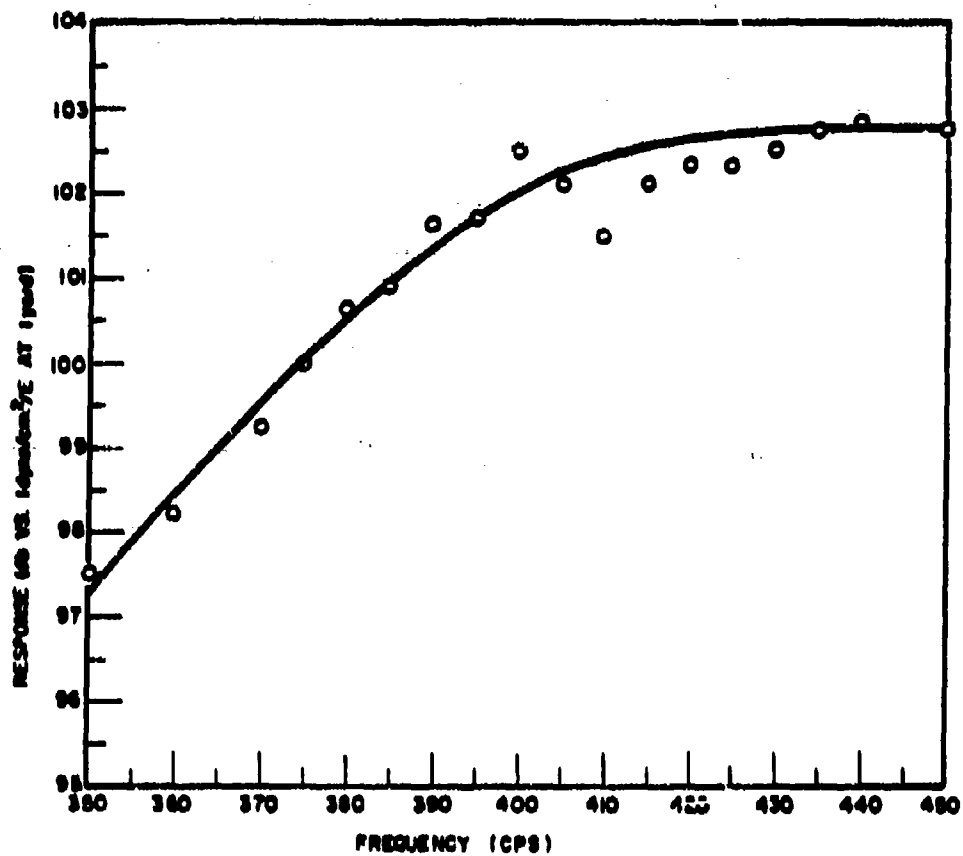


Figure 56 - Relative Response for Constant Voltage Input to Amplifier, Normalized to Value of Voltage Producing one Ampere into Transducer at 400cps

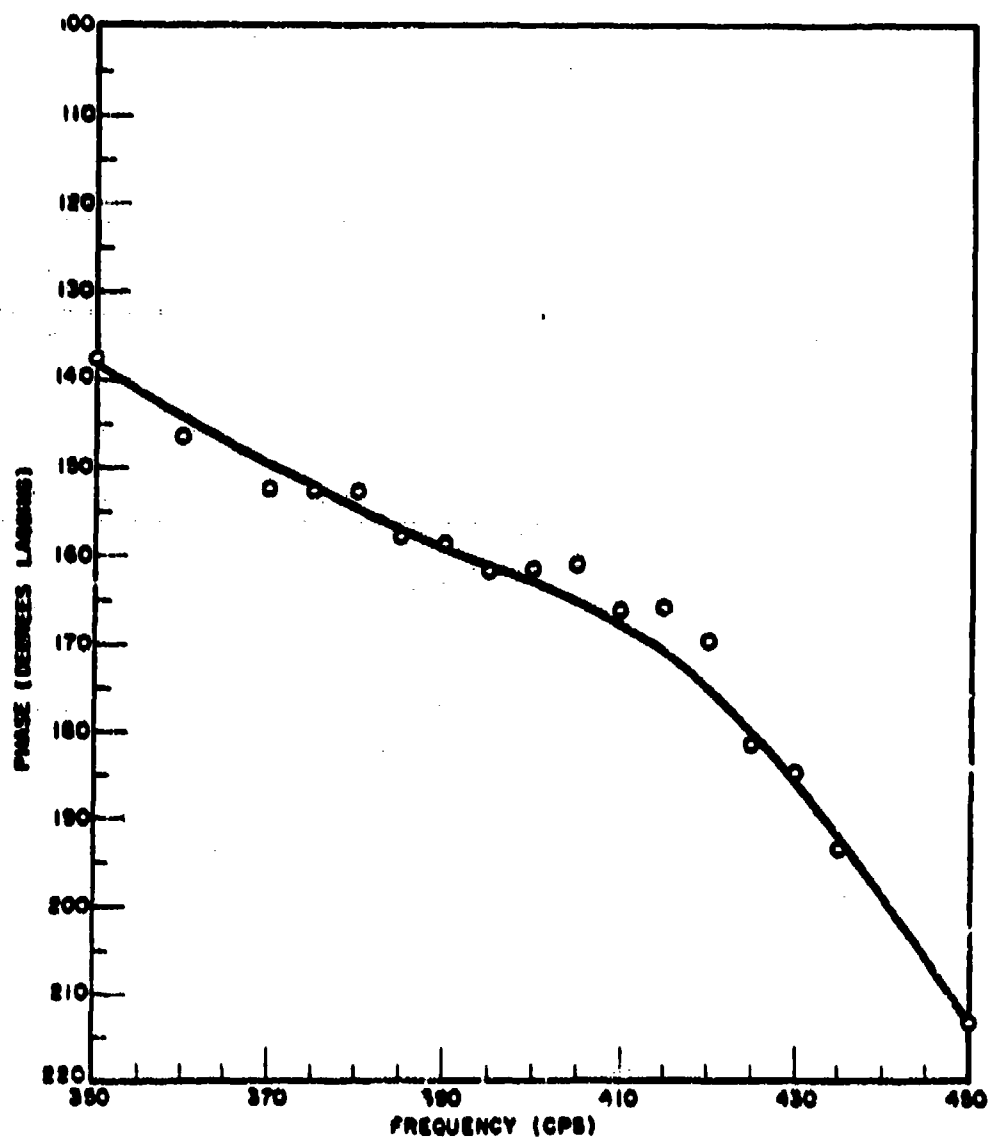


Figure 57 - Pressure Phase at Face of Array Relative to Amplifier Input Voltage for Constant Voltage Input

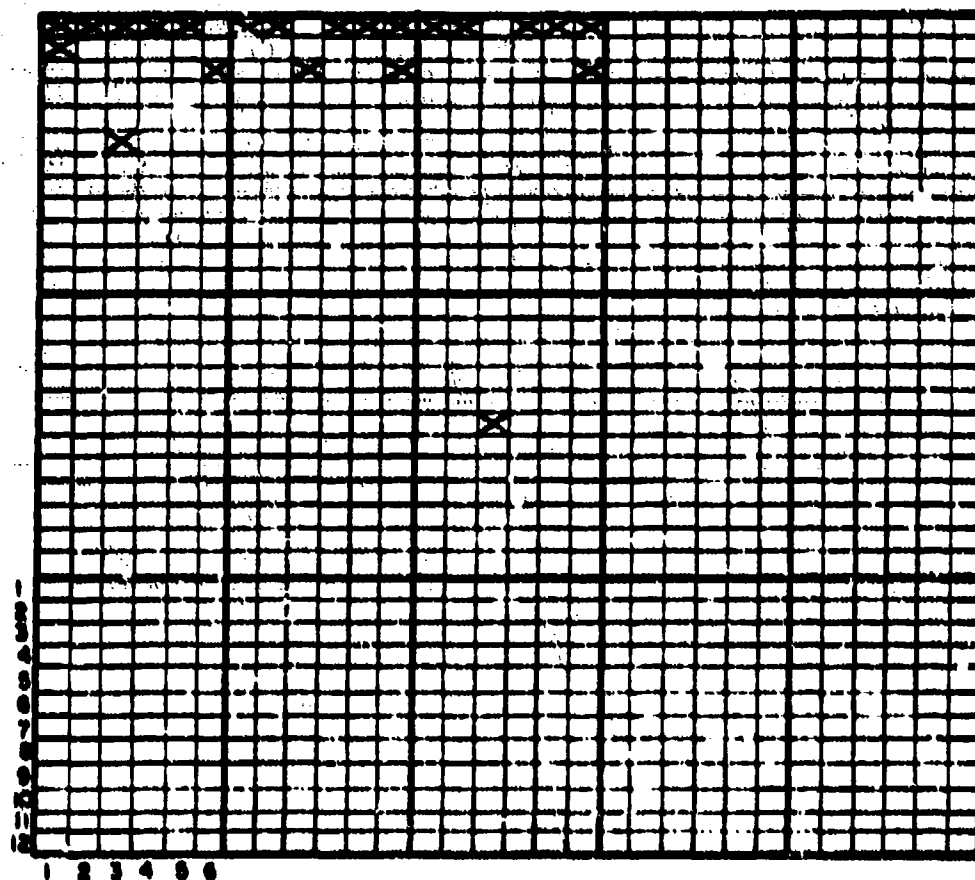


Figure 58 - Location of Accelerometers for Constant Voltage Experiment

UNITED STATES GOVERNMENT
Memorandum

DATE: 7100-016
22 January 2004

REPLY TO
ATTN OF: Burton G. Hurdle (Code 7103)

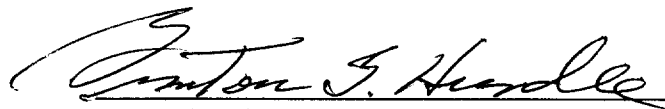
SUBJECT: REVIEW OF REF (A) FOR DECLASSIFICATION

TO: Code 1221.1

REF: (a) "Project ARTEMIS High Power Acoustic Source", A.T. McClinton, R.H. Ferris, W.A. Herrington, Sound Div., NRL Memo Report 1205, 3 Aug 1961 (U)
(b) "Project ARTEMIS High Power Acoustic Source Second Interim Report on Acoustic Performance", A.T. McClinton and R.H. Ferris, Sound Division, NRL Memo Report 1214, 19 September 1961 (U)
(c) "Project ARTEMIS High Power Acoustic Source Third Interim Report on Acoustic Performance", A.T. McClinton, R.H. Ferris, Sound Division, NRL Memo Report 1273, 23 April 1962 (U)
(d) "Project ARETMIS High Power Acoustic Source Effect of Transducer Element Electrical Connection on Interaction in a Consolidated Array", A.T. McClinton, Sound Division, NRL Memo Report 1323, 4 June 1962 (U)
(e) "Test of Project ARTEMIS Source", R.H. Ferris, Sound Division, NRL Memo Report 1648, 15 September 1965 (U)
(f) "Power Limitations and Fidelity of Acoustic Sources", R.H. Ferris and F.L. Hunsicker, Sound Division, NRL Memo Report 1730, November 1966 (U)
(g) "Project ARTEMIS Acoustic Source Acoustic Test Procedure", R.H. Ferris and C.R. Rollins, Sound Division, NRL Memo Report 1769, 5 June 1967 (U)
(h) "Calibration of the ARTEIS Source and Receiving Array on the Mission Capistrano", M. Flato, Acoustics Div., NRL Memo Report 2712, Dec 1973 (U)
(i) "Theoretical Interaction Computations for Transducer Arrays, Including the Effects of Several Different Types of Electrical Terminal Connections", R.V. Baier, Sound Division, NRL Report 6314, 7 October 1965 (U)
(j) "Project ARTEMIS Acoustic Source Summary Report", NRL Report 6535, September 1967 (U)

1. References (a) thru (j) are a series of reports on Project ARTEMIS Reports by the Sound Division that have previously been declassified.
2. The technology and equipment of reference (a) have long been superseded. The current value of these papers is historical

3. Based on the above, it is recommended that reference (a) be available with no restrictions.



BURTON G. HURDLE

NRL Code 7103

CONCUR:

Edward R. Franchi 1/23/2004
E.R. Franchi Date
Superintendent, Acoustics Division

CONCUR:

Tina Smallwood 1/28/04
Tina Smallwood Date
NRL Code 1221.1